DESIGN OF AN AXIAL FLOW FAN FOR A VERTICAL WIND TUNNEL FOR PARATROOPERS

A THESIS SUBMITTED TO
THE GRADUATE SCHOOL OF NATURAL AND APPLIED SCIENCES
OF
MIDDLE EAST TECHNICAL UNIVERSITY

BY
FATİH ÇEVİK

IN PARTIAL FULLFILLMENT OF THE REQUIREMENTS FOR
THE DEGREE OF MASTER OF SCIENCE
IN
MECHANICAL ENGINEERING

DECEMBER 2010

Approval of the thesis:

DESIGN OF AN AXIAL FLOW FAN FOR A VERTICAL WIND TUNNEL FOR PARATROOPERS

submitted by **FATİH ÇEVİK** in partial fulfillment of the requirements for the degree of **Master of Science in Mechanical Engineering Department, Middle East Technical University** by,

Prof. Dr. Canan Özgen
Dean, Graduate School of **Natural and Applied Sciences** _____

Prof. Dr. Süha Oral
Head of Department, **Mechanical Engineering** _____

Prof. Dr. Kahraman Albayrak
Supervisor, **Mechanical Engineering Dept., METU** _____

Examining Committee Members:

Prof. Dr. Haluk Aksel _____
Mechanical Engineering Dept., METU

Prof. Dr. Kahraman Albayrak _____
Mechanical Engineering Dept., METU

Asst. Prof. Dr. Cüneyt Sert _____
Mechanical Engineering Dept., METU

Inst. Dr. Tahsin Çetinkaya _____
Mechanical Engineering Dept., METU

Prof. Dr. Nafiz Alemdaroğlu _____
Aeronautical Engineering Dept., METU

Date: 28.12.2010

I here by declare that all information in this document has been obtained and presented in accordance with academic rules and ethical conduct. I also declare that, as required by these rules and conduct, I have fully cited and referenced all material and results that are not original to this work.

Name, Last name : Fatih Çevik

Signature :

ABSTRACT

DESIGN OF AN AXIAL FLOW FAN FOR A VERTICAL WIND TUNNEL FOR PARATROOPERS

Çevik, Fatih
M.Sc., Department Of Mechanical Engineering
Supervisor: Prof. Dr. Kahraman Albayrak
December 2010, 131 pages

Free fall is one of the important phases of the operation performed by the Special Forces paratroopers. Also civilian parachutists are performing free fall as a sport by doing aerobatic maneuvers when they reach the terminal velocity during falling before opening their parachutes. Vertical wind tunnels are used for training the parachutists and paratroopers. It is safe, cheap and more convenient when compared to jumping out of an airplane.

This thesis consists of aerodynamic design of closed circuit, double return vertical wind tunnel with a flight section that can accommodate four paratroopers, aerodynamic design of a rotor straightener configuration axial flow fan and running CFD analysis of the axial flow fan for different operating conditions by FLUENT software.

Keywords: Axial Flow Fan, Computational Fluid Dynamics, Vertical Wind Tunnel, Terminal Velocity

ÖZ

PARAŞÜTÇÜLER İÇİN DİKEY RÜZGAR TÜNELİNİN EKSENEL FAN TASARIMI

Çevik, Fatih
Yüksek Lisans, Makina Mühendisliği Bölümü
Tez Yöneticisi: Prof. Dr. Kahraman Albayrak
Aralık 2010, 131 sayfa

Serbest düşüş Özel Kuvvetler paraşütçülerinin gerçekleştirdikleri operasyonların önemli bir fazıdır. Sivil paraşütçüler tarafından da, terminal hıza ulaştıktan sonra, paraşütlerini açmalarından önce serbest düşüş sırasında akrobatik manevralar yaptıkları bir spor olarak gerçekleştirilmektedir. Dikey rüzgar tünelleri paraşütçülerin eğitimi için kullanılmaktadır. Uçaktan atlama ile karşılaştırıldığında, güvenli ucuz ve daha uygundur.

Bu tez, kapalı çevrim, çift dönüşlü, uçuş bölümünde dört kişinin uçabildiği bir dikey rüzgar tüneli aerodinamik tasarımından, pervane ve akış düzeltici konfigürasyonuna sahip bir eksenel fanın aerodinamik tasarımından ve FLUENT CFD yazılımı ile eksenel fanın değişik çalışma koşulları için sayısal akışkanlar dinamiği analizlerinden oluşmaktadır.

Anahtar Kelimeler: Eksenel Fan, Hesaplamalı Akışkanlar Dinamiği, Dikey Rüzgar Tüneli, Terminal Hız

To my daughters, İlke, İlgi and my wife Işın

ACKNOWLEDGEMENTS

The author wishes to express his deepest and sincere gratitude to his supervisor, Prof. Dr. Kahraman Albayrak, for accepting him as M.Sc. student, his patience, encouragement and guidance during this thesis study.

The author also would like to thank his wife for her support and his daughters for their love.

The encouragement of his colleagues Barış Gökçe and Dr. İlteriş Koç are greatly appreciated.

The assistance of his friends and colleagues, Mehmet Çavuş and Cumhur Özgür are acknowledged for their technical support and assistance on FLUENT CFD program.

TABLE OF CONTENTS

ABSTRACT iv
ÖZ v
ACKNOWLEDGEMENTS vii
TABLE OF CONTENTS viii
LIST OF TABLES xii
LIST OF FIGURES xiv
LIST OF SYMBOLS xvii
CHAPTERS
1. INTRODUCTION 1
1.1. General Requirements 3
1.2. Wind Tunnels 3
1.2.1. Aeronautical Wind Tunnels 7
1.2.1.1. High Reynolds Number Wind Tunnels 7
1.2.1.2. V/STOL Wind Tunnels 8
1.2.1.3. Free Flight Wind Tunnels 8
1.2.1.4. Spin Wind Tunnels 8
1.2.1.5. Stability Wind Tunnels 8
1.2.1.6. Propeller Wind Tunnels 9
1.2.1.7. Propulsion tunnels 9
1.2.1.8. Icing Wind Tunnels 9
1.2.2. Smoke Tunnels 9
1.2.3. Aero-acoustic Wind Tunnels 10
1.2.4. Automobile Wind Tunnels 10
1.2.5. Water Tunnels 10
1.2.6. General Purpose Wind Tunnels 11
1.2.6.1. People 11

1.2.6.2. Wind Power Devices 11
1.2.6.3. Solar Collectors, Radar Antenna and Satellite Dish 11
1.2.6.4. Bridges 11
1.2.7. Environmental Wind Tunnels 12
1.2.8. Vertical Wind Tunnels 12
1.3. Axial Flow Fans 15
1.3.1. Axial Flow Fan Types 16
1.3.1.1. Propeller Fans 16
1.3.1.2. Tube Axial Fans 17
1.3.1.3. Vane Axial Fans 19
1.3.2. Axial Flow Fan Performance 20
1.4. Fluent CFD Program 23
1.4.1. Fluent Program Introduction 23
2. SUBSONIC WIND TUNNEL DESIGN 24
2.1. Wind Tunnel Component Pressure Losses 25
2.1.1. Universal Friction Coefficient 25
2.1.2. Energy Ratio and Power Considerations 27
2.1.3. Constant Area Components 31
2.1.4. Diffusers 33
2.1.5. Contraction Cone / Nozzle 38
2.1.6. Corners & Guide Vanes 40
2.1.7. Screens and Mesh 42
2.1.8. Honeycomb 44
2.1.9. Model 45
2.2. Wind Tunnel Layout and Pressure Loss Calculations 46
2.2.1. Wind Tunnel Layout 46
2.2.2. Wind Tunnel Component Pressure Loss Calculations 48
2.2.2.1. Basic Data 48
2.2.2.2. Flight Chamber 50
2.2.2.3. Flight Diffuser 51

2.2.2.4. First Diffuser 52
2.2.2.5. First Corner 53
2.2.2.6. Second Diffuser 55
2.2.2.7. Second Corner 56
2.2.2.8. Air Exchange Section 57
2.2.2.9. Fan Collector 58
2.2.2.10. Fan Inlet Duct 59
2.2.2.11. Fan Exit Duct 60
2.2.2.12. Third Diffuser 61
2.2.2.13. Third Corner 62
2.2.2.14. Fourth Diffuser 63
2.2.2.15. Fourth Corner 64
2.2.2.16. Settling Chamber 65
2.2.2.17. Contraction Cone 66
2.2.2.18. Safety Net 67
2.2.2.19. Air Exchange Loss 68
2.2.2.20. Paratroopers 69
2.2.2.21. Total Loss and Power Calculations 69
3. AXIAL FAN DESIGN 72
3.1. Axial Fan Design Approach 72
3.1.1. General Momentum Equations 76
3.1.2. Rotor Blade Design 82
3.1.3. Stator Design 84
3.2. Axial Fan Design and Calculations 87
3.2.1. Basic Assumptions 87
4. FAN CFD MODEL 94
4.1. Introduction 94
4.2. Computational Mesh 95
4.3. Boundary Conditions and Solution Controls 97
4.3.1. Boundary Conditions 97

4.3.2. Solution Controls 100
4.4. CFD Results 103
4.4.1. CFD Results for Design Point 103
4.4.2. CFD Results for Off-Design Points. 104
4.4.3. Rotor and Stator Pressure and Velocity Contours 106
5. RESULTS AND DISCUSSION 110
5.1. General 110
5.1.1. Wind Tunnel 110
5.1.2. Axial Fan Design 111
5.1.3. CFD Analyses 113
5.2. Recommendations for Future Work 113
5.3. Conclusion 114
REFERENCES 116
APPENDICES
A TERMINAL VELOCITY OF PARATROOPERS 119
A.1. Definitions 119
A.2. Drag Force 120
A.3. Human Model 121
A.4. Terminal Velocity Calculation 124
B AIRFOIL SECTIONS AND DATA 128
B.1. F Series Airfoil 128
B.2. Other Airfoil Sections 131

LIST OF TABLES

TABLES:

Table 1 Comparison of open circuit and closed circuit wind tunnels 6
Table 2 Wind tunnel types 6
Table 3 Basic Specifications of Commercial Vertical Wind Tunnels 15
Table 4 Difference between fans, blowers and compressors 16
Table 5 Flight chamber pressure loss calculation results 50
Table 6 Flight diffuser pressure loss calculation results 51
Table 7 First diffuser pressure loss calculation results 52
Table 8 First corner pressure loss calculation results 53
Table 9 Second diffuser pressure loss calculation results 55
Table 10 Second corner pressure loss calculation results 56
Table 11 Air exchange section pressure loss calculation results 57
Table 12 Fan collector section pressure loss calculation results 58
Table 13 Fan inlet duct section pressure loss calculation results 59
Table 14 Fan exit duct section pressure loss calculation results 60
Table 15 Third diffuser pressure loss calculation results 61
Table 16 Third corner pressure loss calculation results 62
Table 17 Fourth diffuser pressure loss calculation results 63
Table 18 Fourth corner pressure loss calculation results 64
Table 19 Settling chamber section pressure loss calculation results .. 65
Table 20 Contraction cone section pressure loss calculation results .. 66
Table 21 Safety net pressure loss calculation results 67
Table 22 Air exchange pressure loss calculation results 68
Table 23 Paratroopers pressure loss 69
Table 24 Rotor parameters summary 91
Table 25 Stator parameters summary 91

Table 26 Gauge total pressures about rotor..... 103
Table 27 CFD results for 600 RPM 105
Table 28 CFD results for 450 RPM 105
Table 29 Human model section weights 122
Table 30 Human model section dimensions..... 123

LIST OF FIGURES

FIGURES:

Figure 1 Schematic view of an open circuit wind tunnel [36] 4
Figure 2 Schematic view of a closed circuit wind tunnel [37] 5
Figure 3 Direct drive and belt driven propeller fan [38] 17
Figure 4 Belt driven tube axial fan [41] 18
Figure 5 Direct drive tube axial fan [38] 18
Figure 6 Belt driven vane axial fan [39] 19
Figure 7 Direct drive vane axial fan [40] 20
Figure 8 Typical performance curve of axial flow fans [12] 21
Figure 9 Schematic view of different flow conditions [16] 22
Figure 10 Friction Factor for Smooth Pipe 26
Figure 11 Jet power per unit area at standard conditions 28
Figure 12 Diffuser geometry and notation 33
Figure 13 Diffuser design limitations [9] 34
Figure 14 Typical contraction cone / Nozzle [9] 38
Figure 15 Borger curves for contraction surfaces [23] 39
Figure 16 Guide vane profiles [3] 41
Figure 17 Mesh Structure 43
Figure 18 Three types of honeycomb[3] 44
Figure 19 Vertical wind tunnel model 47
Figure 20 Turning vanes 54
Figure 21 System curves 70
Figure 22 Cascade flow[6] 76
Figure 23 General blading arrangement [6] 78
Figure 24 Relative velocity vectors [6] 79
Figure 25 Absolute velocity vectors [6] 80

Figure 26 Profile drag vs lift coefficient for F series airfoil [6] 81
Figure 27 Rotor blade element geometry [6] 83
Figure 28 Deviation angle coefficient vs stagger angle [6] 84
Figure 29 Stator vane element geometry [6] 85
Figure 30 Stator vane design data [6] 86
Figure 31 Stator vane camber and stagger angle [6] 86
Figure 32 Rotor section profiles 92
Figure 33 Stator section profiles 92
Figure 34 Rotor and stator model (top view) 93
Figure 35 Rotor and stator model (oblique view) 93
Figure 36 Rotor and stator surface mesh 95
Figure 37 Rotor and stator surface mesh with casing 96
Figure 38 Rotor tip clearance 96
Figure 39 Fluid zones 98
Figure 40 Inlet boundary condition 98
Figure 41 Exit boundary condition 99
Figure 42 Fluid zone definition around rotor 99
Figure 43 Grid interface definitions 100
Figure 44 Solver form 101
Figure 45 Viscous panel options 102
Figure 46 Solution controls 102
Figure 47 Fan performance curve 106
Figure 48 Rotor static pressure contours (pressure side) 107
Figure 49 Rotor static pressure contours (suction side) 108
Figure 50 Rotor static pressure contours (Off-design) 109
Figure 51 Stator static pressure contours 109
Figure 52 Spread eagle position 119
Figure 53 Human Model 122
Figure 54 Terminal velocity, no additional weight 125
Figure 55 Terminal velocity, 30kg additional weight 126

Figure 56 Terminal velocity, 60kg additional weight 127
Figure 57 Camber line of F Series airfoil [6] 129
Figure 58 Airfoil coordinate determination [6] 130
Figure 59 Sample airfoil 131

LIST OF SYMBOLS

L	:	Length (m²)
$\bar{\tau}_w$	:	Wall shear stress (Pascal)
C_w	:	Circumference
Δp	:	Pressure difference, pressure drop
f	:	Friction coefficient
Re	:	Reynolds number
D_h	:	Hydraulic diameter
E_R	:	Energy Ratio
P	:	Power (Joule/s, Watt)
A	:	Area (m²)
V	:	Velocity, Average Velocity
K	:	Local pressure loss coefficient
K_0	:	Pressure loss coefficient
q	:	Dynamic pressure (Pascal)
ϕ	:	Turning angle (°)
θ	:	Blade element camber angle (°)
θ	:	Blade element camber angle (°)
δ	:	Flow deflection angle (°)
σ	:	Solidity
β	:	Porosity
ε	:	Influence coefficient
ε	:	Flow swirl coefficient
C_L	:	Lift coefficient
C_D	:	Drag coefficient

C_{Dp}	:	Pressure drag coefficient
C_{Ds}	:	Secondary drag coefficient
μ	:	Viscosity (N·s / m²)
β_1	:	Angle between rotor inlet velocity and fan axis (°)
β_2	:	Angle between rotor exit velocity and fan axis (°)
β_m	:	Angle between mean rotor velocity and fan axis (°)
Q	:	Volumetric flow rate (m³/s)
H	:	Total pressure (Pascal)
λ	:	Flow coefficient
Δh	:	Local total pressure change between two points (Pascal)
ΔH	:	Total pressure change between two points (Pascal)
Ω		Angular velocity (radians/s)
T	:	Torque (N·m)
Th	:	Thrust (N)
K_{th}	:	Theoretical pressure rise coefficient
ξ		Stagger angle (°)
AR	:	Blade aspect ratio
s	:	Blade spacing (m)
c	:	Chord length (m)
η_{bl}	:	Blading efficiency
η_{hyd}	:	Hydraulic efficiency
x	:	Relative blade station with respect to tip radius
ω	:	Angular velocity (radians/s)
d	:	Airfoil nose droop (%)
t	:	Blade thickness (m)
i	:	Local incidence angle (°) between V_1 and β_1

Subscripts

0	:	Fan inlet, prerotator inlet
1	:	Prerotator exit, Rotor inlet
2	:	Rotor exit, Stator inlet
3	:	Stator exit, Fan exit
a	:	Axial
θ	:	Tangential
c	:	coefficient
l	:	local
lt	:	test

CHAPTER 1

INTRODUCTION

It is humankind's dream to fly from the early times of the history. In the Greek Mythology, "Daedalus" and "Icarus" [1]; a father and son, escape from the prison of the Hernia. They had flown by the help of the wings, which they built from the bird feathers. They glued the wings to their bodies with wax. "Icarus" flew higher in the sky close to the sun. It was unfortunate that the sun melted the wax and made feathers fall apart.

"Leonardo de Vinci" is well known for his effort to build flying machines and observations how birds use their wings to fly. Although there are some scientific and artistic studies in history, it took a very long time until men successfully use machines to fly with. In the 19th century, one of the pioneers of aviation was "Otto Lilienthal" (1848–1896) of Germany who was famous for piloting the gliders that he built. He performed more than 2000 flights with gliders before he died in a flight accident [2]. In the very early stages of the 20th century, "Orville Wright" and "Wilbur Wright" brothers introduced the first powered flight to the mankind. Then the progress in aviation was unstoppable.

However, no machine gives the enthusiasm of flying like a bird. The time between the jumping out of a plane and opening the parachute is the time when a man feels as close as possible to flying. This phase is called the "Free Fall Phase". It is becoming a very wide spreading sport and there are several competitions all over the world. The competitions are about the

aerobatic maneuvers performed in the air and can be among individuals or among teams composed of different number of parachutists.

The concept of using a vertical wind tunnel to imitate flying aroused in USA. In 1964, Jack Tiffany, a US Air Force Officer, flew in a vertical wind tunnel at Wright Peterson Air Force Base. After that, the vertical wind tunnels were used for training of paratroopers, parachutists. The idea went commercial in the 1980's. There are several facilities all over the world and anybody who wants a taste of flying can fly in any of these facilities.

Free falling phase has a great importance for the military applications also. Especially Special Forces' paratroopers jump from very high altitudes in a very narrow time window and they keep falling until the last second just before opening their parachutes that they can make safe landings. The paratroopers can face some problems:

- The collision in the air between two paratroopers can knock them unconscious.
- The loss in attitude control in the air can make the paratrooper land far away from the targeted point behind the enemy lines.
- The loss of orientation at night operations can put the paratrooper in unwanted situations when opening the parachute.

To overcome these problems, paratroopers need excessive training. A vertical wind tunnel will give them the opportunity of having safe and effective training in an economical way.

This thesis will describe the general requirements for a vertical wind tunnel with military capabilities. In a military vertical wind tunnel, the velocity that must be obtained in the flight chamber is more than the commercial vertical wind tunnels. After that, a literature survey about the wind tunnels, axial fans and very short information about CFD method will be presented. Then the methodology of the design of the duct system of the vertical wind

tunnel will be given. In addition, the conceptual design of the axial fan required to supply sufficient pressure rise and volumetric flow rate will be given. A CFD confirmation of the fan design is also performed in this thesis. The thesis will be concluded by the discussion about the results and the possible studies that can be performed in the future.

1.1. General Requirements

The general requirements for a vertical wind tunnel for paratroopers training can be specified as follows:

- The wind tunnel must be operable in all weather conditions.
- At least four paratroopers must fly at the same time.
- The air speed must be adjustable to train paratroopers having different height / weight and operational flying configuration.
- The wind tunnel must have uniformly distributed flow in the flying chamber.
- Minimum height of the flying chamber must be at least 3 meters. More height is favored.
- The wind tunnel must be energy efficient.
- Must have power unit to supply and sustain enough flow rate.

1.2. Wind Tunnels

In aerodynamics and hydrodynamics, experimental information is useful in solving problems. There are several ways to obtain experimental information [3]. These methods can be summarized as:

- Road test
- Flight experiments
- Rocket sleds
- Whirling arms

- Shock tubes
- Ballistic ranges
- Wind tunnels
- Rocket flights
- Flying scale models
- Wind tunnels

Although every method has advantages and disadvantages, wind tunnels are considered as one of the important ones among the alternatives.

There are many ways to classify the wind tunnels. But two major classifications are due to the circuit type and test section type.

The circuit can be either closed circuit and open circuit. In an open circuit wind tunnel, the air is taken from outside environment and discharged to outside environment again. In Figure 1, schematic view of an open circuit wind tunnel is given. The air generally follows a straight path from the entrance to the exit of the wind tunnel

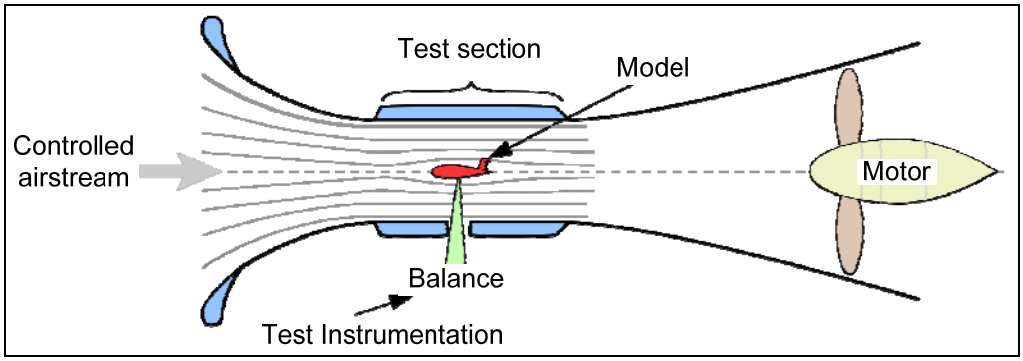

Figure 1 Schematic view of an open circuit wind tunnel [36]

In closed circuit wind tunnels, the air is circulated by the help of a power unit continuously. The schematic view of a closed circuit wind tunnel is given in Figure 2. Sometimes, a small amount of air is exchanged with the

environment to increase the air quality and have some temperature control.

The test section of the wind tunnels can be either open jet (no solid boundaries around the test section) or closed jet (solid boundaries around the test section). In some wind tunnels, the test sections also have slotted walls.

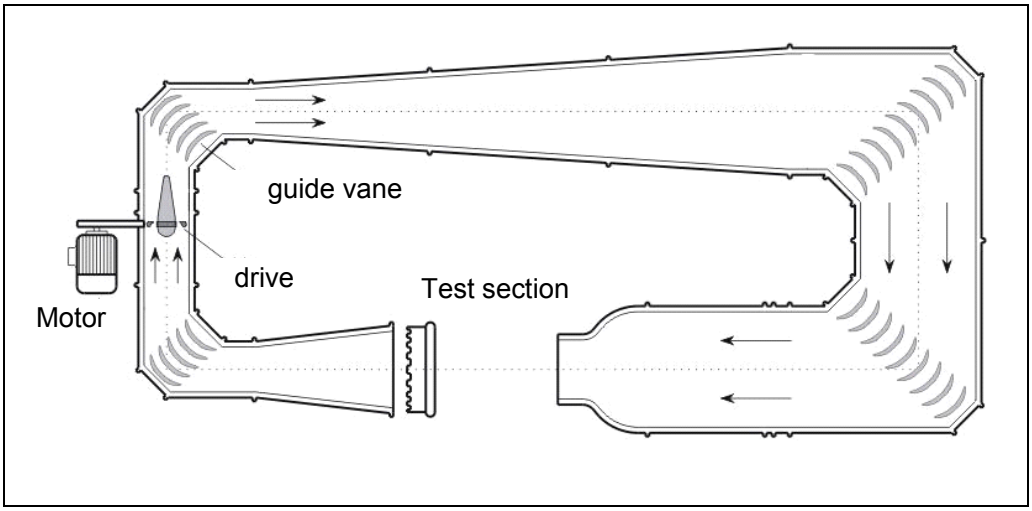

Figure 2 Schematic view of a closed circuit wind tunnel [37]

Open circuit and closed circuit wind tunnels have some major advantages and disadvantages. A comparison of closed circuit wind tunnels and open circuit wind tunnels is given in Table 1.

Table 1 Comparison of open circuit and closed circuit wind tunnels

	Advantage	Disadvantages
Open Circuit Wind Tunnels	Less construction cost	Flow quality is easily affected from wind or room size
	No purging problem in flow visualization	The tunnel requires more energy (for a given size and speed)
		The open circuit tunnels are more noisy
Closed Circuit wind Tunnel	The quality of the flow can be well controlled and independent of atmosphere	Initial investment is higher
	The tunnel requires less energy (for a given size and speed)	Precautions must be taken if used for flow visualization
	Less noisy	Needs cooling if used extensively

Having open and closed test sections as one pair of edges and open and closed circuit as the other pair of edges, theoretically infinite number of configurations can be designed. There are conventional configurations, which are well known in scientific world. The definitions of the most known wind tunnel types are given in Table 2.

Table 2 Wind tunnel types

Wind tunnel type	Circuit Type	Test Section
Eiffel	Open	Open
NPL	Open	Closed
Göttingen	Closed	Open
Prandtl	Closed	Closed

There are many ways to classify the wind tunnels. Barlow, Rae and Pope[3] define various types wind tunnels and their usage.

1.2.1. Aeronautical Wind Tunnels

Most of the wind tunnels have been designed for aeronautical research. For low speed tunnels, there are other usage areas. For high speed tunnels which are capable of transonic, sonic and supersonic speeds are still being designed and used for aeronautical purposes.

Aeronautical wind tunnels can be classified by their usage as following:

1.2.1.1. High Reynolds Number Wind Tunnels

It is not always possible to use a full scale model and perform experiments with full scale Reynolds numbers in a wind tunnel. Full scale Reynolds numbers are obtained by different methods.

The earliest methods are to use pressurized wind tunnels. Increasing the pressure in wind tunnel by a factor directly increases the Reynolds number with that factor. There are pressurized wind tunnels in USA and England and these can be pressurized up to 20 atmosphere.

Another method is to use a different fluid than air. For same power input, use of Freon 12 can increase the Mach number by a factor of 2.5 and Reynolds number by a factor of 3.6 [3]. Nowadays, fluid, which is named “R-134a”, is used instead of Freon-12 for environmental considerations.

In addition, there are cryogenic wind tunnels that are built to control the Reynolds number. The fluid inside the circuit is cooled by using liquid nitrogen. Such tunnels can be operated at constant dynamic pressure. Reynolds number is controlled by changing the temperature. The cryogenic tunnels can also be used to keep temperature constant and changing the dynamic pressure and Reynolds number similar to pressurized wind tunnels.

1.2.1.2. V/STOL Wind Tunnels

These tunnels are used for experimenting on V/STOL vehicles. These tunnels require larger test sections due to downwash angles generated during transition from vertical flight to horizontal flight. They are in the range of 60 – 100 miles per hour.

1.2.1.3. Free Flight Wind Tunnels

Free flight tunnels are generally open circuit type. In these tunnels, dynamically similar models are flown under the effect of gravity. The tunnels are tilted to match the glide path of the model. The dynamics of the model can also be studied in these tunnels by controlling the control surfaces. Today, free flight wind tunnels are not operational. Since the simulations take place at very low Reynolds numbers, additional care must be considered while projecting the data to high Reynolds numbers.

1.2.1.4. Spin Wind Tunnels

In spin tunnels, the tendency of aircraft to enter spin after a stall recovery is studied. The spin tunnels are examples of vertical wind tunnels. Usually the air is sucked up by a propeller in the open circuit spin tunnels. There are also closed circuit spin tunnels with annular return.

Dynamically similar spinning model is inserted to air stream, the air velocity is adjusted to hold the model at a specified height and the motion of the model is recorded to be analyzed later. There are also spin tunnels that have balances to measure the force over a range of speeds and attitudes.

1.2.1.5. Stability Wind Tunnels

Stability wind tunnels are not very common. In the test section of stability wind tunnels, there are some rotating vanes to investigate the model at different conditions. Also, there are tunnels with curved test sections. In

this tunnel, turning flight can be simulated. There are some techniques to investigate stability in conventional tunnels, i.e. oscillating the model.

1.2.1.6. Propeller Wind Tunnels

The propeller wind tunnels are very similar to conventional wind tunnels. Often they usually have open test section with a circular cross section. The behaviors of propellers, the location of engine nacelles on the wings or the design of engine cowls are investigated in propeller wind tunnels.

1.2.1.7. Propulsion tunnels

The evaluation of aircraft engines are investigated in propulsion wind tunnels. They are generally open circuit type to avoid exhaust generated by the engines. For both jet and reciprocating engines, velocity, atmospheric variation and temperature must be simulated.

1.2.1.8. Icing Wind Tunnels

Icing wind tunnels are generally a variation of conventional wind tunnels with the addition of a refrigeration system. The ice formation on air vehicles are still a serious safety problem in aviation. The water droplets are added to free stream. The air circulating in the tunnel is cooled down to 0°C. There must be good insulation around the tunnel to keep it below 0°C.

1.2.2. Smoke Tunnels

Smoke tunnels are used for flow visualization. They are open circuit type. Video recording and photographs are primary data collection techniques. Smoke sources are generally vaporized light oils, kerosene or propylene glycol and other substances.

Smoke can also be used in many general purpose tunnels but the results are not always as good as specially designed smoke tunnels.

1.2.3. Aero-acoustic Wind Tunnels

The civil aviation authorities are putting more severe restriction on air vehicle generated noise either from engine or air vehicle itself. Also the flow related noise has special importance in military for navy or air forces. There are wind tunnels specially designed to study the noise generated by the air stream flowing on air vehicles. Increasing knowledge in material properties, the technology in measurement devices allow aero-acoustic wind tunnels to be built and used for noise measurement and searching for acoustic treatment for quieter vehicles.

1.2.4. Automobile Wind Tunnels

There are wind tunnels specialized for automobiles all over the world. The basic missions of these wind tunnels are to design the best aerodynamic shape for fuel efficiency, the effect of external flow on the performance of the air conditioning and air circulating system of the vehicle, the behavior of the vehicle in extreme atmospheric conditions like heavy rain snow or long durations that the vehicle is exposed to solar radiation.

Also, the automobile wind tunnels have great importance for car racing teams in Formula-1 or NASCAR organizations. Increasing the performance split second for each lap brings the victory. The earned experience is used for designing more efficient and safe commercial automobiles

1.2.5. Water Tunnels

Water tunnels work as the same principle as low speed wind tunnels. In water tunnels, some effects like cavitation problems can be investigated which is not possible by wind tunnels. Water tunnels are smaller than the wind tunnels for same Reynolds number; however, it has also its own difficulties to work with water as the operating fluid.

1.2.6. General Purpose Wind Tunnels

Although most of the tunnels are built for aviation industry, some tunnels have been used for other areas with minor modifications. Below are the areas how the wind tunnels are used for different applications.

1.2.6.1. People

The wind tunnels are used for increasing the performance of bikers or skiers. The athlete can learn which posture gives him the minimum drag. In addition, ski jumpers can learn to have best lift to drag ratio to glide further.

1.2.6.2. Wind Power Devices

The wind tunnels are also used to simulate the conditions that a wind power device can have during its life cycle. Experiments in the wind tunnel have significant importance for the integrity of the system. Also, the efficiency is worth studying to increase the energy taken for the same size of wind mills.

1.2.6.3. Solar Collectors, Radar Antenna and Satellite Dish

The tests are performed to obtain the loads on the solar collectors. The shapes of the collectors have different aerodynamic pressure distribution in different wind conditions that must be considered during design of the foundation. In addition, elastic movements under the influence of the air flowing around the collector may change the focal point which will decrease the efficiency.

Radar antennas and satellite dishes are also subject to wind tunnel testing for obtaining the data for structural integrity.

1.2.6.4. Bridges

The natural winds flowing over the bridges have great importance. The wind tunnels supply useful information for long span bridges. Even at very

small wind speeds, the aerodynamic excitation can led fatigue crack grew on the beams of the bridge structure. The effects are caused by a phenomenon called vortex shedding. The result of the vortex shedding may be seen as vertical movement or torsional oscillations that can be a very serious problem for the bridges. Also, flutter instability is another problem which must be investigated before the bridge has been built in wind tunnels.

1.2.7. Environmental Wind Tunnels

The environmental tunnels are built for simulating flow near earth's surface. The boundary layer on the earth's surface usually has a thickness between ~300 and ~600 m[3]. The main aim of these tunnels is to study the flow in the vicinity of the buildings, static and dynamic loads on the buildings, soil erosion, air pollution and snow drift. In these tunnels, the flow quality is generally not a concern. The flow is not expected to be smooth and straight. The flow is disturbed to have a non-uniform flow in time and space.

Also for military, it is important to know the threshold pattern for an attack with a chemical or biological agent. These studies are also a subject of environmental wind tunnels. Another subject in environmental wind tunnels is Aeolian vibrations and galloping of power transmission wires. The galloping becomes wild and it must be eliminated during design.

1.2.8. Vertical Wind Tunnels

The main subject of this manuscript is to design a vertical wind tunnel for paratroopers training. There are various vertical wind tunnels that are in use all over the world. Some enterprises have commercial vertical wind tunnels. Any person can fly in these tunnels under the supervision of an experienced trainer. Also, there are some special wind tunnels which are not open to public and used for training of Special Forces paratroopers. It is possible to get information about the vertical wind tunnels in the World

Wide Web, in either the related enterprises' web sites or different associations gathered for free flights.

The vertical wind tunnels are great variety. They can be closed circuit type or they can be open circuit type, and they can have closed flying chamber or open flying chamber.

The propelling of air is performed by aircraft propellers designed or modified for vertical wind tunnels. Also, impellers in ducted fans are the means for propelling the air.

The required power is coming from the diesel engines especially for outdoor vertical wind tunnels and electric motors directly coupled with the ducted impellers. Even some facilities do not have any duct system.

The speed control during the tunnel operation can be obtained by either changing the angular speed of the impeller or changing the stagger angle. The types of control are named as "variable speed control" or "variable pitch control" respectively.

The open circuit type tunnels have limitations from the environmental conditions. It is difficult to operate them for all conditions in winter and summer time. However, for the closed circuit type tunnels the air flowing inside the circuit is independent from the outside conditions. The interaction through the tunnel walls can be controlled or taken into consideration during the design phase of the tunnel.

Any vertical tunnel must be optimized for the power that it uses for its life cycle. Sometimes bearing an initial investment cost could yield low operating costs through the life time of the tunnel. Also the maintenance cost and safety aspects must be taken into consideration when selecting the equipment that will be used.

For the closed circuit tunnels, it is a good idea to exchange some air with the surroundings. This operation will help to keep temperature at a limit a

little above the environment temperature depending on the amount of air exchange. Also, some fresh air will help comforting the paratroopers inside the flying chamber.

The flying chamber of the vertical wind tunnel can be open or closed section. Ideal flying chamber shape is the circular one because of aerodynamic symmetry. However, for the construction point of view, polygonal shapes like hexagonal or octagonal cross sections are preferred.

The vertical wind tunnels can be portable. That is the tunnel parts are easily disassembled and carried to another place than reassembled again. Some tunnels are not portable and they supply comprehensive facilities for users. These tunnels are preferred by professionals and teams who are regularly participating in different competitions.

There are some companies that are building vertical wind tunnels. The most famous of these companies are “Skyventure”, “Bodyflying Association” and “Aerodrome”. In Table 3 some data of vertical wind tunnels of “Skyventure” corporation are given. All the data are given for standard sea level condition, which is defined as 21°C and 75% relative humidity. For all tunnels, the air is driven by vane axial fans directly coupled to an electric motor.

Table 3 Basic Specifications of Commercial Vertical Wind Tunnels

Model	Diameter of Flying Chamber ft	Power Pack Kw	HP	Max. HP	Max Velocity mph	Max Draw Kw/Hr	Peak Demand Kw
10O3-600	10	3x200	600	672	130	462	497
10R2-600	10	3x200	600	672	130	462	497
12O3-750	12	3x250	750	840	134	578	622
12O3-950	12	3x350	950	1064	142	732	787
12O3-1200	12	3x400	1200	1344	154	924	995
12R4-800	12	4x200	800	896	135	616	663
12R4-1000	12	4x250	1000	1120	147	770	829
14O4-1200	14	4x300	1200	1344	135	924	995
14O4-1600	14	4x400	1600	1792	148	1232	1326
14R6-1200	14	4x300	1200	1344	143	924	995
14R6-1400	14	4x350	1400	1568	151	1078	1160
14R6-1600	14	4x400	1600	1792	160	1232	1326

1.3. Axial Flow Fans

Axial fans, blowers and compressors are all equipments that move air. They are differentiated by the method they use for moving air and by the pressure rise they can supply. The American Society of Mechanical Engineers (ASME) uses specific ratio that is the ratio of discharge pressure to suction pressure to classify the air moving equipments. The range of specific pressure is given in Table 4.

Table 4 Difference between fans, blowers and compressors

Equipment	Specific Ratio	Pressure Rise (Pascal)
Fans	< 1.11	< 11108
Blowers	1.11 – 1.20	11108 – 20201
Compressors	> 1.20	> 20201

Axial Flow Fans are the devices that discharge the working fluid parallel to its axis of rotation. The working fluid is generally air and mostly they are operated in the incompressible range. Axial flow fans are generally used in mines, tunnels, underground transportation, all kinds of vehicles and industrial facilities for air conditioning and ventilation purposes in normal and emergency situations.

In an axial flow fan, it is desired to have ideally axial flow that there is no radial velocity component. The pressure rise is supplied by the rotation of the impeller that imposes a tangential velocity component to the flow and the diffusion after the flow passes the impeller.

The system requirements are generally specified by a pressure rise and a corresponding volumetric flow rate. For each volumetric flow rate and pressure loss pair, a specific design must be used to match the requirements of the system.

The types of axial fans can be classified in three groups. They are propeller fans, tube axial fans, vane axial fans. Another application is multi stage axial fans. By use of multistage axial fans, it is possible to have higher pressure rise with the same volumetric flow rate.

1.3.1. Axial Flow Fan Types

1.3.1.1. Propeller Fans

Propeller fans are used for high flow rates with little pressure rise. Generally, they are not combined with extensive ducts or systems that

require high pressure increase. They are considered to be inexpensive because of relatively simple construction. Their maximum efficiency is achieved near free delivery. They are used for rooftop ventilation or as panels mounted on walls of structures. They can generate flow in reverse direction, which is suitable for ventilation applications.

The energy efficiency is low compared with other types of axial flow fans. In addition, they are considered to be noisy. The drive system can be either direct drive that is the motor is directly coupled to impellers or indirect drive that is the mechanical motion is transferred by belt to the hub.

Examples of propeller fan are given in Figure 3 .

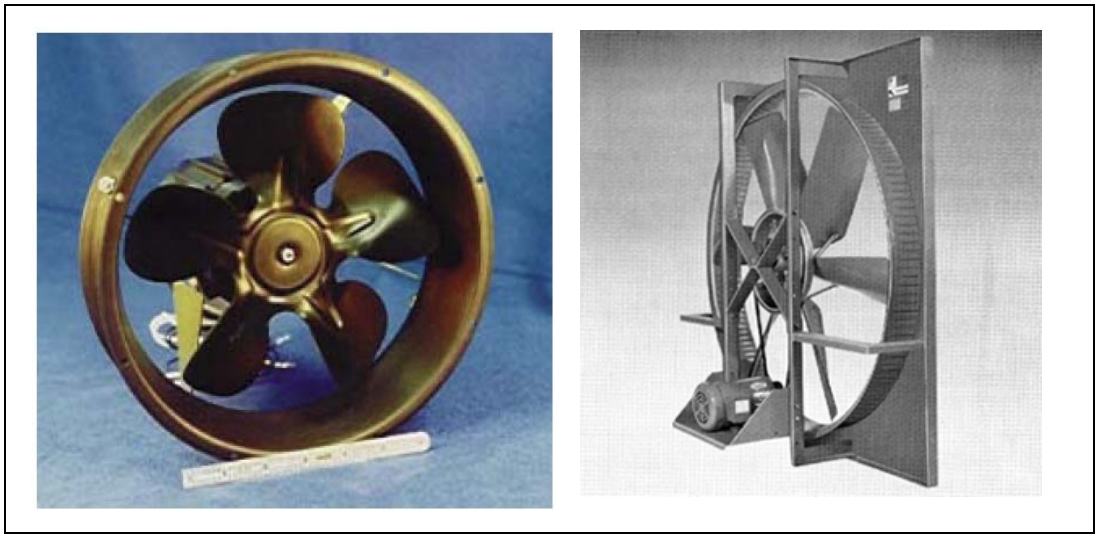

Figure 3 Direct drive and belt driven propeller fan [38]

1.3.1.2. Tube Axial Fans

Tube axial fans are essentially propeller fans placed inside a cylindrical shell, which is about one diameter long generally. Tube axial fans can generate higher pressure rise and operate at better efficiencies than the propeller fans. They are used in ducted HVAC applications. It can generate flow in reverse direction, which is very useful for most ventilation

applications. The hub diameter is about 30% to 50% of the impeller diameter. Tube axial fan performs better when used as exhausting fans.

The motor orientation can be either upstream or downstream of the impeller. Figure 4 and Figure 5 are the examples of belt drive and direct drive of tube axial fans.

The cost of the vane axial fans are more compared to the propeller fans but relatively less noisy. The energy efficiency is about 65%.

Figure 4 Belt driven tube axial fan [41]

Figure 5 Direct drive tube axial fan [38]

1.3.1.3. Vane Axial Fans

A vane axial fan is very similar to a tube axial fan, except it has additional guide vanes to direct the flow into a more suitable path to the impellers or to remove the swirl component of the velocity to have additional gain of static pressure. The hub diameter is 50% to 80% percent of the impeller diameter. Vane axial fans can generate high volumetric flow rates and fairly high static pressure rise compared to the previous axial fan types. The shell is generally one diameter long. In some application, the motor is buried in a tail cone that increases aerodynamic efficiency by a controlled diffusion of the flow. The tolerance between the tip of the impeller blades and the shell has an effect on efficiency. Also using airfoil blades has a positive effect on performance and efficiency. The overall efficiency of well designed vane axial fan can exceed 85%. In Figure 6 and Figure 7, examples of vane axial fan are given.

Figure 6 Belt driven vane axial fan [39]

Figure 7 Direct drive vane axial fan [40]

1.3.2. Axial Flow Fan Performance

Axial fans have typical performance curves. The plot of pressure increase versus the volumetric flow rate gives information about the performance of axial flow fans. The curve generally starts from zero resistance i.e. free delivery. As the resistance increase, the flow rate decrease. In a typical operating range, the axial fan can operate smoothly. But when the operating point falls in the stalling region, the fan is not capable of operating smoothly; any oscillation in the static pressure will have an effect on the blades as oscillating loads and may lead to fatigue. A sample fan performance curve is given in Figure 8.

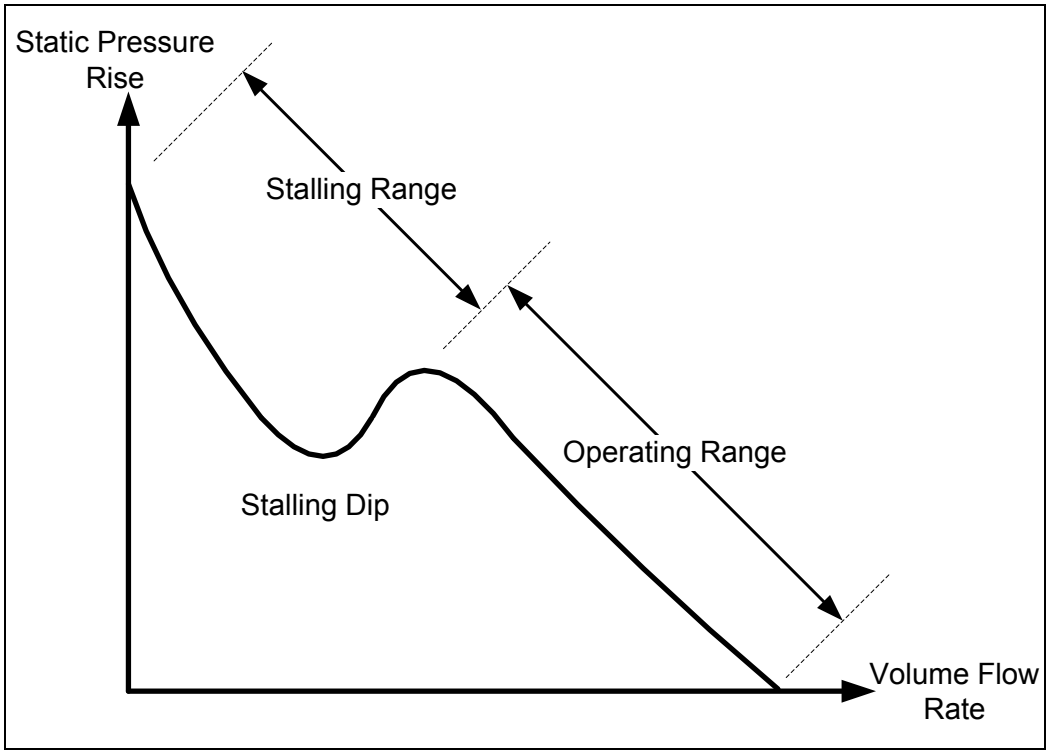

Figure 8 Typical performance curve of axial flow fans [12]

The static pressure rise is the results of increased flow incidence relative to the fan blades. The increase of incidence angle up to a certain point will increase the lift force on the blades. When the stall occurs, the lift on the blades starts to decrease because of the flow separation on the suction side of the blades. In the stall region, some of the energy coming from the blades is used to increase the radial component of the velocity which increases the static pressure, until there is no flow.

In reference [16] the flow behavior on the fan blades are given with respect to a typical axial fan curve.

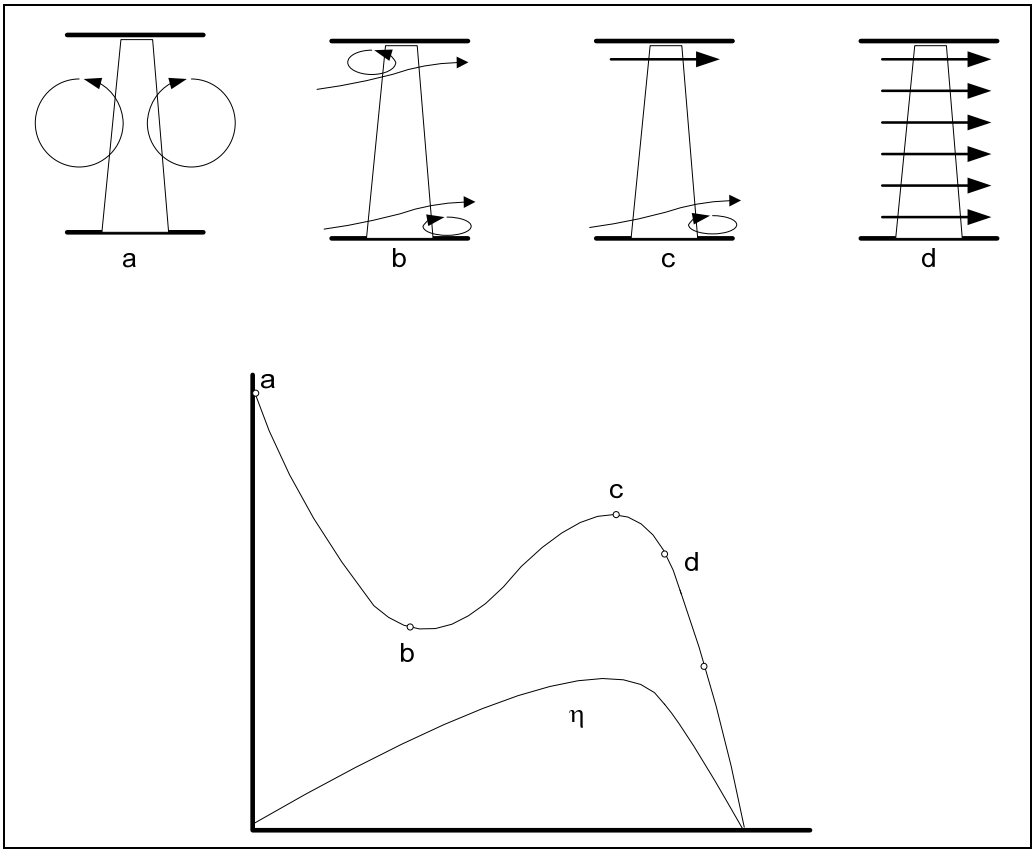

Figure 9 Schematic view of different flow conditions [16]

A flow illustration of different points on fan performance curve is given in Figure 9.

At point “a”, there is no axial flow; all energy is used to increase static pressure as a result of the centrifugal force exerted by the fan blades. At point “b” and “c” of the performance curve, for a given static pressure there is a chance of flow instability, which is a rapid change in the volumetric flow rate. At point “d” and further, the normal operating range of the axial flow fan is obtained.

In fan design, it is customary to keep the peak pressure between 30% and 50% above the normal operating pressure. The design can be considered as safe and fluctuations can be eliminated.

1.4. Fluent CFD Program

For the analysis of the axial flow fan design in this manuscript, FLUENT CFD software is used.

1.4.1. Fluent Program Introduction

FLUENT is a state-of-the-art computer program for modeling fluid flow and heat transfer in complex geometries. FLUENT provides complete mesh flexibility, including the ability to solve flow problems using unstructured meshes that can be generated about complex geometries with relative ease. Supported mesh types include 2D triangular and quadrilateral, 3D tetrahedral, hexahedral, pyramid, wedge, polyhedral and mixed (hybrid) meshes. FLUENT also allows users to refine or coarsen the grid based on the flow solution.

FLUENT is written in the C computer language and makes full use of the flexibility and power offered by the language. Consequently, true dynamic memory allocation, efficient data structures, and flexible solver control are all possible. In addition, FLUENT uses a client/server architecture, which allows it to run as separate simultaneous processes on client desktop workstations and powerful compute servers. This architecture allows for efficient execution, interactive control, and complete flexibility between different types of machines or operating systems.

All functions required to compute a solution and display the results are accessible in FLUENT through an interactive, menu-driven interface.

Additional information can be obtained from the FLUENT user manual and other FLUENT documentation [5].

CHAPTER 2

SUBSONIC WIND TUNNEL DESIGN

In this chapter, the design methodology of a wind tunnel is presented. The design methodology is to use the standard components one after another. Calculating the losses in each component and summing them will allow calculating the total pressure loss of the whole circuit. Then the power required to operate the wind tunnel is calculated. The calculation method can be applied either open circuit wind tunnel or closed circuit wind tunnel using any combination of standard components in any order. The flow conditions in the test section such as velocity, stagnation temperature and pressure and the external atmospheric pressure are required variables [9].

For the rapid solution, there are some restrictions. These restrictions can be stated as follows:

- The cross-sectional geometries are limited to most common known shapes such as circular, rectangular and flat-oval (semi-circular sidewalls with flat floor and ceiling).
- The air exchanges are included in the calculations as standard inlet and exit.
- The derive system is assumed to be located in one or more parallel, annular ducts.

2.1. Wind Tunnel Component Pressure Losses

In this section, necessary formulation to calculate the pressure losses for each component of a wind tunnel and some general concept such as energy ratio is given.

2.1.1. Universal Friction Coefficient

For constant area cross-sections, a relation to wall shear stress can be given such that the pressure loss is entirely balanced by the skin friction force on the walls.

$$L_w \bar{\tau}_w C_w = A_w \Delta p_w \qquad (1)$$

In equation (1), L_w is the length of the component, C_w is the circumference, $\bar{\tau}_w$ is the average wall shear stress, A_w is the cross-sectional area and Δp_w is the pressure drop along the component.

For a circular cross-sectional pipe, the equation of wall shear stress is given [19]:

$$\tau_w = \frac{1}{4} f \left(\frac{1}{2} \rho \bar{V}^2 \right) \qquad (2)$$

In equation (2), $\bar{V}$ is the average velocity at the cross-section ρ is the density, f is the “Darcy friction factor” and τ_w is the wall shear stress which is constant throughout the circumference. The pressure loss through the component is function of wall shear stress. Other than circular cross-section, wall shear stress will vary along the circumference depending on the geometric shape. The dependence will not be considered in the thesis as the range of the geometric shapes suitable for wind tunnels are limited.

For smooth pipes at high Reynolds numbers, “Prandtl universal law of friction” relates Reynolds number and the friction factor [18].

$$\frac{1}{\sqrt{f}} = 2\log_{10}\left(\mathrm{Re}\sqrt{f}\right) - 0.8 \qquad (3)$$

Where

$$\mathrm{Re} = \frac{\rho \bar{V} D_h}{\mu} \qquad (4)$$

In equation (4), D_h is the hydraulic diameter and calculated as $D_h = 2\sqrt{A/\pi}$. Equation (3) can be solved iteratively by Newton-Raphson method.

For general cross section the hydraulic diameter is defined as $D_h = \frac{4A}{S}$ where A is the cross sectional area and S is the wetted perimeter.

For some Reynolds numbers, the friction factor is calculated for pipe diameter equal to 1 meter for sea level standard conditions for density and viscosity. The results are given in Figure 10.

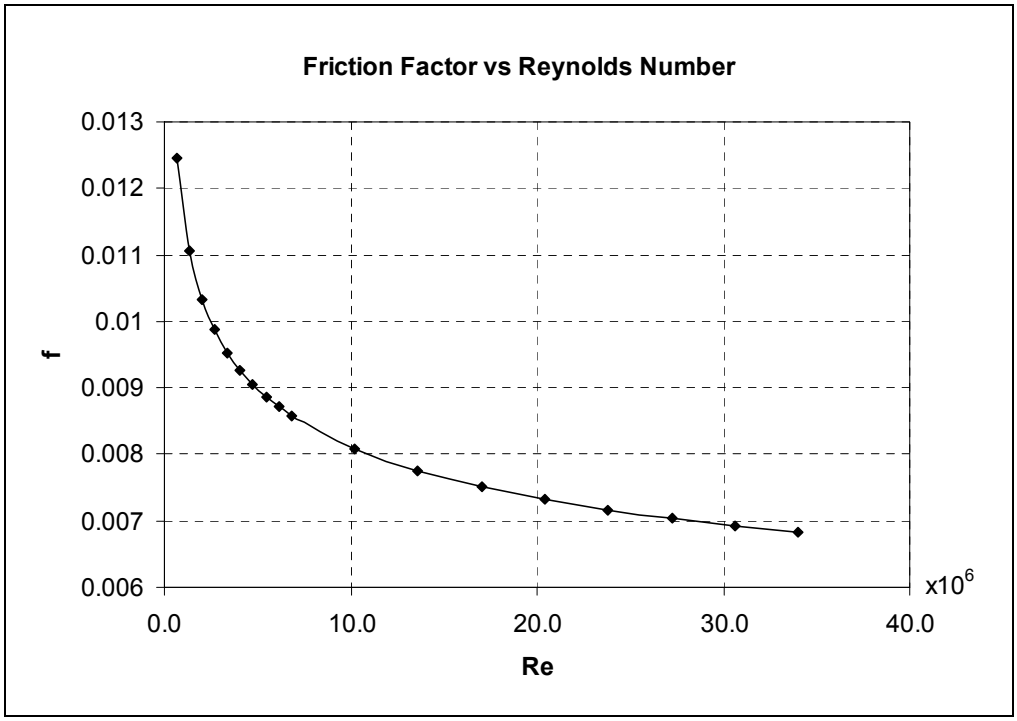

Figure 10 Friction Factor for Smooth Pipe

2.1.2. Energy Ratio and Power Considerations

In a wind tunnel, the ratio of the power in the test section to the rate of flow losses in the circuit are a measure of energy efficiency of the tunnel [3]. Sometimes the denominator can be changed as the electrical power input the motor or the mechanical power input to the shaft of the fan. However, for the aerodynamic point of view it is best to use the test section power, which excludes the effect of the mechanical loss in the fan and electrical loss in the electrical motor. In equation (5), P_t is the jet power in the test section and P_c is the rate of the flow losses in the circuit. P_c is the sum of rate of flow losses for all components of the wind tunnel. It is calculated as the product of the pressure loss ΔH_l and volumetric flow rate Q_l for each component. E_R is the "energy ratio" of the wind tunnel.

"The energy ratio for closed circuit wind tunnels and open circuit wind tunnels other than free-jet facilities are greater than unity." [3]. The energy ratio is changing between 3 and 7 for typical closed jet wind tunnels. The energy ratio for free-jet facility is always less than 1, which is the reason there are not any large size free-jet facilities.

$$E_R = \frac{P_t}{P_c} \tag{5}$$

The jet power is defined as the power of the fluid flowing in the test chamber. It gives an instructive idea about the magnitude of power required for the wind tunnel to operate. The jet power in a wind tunnel can be expressed in terms of density, test section area and test section flow velocity.

$$P_t = \frac{1}{2}\dot{m}_t V_t^2 = \frac{1}{2}\rho_t A_t V_t^3 \tag{6}$$

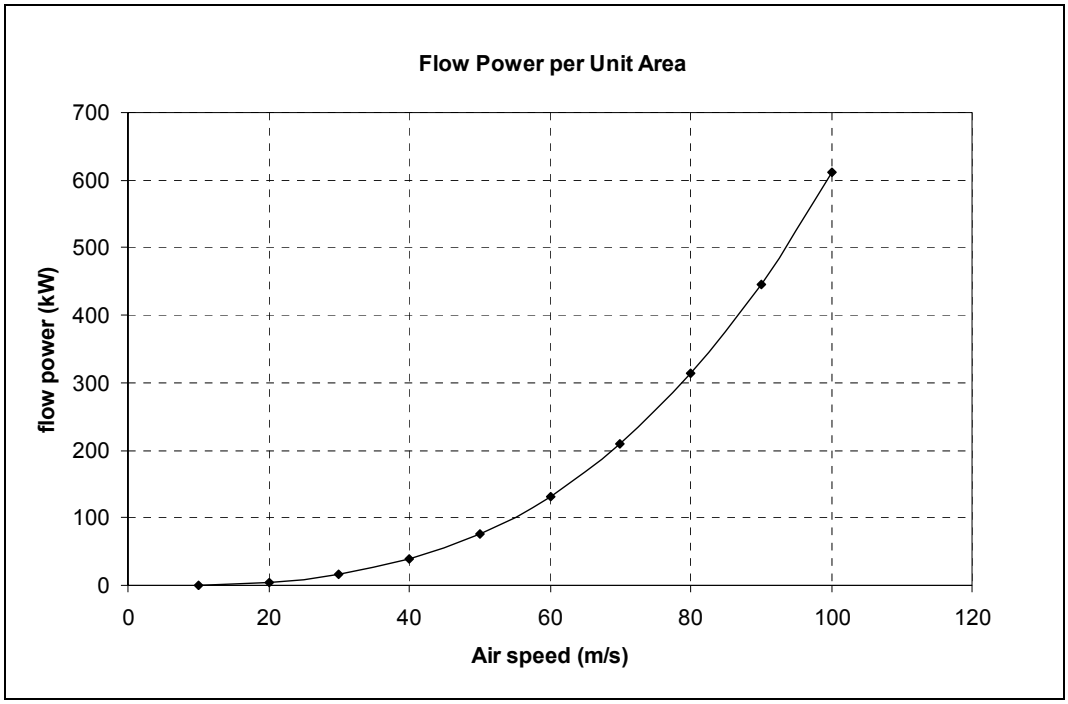

Figure 11 Jet power per unit area at standard conditions

In Figure 11, the jet power per unit area is given as a function of air speed, standard density at sea level. For open and closed return wind tunnel circuits, jet power that is greater than the power source can be sustained by the use of different components like diffusers.

Wattendorf [4] calculated the total loss in closed return wind tunnel by splitting it into components and analyzing the losses in each component [3]. The typical components of wind tunnels can be listed as follows:

- Constant area sections
- Corners
- Expanding sections / diffusers
- Contracting sections
- Straightener section
- Fan / Propeller

Wallis [6] has a similar but extensive approach. Also Eckert at all [9] use the same approach and compare the measured performance of wind tunnels and the calculated performance.

Other than wind tunnel components, there are other equipments that cause energy losses:

- Honeycomb
- Nets and screens
- Model

Except for the fan or propeller, energy loss occurs. The mechanical energy is transformed into heat that rises the temperature of the fluid and the solid materials that are in contact with the fluid. The reason for the transformation of the mechanical energy to the heat energy is the viscous action between the fluid and the boundaries. The term “loss” refers to the transformation of mechanical energy into heat through out the thesis.

The momentum equation for a uniform, incompressible, irrotational, steady flow neglecting the gravity term is given as follows:

$$p_{static} + \frac{1}{2}\rho V^2 = p_{total} = \text{constant} \qquad (7)$$

The equation is called the “Bernoulli” [19] equation and it is valid between two points in a flow if there are no losses between sections. However, in real life there are always losses between the sections.

For upstream and downstream end sections of a constant area component of the wind tunnel, the continuity equation for steady incompressible flow is given as:

$$\bar{V}_1 A_1 = \bar{V}_2 A_2 \qquad (8)$$

A_1 and A_2 are the cross sectional areas and $\bar{V}_1$ and $\bar{V}_2$ are the corresponding average velocities. If A_1 and A_2 is same, then $\bar{V}_1$ and $\bar{V}_2$ are same i.e. the velocity pressure is not changing. Then considering equation (7), the diminution in total pressure is equal to the diminution in static pressure due to the friction loss. The total pressure drop is ΔH.

All of the wind tunnel components can be analyzed successively and the total pressure loss that the fan must overcome can be calculated.

The loss in a section is the mean loss of total pressure. The loss can be expressed in a non-dimensional form which is called the local loss coefficient.

$$K_l = \frac{\Delta H_l}{\frac{1}{2}\rho_l \bar{V}_l^2} = \frac{\Delta H_l}{q_l} \tag{9}$$

In equation (9), K_l is the local loss coefficient; ΔH_l is the total pressure loss; ρ_l is the local density; $\bar{V}_l$ is the local average velocity and q_l is the dynamic pressure.

In the above equation, dynamic pressure and total pressure are measurable quantities. Time rate of energy loss in a section is function of total pressure and volumetric flow rate and can be expressed as follows:

$$\Delta E_l = A_l V_l \Delta H_l = Q_l \Delta H_l \tag{10}$$

Substituting ΔH_l from equation (9) the following relation is obtained. The equation implies that the loss coefficient is the ratio of the total energy loss of the component to the rate of flow kinetic energy in to the section.

$$\Delta E_l = K_l(\frac{1}{2}\dot{m}V_l^2) \tag{11}$$

Applying some mathematical manipulation, the local loss coefficients can be referred to the test section dynamic pressure. Starting with equation (9) the following relationship between the local loss coefficient and local loss referenced to test section dynamic pressure is obtained.

$$K_{lt}q_t = \Delta H_l = K_l q_l \Rightarrow K_{lt} = K_l \frac{q_l}{q_t} \tag{12}$$

Using the above relation equation (11) turns into

$$\Delta E_l = K_{lt}(\frac{1}{2}\dot{m}V_t^2) = K_{lt}P_t \tag{13}$$

Then total rate of loss in the circuit can be calculated using the following relation

$$P_c = \sum_l \Delta E_l = \sum_l K_{lt}P_t \tag{14}$$

Substituting equation (14) into equation (5) the energy ratio of wind tunnel can be expressed as the inverse of sum of the local loss coefficients referenced to test section.

$$E_r = \frac{1}{\sum_l K_{lt}} \tag{15}$$

The loss does not include fan, as the fan must supply the loss energy into the wind tunnel system to have a steady flow.

2.1.3. Constant Area Components

In general, test sections in wind tunnels are constant area sections. Other than the test sections, some wind tunnels have sections with cross sectional area conversion like from circular to some polygonal shape etc.

The test sections area can be circular, square, rectangular, hexagonal, octagonal or elliptical in shape. In theory the options are limitless, however the requirement for the wind tunnels, the object to be tested and construction technology derive the shapes of the test section.

In literature, the pressure loss for constant area pipes is given as follows:

$$\Delta p = \Delta H = \rho f \frac{L}{D_h} \frac{\bar{V}^2}{2} \tag{16}$$

Where Δp is the static pressure drop, ΔH is the total pressure drop f is the friction coefficient, L is the length of the pipe, D_h is the hydraulic diameter, ρ is the density and $\bar{V}$ is the average velocity.

Then the loss coefficient for constant area components is given as follows:

$$K_t = f \frac{L}{D_h} \tag{17}$$

In equation (17), f is the friction coefficient, L is the length of the test section and D_h is the hydraulic diameter.

Depending upon the need, the test section must be designed properly. The test section can be classified as open jet or closed jet.

For closed jet the friction factor f is solved by using the equation (3) and (4). The Reynolds number must be calculated by using the hydraulic diameter of the section. The loss is directly proportional to the length of the test section. Increasing in length will increase the power required to sustain steady flow.

For open jet test sections, it is reasonable to use f=0.008 for the value of the friction factor [3]. Compared to closed jet test sections, open jet test sections require much more power, hence the operational cost will increase. The loss coefficient for open jet test sections is given in equation (18).

$$K_t = 0.0845\frac{L}{D_h} - 0.0053(\frac{L}{D_h})^2 \quad (18)$$

2.1.4. Diffusers

Diffuser is the component of the wind tunnel which reduces the speed by increasing the cross-sectional area. It can be circular, rectangular or polygonal. When it is used just after the test section, the geometry of the cross section may change through out the diffuser.

When diffusers are placed just after the high speed sections, the design must be carefully examined. Any flow separation in the diffuser will affect other components and performance of the wind tunnel. In diffuser design, a parameter called equivalent cone angle is used.

Equivalent cone angle is calculated by using a hypothetical cone, having the same area for inlet and exit of the diffuser. A representative drawing is given in Figure 12.

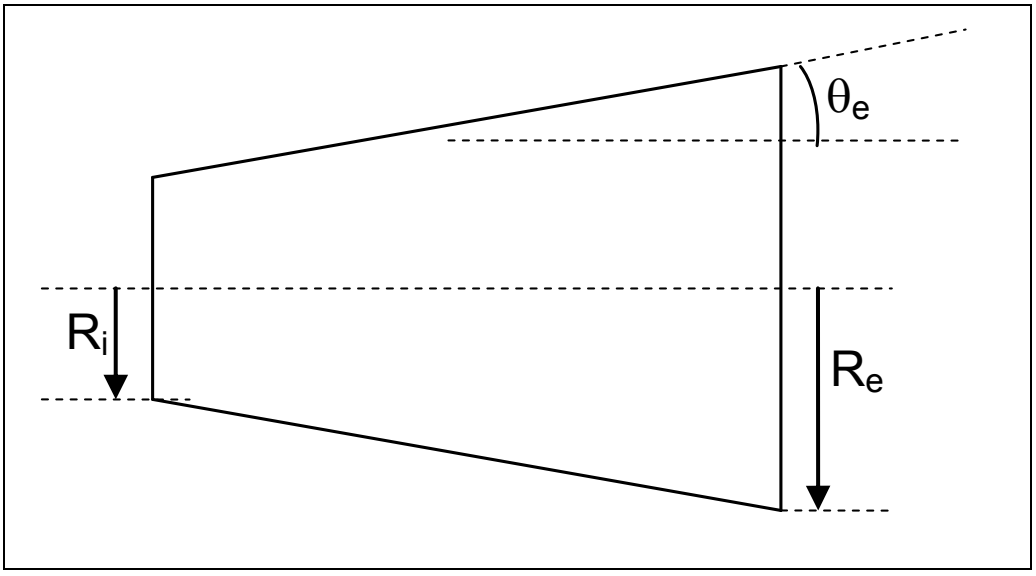

Figure 12 Diffuser geometry and notation

$$\theta_e = \tan^{-1}\left(\frac{\sqrt{A_e/\pi} - \sqrt{A_i/\pi}}{L_d}\right) \tag{19}$$

Equivalent cone angle must be less than some value for the diffuser to operate as designed. When the diffuser has sharp corners, the equivalent cone angle will have 0.5°~1.0° lower limit than for the rounded cross-sections. The equivalent cone angle must be less than 4-5°[9] for diffusers.

In Figure 13, the limits for diffuser design are given. The design must satisfy the given curves not to have separation in the diffuser. The figure also includes diffuser data of various wind tunnels.

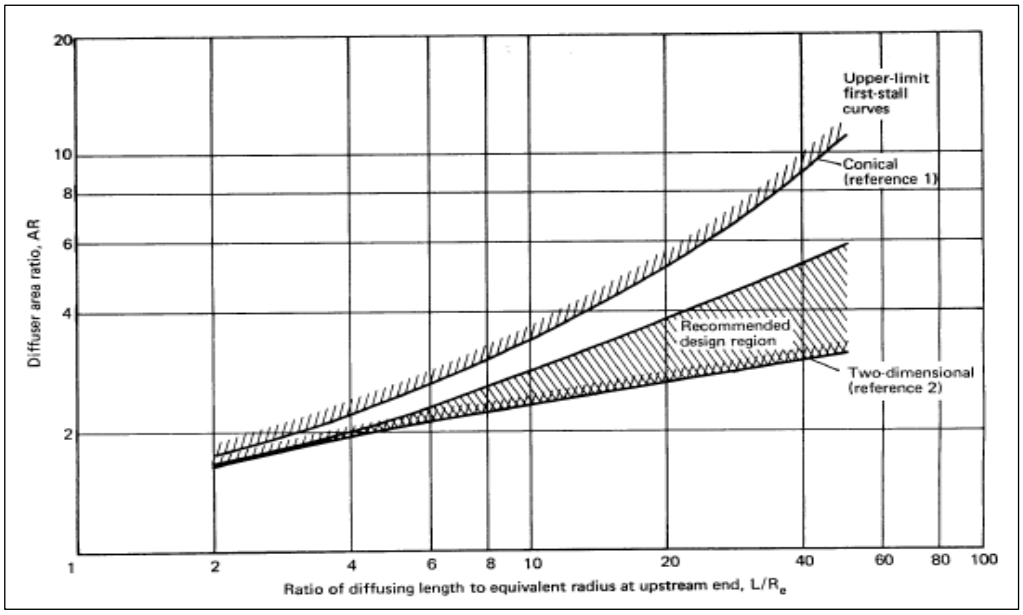

Figure 13 Diffuser design limitations [9]

Eckert W.T., et al [9] compiles formulation to calculate pressure loss coefficients for various types of diffusers as polynomials. The total loss coefficient is sum of friction losses and expansion losses.

$$K_{ld} = K_f + K_{\exp} \tag{20}$$

Where the friction coefficient of the diffuser is calculated as follows:

$$K_f = \left(1 - \frac{1}{AR^2}\right)\frac{f_i}{8\sin(\theta_e)} \tag{21}$$

In above equation, AR is the ratio of the diffuser exit area to the diffuser inlet area, f_i is the friction coefficient of the diffuser inlet and θ_e is the equivalent cone angle.

$$K_{\exp} = K_e\left(2\theta_e\right)\left(\frac{AR-1}{AR}\right)^2 \tag{22}$$

The expansion loss coefficient is calculated by using polynomials that are functions of equivalent cone angle in degrees and the aspect ratio.

For circular cross sections:

$0.0 \le 2\theta_e \le 3.0$

$$K_e(2\theta_e)_{circular} = 0.1033395 - 0.0119465(2\theta_e) \tag{23}$$

$3.0 < 2\theta_e \le 10.0$

$$\begin{aligned} K_e(2\theta_e)_{circular} &= 0.170925 - 0.0584932(2\theta_e) \\ &+ 0.00814936(2\theta_e)^2 + 0.000134777(2\theta_e)^3 \\ &- 0.0000567258(2\theta_e)^4 - 0.000000415879(2\theta_e)^5 \\ &+ 0.000000210219(2\theta_e)^6 \end{aligned} \tag{24}$$

$10.0 \le 2\theta_e$

$$K_e(2\theta_e)_{circular} = -0.0966135 + 0.02336135(2\theta_e) \tag{25}$$

For square cross sections:

$0.0 \le 2\theta_e \le 3.0$

$$K_e(2\theta_e)_{square} = 0.0962274 - 0.00207582(2\theta_e) \tag{26}$$

$$3.0 < 2\theta_e \leq 10.0$$

$$\begin{aligned} K_e(2\theta_e)_{square} &= 0.122156 - 0.022948(2\theta_e) \\ &+ 0.0050704(2\theta_e)^2 - 0.000408644(2\theta_e)^3 \\ &- 0.0000384056(2\theta_e)^4 + 0.00000874969(2\theta_e)^5 \\ &- 0.000000365217(2\theta_e)^6 \end{aligned} \tag{27}$$

$$10.0 \leq 2\theta_e$$

$$K_e(2\theta_e)_{square} = -0.1321685 + 0.0293315(2\theta_e) \tag{28}$$

For 2D rectangular cross sections:

$$0.0 \leq 2\theta_e \leq 3.0$$

$$K_e(2\theta_e)_{2Drectangular} = 0.1 - 0.005333333(2\theta_e) \tag{29}$$

$$3.0 < 2\theta_e \leq 9.0$$

$$\begin{aligned} K_e(2\theta_e)_{2Drectangular} &= 0.323334 - 0.0582939(2\theta_e) \\ &- 0.0497151(2\theta_e)^2 + 0.019909(2\theta_e)^3 \\ &- 0.0019863(2\theta_e)^4 - 0.0000206857(2\theta_e)^5 \\ &+ 0.00000381387(2\theta_e)^6 \end{aligned} \tag{30}$$

$$9.0 < 2\theta_e \leq 10.0$$

$$K_e(2\theta_e)_{2Drectangular} = 5.72853 - 1.21832(2\theta_e) + 0.0708483(2\theta_e)^2 \quad (31)$$

$$10.0 \le 2\theta_e$$

$$K_e(2\theta_e)_{2Drectangular} = -1.36146 + 0.198646(2\theta_e) \quad (32)$$

For some cross sections K_e is not defined. It is assumed combinations of the defined values just for numerical purposes.

$$K_e(2\theta_e)_{2Dcircular} = K_e(2\theta_e)_{2Drectangular}\left(\frac{K_e(2\theta_e)_{circular}}{K_e(2\theta_e)_{square}}\right) \quad (33)$$

$$K_e(2\theta_e)_{2Daverage} = \left(\frac{K_e(2\theta_e)_{2Drectangular} + K_e(2\theta_e)_{2Dcircular}}{2}\right) \quad (34)$$

$$K_e(2\theta_e)_{3Daverage} = \left(\frac{K_e(2\theta_e)_{square} + K_e(2\theta_e)_{circular}}{2}\right) \quad (35)$$

How planar the diffuser is calculated from equation (36). In that equation "h"'s are heights for rectangular shape cross sections and "w"'s are widths of the rectangular cross section. If the cross sections are circular, both "h" and "w" are radii.

$$\delta_s = min\left(\frac{h_2 - h_1}{w_2 - w_1}, \frac{w_2 - w_1}{h_2 - h_1}\right) \quad (36)$$

Then the expansion loss can be expressed as:

$$K_{\exp} = \left(K_e(2\theta_e)\right)_{basic} + (1-\delta_s)\left(\left(K_e(2\theta_e)\right)_{additional} - \left(K_e(2\theta_e)\right)_{basic}\right) \quad (37)$$

Where based on the geometries of each end of diffuser, $K_e(2\theta_e)_{basic}$ is selected among $K_e(2\theta_e)_{circular}$, $K_e(2\theta_e)_{3Daverage}$, $K_e(2\theta_e)_{square}$ and the additional loss factor $K_e(2\theta_e)_{additional}$ can be selected among $K_e(2\theta_e)_{2Dcircular}$, $K_e(2\theta_e)_{2Daverage}$, $K_e(2\theta_e)_{2Drectangular}$.

2.1.5. Contraction Cone / Nozzle

Contraction cone is the section just before the test section in a wind tunnel. The average flow speed can be increased up to 20 times the inlet speed. Typical values for a contraction ratio are in the range 6 – 10. The inlet and exit of the nozzle can have various shapes. Despite its name, it is never a cone in real life. A typical sketch of the contraction cone is given in Figure 14

Nozzles must be designed carefully. Any problem in the design will degrade the quality of the flow in the test section, an increase in power required and increase in acoustic noise. A study of axisymmetric nozzle problems are discussed in reference [22]

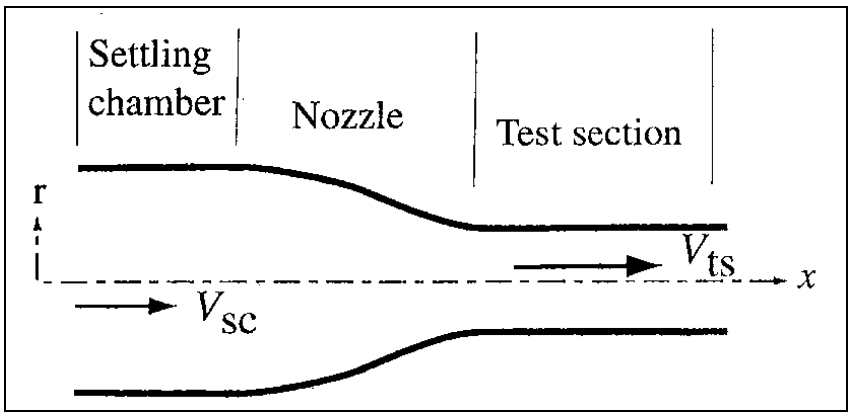

Figure 14 Typical contraction cone / Nozzle [9]

For non-axisymmetric nozzles, there are additional problems. For rectangular cross sections when streamlines cross the edges, secondary flows occur in the corners. This increases the possibility of flow separation. In many tunnels, to avoid the problem a 45° fillet is attached at the inlet section and carried through test section and first diffuser.

For nozzle design, there are many methods given in the literature. The method given in [23] is to define two curvatures in the ‘xy’ plane. The

slopes of both curvatures are same in the axis center. In the connection point, the second derivative changes sign. The ends of both curves are inlet and exit diameter of the nozzle. The Borger curves are given in Figure 15.

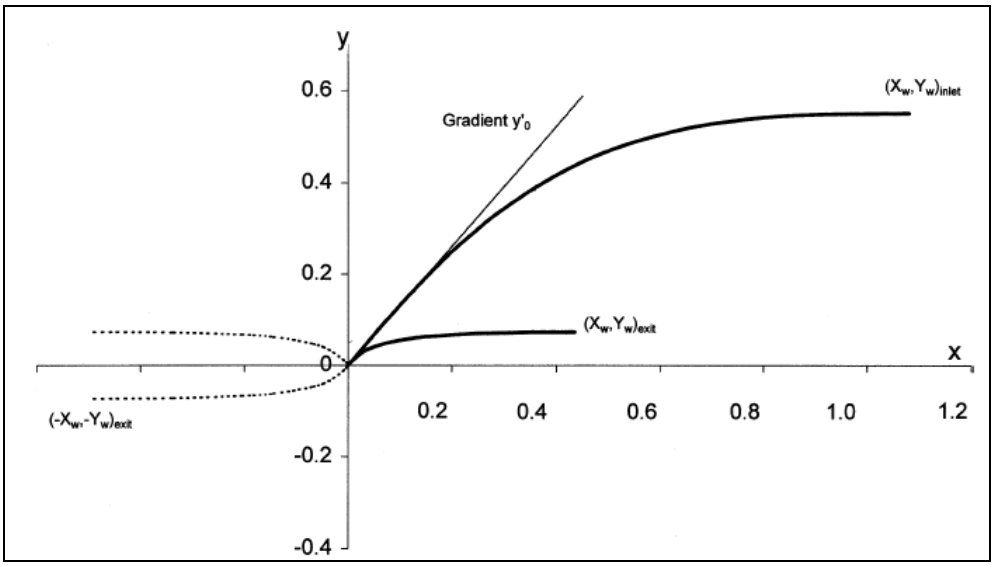

Figure 15 Borger curves for contraction surfaces [23]

If inlet and exit cross sectional area are circular, then the loss for a nozzle is smallest. However, in real life the nozzle shapes are different than circular for various reasons, such as construction difficulties, test section geometry, etc. An approximation can be made such that keeping the area same as circular cross section nozzle. Area change through out the nozzle is also an option if the inlet and exit area of the nozzle must have different shapes.

The total pressure loss coefficient of a typical nozzle is given as follows.

$$K_{nl} = 0.32 f_e \frac{L_n}{D_{he}} \tag{38}$$

Where, f_e is the universal friction coefficient calculated using the exit parameters, L_n is the nozzle length and D_{he} is the hydraulic diameter at the exit.

The nozzle loss is considered very small compared with other components in the wind tunnel. For ease of calculations, equation (38) is used for calculating any nozzle that has different inlet and exit shapes.

2.1.6. Corners & Guide Vanes

In wind tunnels, corners are one of the major pressure loss components. Generally, the cross sectional area does not change through out the corner. To have a straight flow and prevent losses, guide vanes (turning vanes) are installed to the corners. The guide vanes can be bent plates or cambered airfoil like structures. It is important to have mechanical installation provisions to adjust the vanes in the corners. The turning amount of the flow must be correct, not much, not less.

It is possible to minimize the losses in corner selecting efficient cross sectional shapes and optimizing the gap to chord ratio. Using blunt leading edges will give the advantage of being less sensitive to incoming flow than the sharp leading edge airfoils.

The vane camber lines can be designed according to the cascade theory. The flow can be assumed two-dimensional. Several guide vane profiles are experimented and labeled according to their loss coefficients. The experiments and results can be found in references [24], [25], [26], [27]. Typical loss coefficients of some guide vanes are given in Figure 16.

Eckert et al [9], use the below formula to estimate the loss coefficients of constant area corners and guide vanes.

$$K_l = K_{TV}(\phi)\left(\frac{2}{3} + \frac{29.705}{(\log_{10}\mathrm{Re}_V)^{2.58}}\right) + f_i\frac{L}{D_{hi}} \qquad (39)$$

Where $K_{TV}(\phi)$ is a polynomial function of turning angle ϕ, D_{hi} is the hydraulic diameter at the inlet, f_i is friction coefficient due to inlet conditions, and Re_v is the Reynolds number with respect to chord length of the vanes and L is the reference length to calculate the skin friction for corner walls.

$$\mathrm{Re}_V K_l = \frac{\rho V c}{\mu} \tag{40}$$

The function $K_{TV}(\phi)$ is given below and turning angle ϕ is in degrees.

$$0^\circ \le \phi \le 30^\circ$$

$$K_{TV}(\phi) = \begin{matrix} 1.395066\times10^{-2} + 5.672649\times10^{-4}\phi \\ +7.08159\times10^{-5}\phi^2 + 1.394685\times10^{-6}\phi^3 \\ -4.885101\times10^{-8}\phi^4 \end{matrix}$$

$$30^\circ < \phi \le 90^\circ \tag{41}$$

$$K_{TV}(\phi) = \begin{matrix} -1.605670\times10^{-1} + 1.446753\times10^{-2}\phi \\ -2.570748\times10^{-4}\phi^2 + 2.066207\times10^{-6}\phi^3 \\ -6.335764\times10^{-9}\phi^4 \end{matrix}$$

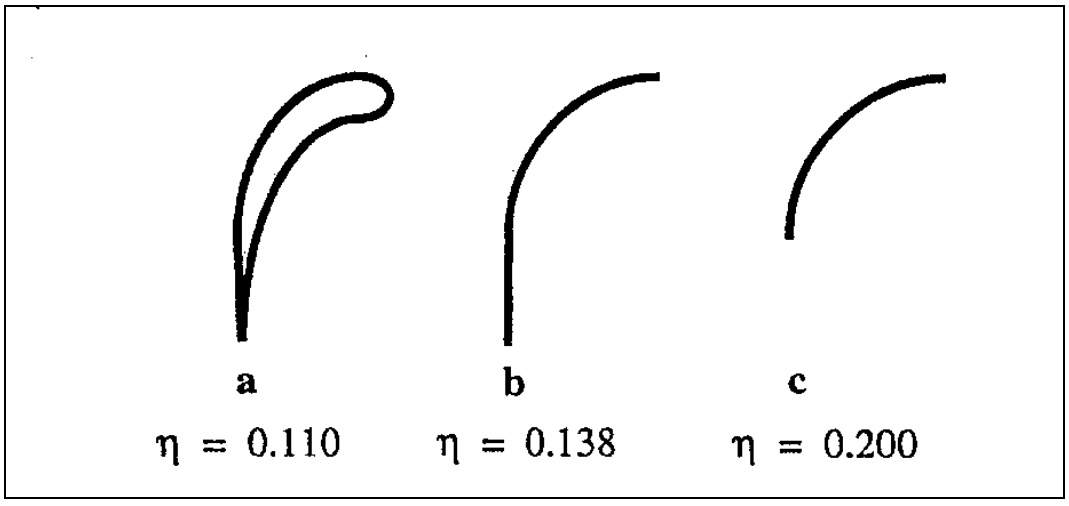

Figure 16 Guide vane profiles [3]

For a 90° turn equation (39) turns into

$$K_{l,\phi=90^\circ} = \left(0.1 + \frac{4.55}{(\log_{10} \mathrm{Re}_V)^{2.58}} \right) + f_i \frac{L}{D_{hi}} \tag{42}$$

For small turns without guide vanes the loss coefficient can be calculated using the following formula.

$$K_l = K_{NV}(\phi) + f_i \frac{L}{D_{hi}} \tag{43}$$

Where the polynomial function $K_{NV}(\phi)$ is given below.

$$K_{NV}(\phi) = \begin{array}{c} 4.313761\times10^{-5} - 6.021515\times10^{-4}\phi \\ +1.693778\times10^{-4}\phi^2 - 2.755078\times10^{-6}\phi^3 \\ +2.323170\times10^{-7}\phi^4 - 3.775568\times10^{-9}\phi^5 \\ +1.796817\times10^{-11}\phi^6 \end{array} \tag{44}$$

2.1.7. Screens and Mesh

There are several factors that screens are used in wind tunnels. One reason can be stated as to protect the fan. The other reason can be stated as to control flow separation in wide angle diffusers. It is also used for turbulence control for flow conditioning at the nozzle entrance.

For the energy aspect, the screens are source of great energy losses. Eckert et al [9], gives the formula for pressure loss coefficient based on three parameters. These parameters are “porosity” β_s and Reynolds number depending on the wire diameter. The two parameters can give the characteristic of a screen. The third parameter is K_{mesh} and it is takes different values for smooth and rough materials. The mesh structure and nomenclature is given in Mesh Structure

In literature another parameter, “screen solidity” σ_s is also defined as:

$$\sigma_s = (1 - \beta_s) \tag{45}$$

As porosity goes to one the screen diminishes and as porosity goes to zero the screen becomes solid.

The local loss coefficient of the mesh is given as:

$$K_l = K_{mesh} K_{Rn} \sigma_s + \frac{\sigma_s^{\,2}}{\beta_s^{\,2}} \tag{46}$$

Where, K_{mesh} is the parameter depending on the material of the mesh. For circular cross section, metal wires it can be selected between 1.0 and 1.3 depending on if it new or used. For textile wires, the factor is used as 2.1 [3].

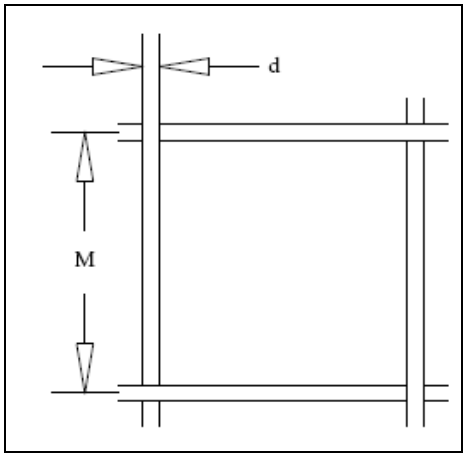

Figure 17 Mesh Structure

The porosity is defined as:

$$\beta_s = \left(1 - \frac{d}{M}\right)^2 \tag{47}$$

The solidity is calculated by using the porosity as given in equation (45).

The Reynolds effect coefficient is given by the following equation.

$$K_{Rn} = \begin{cases} \left[0.785\left(1 - \dfrac{\mathrm{Re}_w}{354}\right) + 1.01 \right] & 0 \le \mathrm{Re}_w \le 400 \\ 1 & 400 \le \mathrm{Re}_w \end{cases} \quad (48)$$

And, Reynolds number referenced to wire diameter is

$$\mathrm{Re}_w = \frac{\rho V d}{\mu} \quad (49)$$

2.1.8. Honeycomb

It is important to have uniform flow in the test section of the wind tunnel. And, how it is obtained is a problem always. Through out the history, many aerodynamicists work on the problem. One of the major solutions is to use honeycombs. Prandtl [28] states that, “a honeycomb is a guiding device through which the individual air filaments are rendered parallel”. Some honeycomb shapes are given in Figure 18.

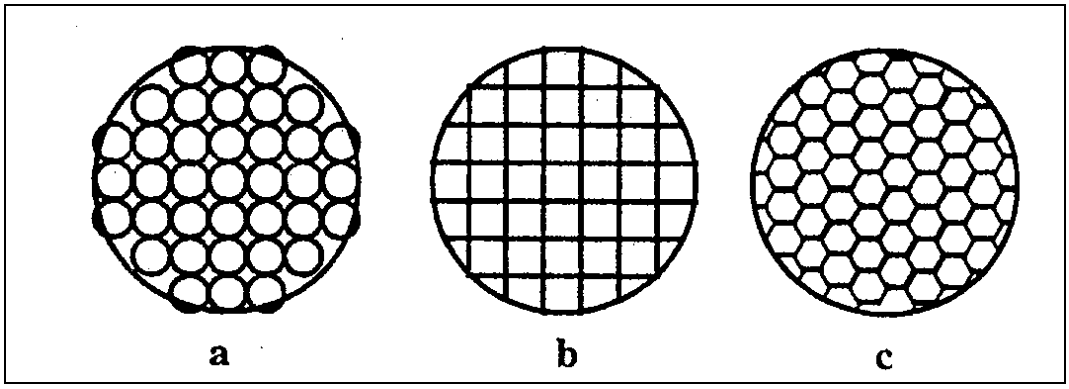

Figure 18 Three types of honeycomb[3]

The parameters to define pressure loss coefficients of honeycombs are the length in flow direction, hydraulic diameter of individual cell and porosity as defined for the screens. Typical values are 6-8 for length to hydraulic diameter ratio and the porosity is in the neighborhood of 0.8.

The formula for pressure loss coefficients of honeycomb is given as:

$$K_{lh} = f_h \left(\frac{L_h}{D_h} \right) \left(\frac{1}{\beta_h} \right) + \left(\frac{1}{\beta_h} - 1 \right)^2 \tag{50}$$

Where the length in flow direction is L_h, the hydraulic diameter of individual cell is D_h, the porosity is β_h and the friction factor is f_h.

For the friction factor, equation (51) is used.

$$f_h = \begin{cases} 0.375 \mathrm{Re}_\Delta^{\,2} \left(\frac{\Delta}{D_h} \right)^{0.4} ; \mathrm{Re}_\Delta \le 275 \\ 0.214 \left(\frac{\Delta}{D_h} \right)^{0.4} ; \mathrm{Re}_\Delta > 275 \end{cases} \tag{51}$$

Re_Δ is the Reynolds number referenced to surface roughness and Δ is the surface roughness of the honeycomb material.

The pressure loss coefficients for the honeycombs given in Figure 18 are 0.30, 0.22 and respectively 0.20.

2.1.9. Model

The models generally have comparably small cross sections with respect to the test section cross area. The blockage effect is calculated by equation (52)[9]:

$$K_l = C_D \frac{S_m}{A_t} \varepsilon \tag{52}$$

C_D is the drag coefficient related to model projection area S_m, A_t is the test section cross sectional area and ε is the downstream influence coefficient.

The equation (52) is considered for models supported by some structure and fixed relative to the test section, however in vertical wind tunnels models are the flying paratroopers who are not fixed but floating.

The force on the floating paratroopers can be expressed as:

$$D = \frac{1}{2}\rho_t V_t^2 C_D S_m \quad (53)$$

The drag force must be equal to weight of the paratrooper.

$$W = D \quad (54)$$

Manipulating the equations (52), (53) and (54), the following relation for the flying paratrooper and pressure loss coefficient is obtained.

$$K_l = \frac{W_P / A_t}{q_t} \quad (55)$$

Where the dynamic pressure of the test section is $q_t = \frac{1}{2}\rho_t V_t^2$.

2.2. Wind Tunnel Layout and Pressure Loss Calculations

In this section, a general layout of a double return closed test section and closed circuit wind tunnel is described. Then the pressure loss coefficients of all components are calculated. The calculations are carried out for a single velocity chosen from Figure 54, Figure 55 and Figure 56.

Then a system operating envelope is drawn from different velocity and flying people configuration. A point that requires maximum operating power is selected as fan design point.

2.2.1. Wind Tunnel Layout

From the basic requirements, it is decided to have a shape, which has an equivalent cross sectional area of a 4 meters diameter circular shape. The basic shape of the flight chamber is chosen as an octagonal shape, which has an area of a 4 meters diameter circle area$12.556 m^2$.

The schematic model of the vertical wind tunnel is shown in Figure 19.

The calculation will start from the flight chamber. It will be performed one by one for all components in the flow direction, sequentially. As an

addition, a loss for air exchange with the surroundings will be calculated and added to the system loss. The maximum air exchange amount will be used as %20 percent of the total volumetric flow rate.

For each section the defined parameters are as follow, inlet (upstream) cross sectional area and shape, exit (down stream) cross sectional area and shape, length, hydraulic diameter for inlet and exit. Then the local friction coefficient for each component is calculated by using the universal friction coefficient.

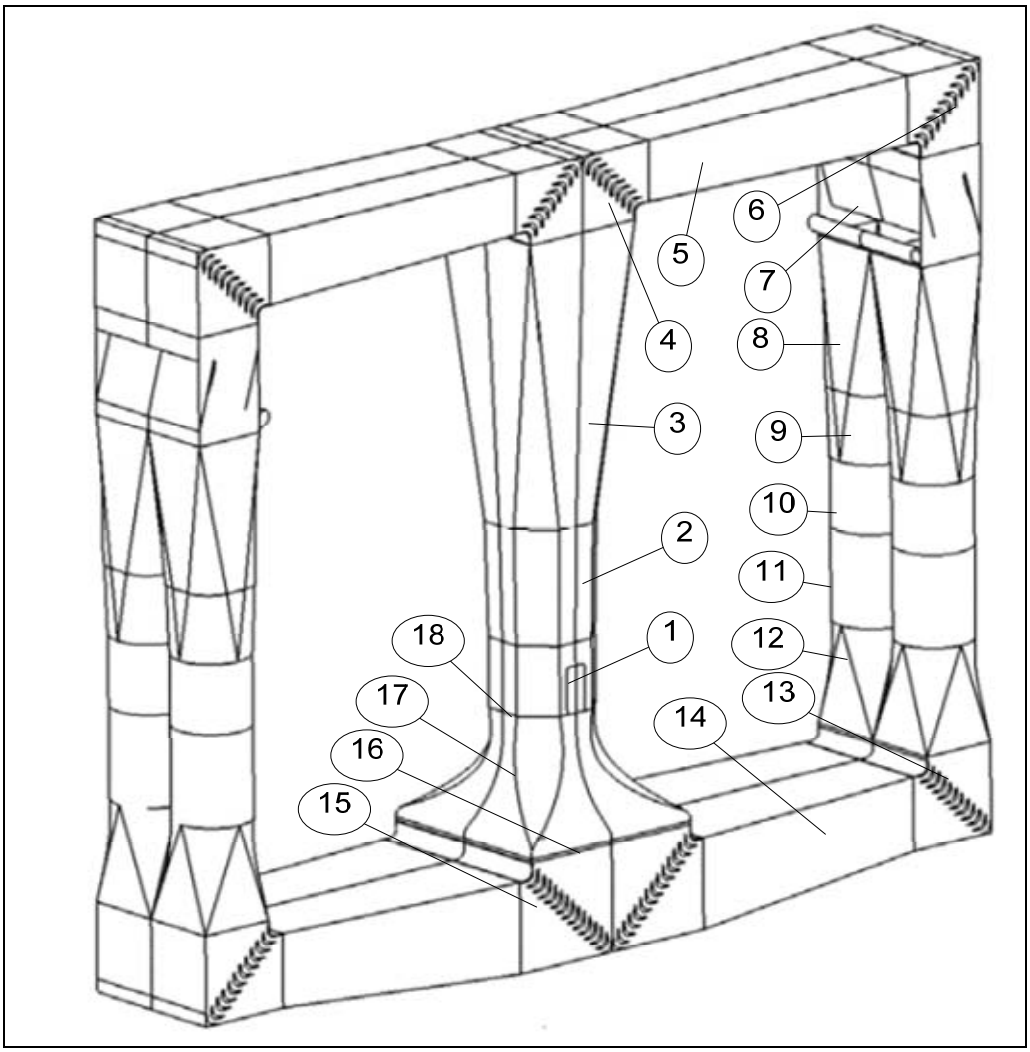

Figure 19 Vertical wind tunnel model

The sections given in Figure 19 are:

1. Flight Chamber
2. Flight Diffuser
3. First Diffuser
4. First Corner
5. Second Diffuser
6. Second Corner
7. Air Exchange Section
8. Fan Collector
9. Fan Inlet Duct
10. Fan
11. Fan Exit Duct
12. Third Diffuser
13. Third Corner
14. Fourth Diffuser
15. Fourth Corner
16. Settling Chamber
17. Contraction Cone
18. Safety Net

The tunnel is double return type and each return is divided into two to avoid interference between axial flow fans. There are four axial fans and they supply necessary volumetric flow rate.

2.2.2. Wind Tunnel Component Pressure Loss Calculations

For each component, the pressure losses are calculated. Then the pressure losses are summed to calculate the total pressure loss. After that energy ratio is used for calculating the power required.

2.2.2.1. Basic Data

The following basic data for the calculations will be used

Velocity of air (average) is $\bar{V}_t = 65.00$ m/s

Dynamic pressure for the flight chamber is $q_t = 2587.81$ pascal.

Density of air is $\rho_t = 1.225$ kg/m³

Volumetric flow rate is $Q = 816.79$ m³/s

Mass flow rate is $\dot{m} = 1000.57$ kg/s

Drag coefficient for human $C_D = 1.00$

Mass of one paratrooper $m = 130.00$ kg

Number of paratroopers flying at the same time is four.

The absolute viscosity at standard conditions is $\mu = 1.79x10^{-5}$ Pa s.

2.2.2.2. Flight Chamber

The flight chamber data and calculated values are given in Table 5. Equation (17) is used for calculating the pressure loss coefficients.

Table 5 Flight chamber pressure loss calculation results

Basic Data	Length (m)	3.00
Inlet	Shape	Octagon
	Area (m²)	12.566
	Wetted perimeter (m)	12.906
	Hydraulic diameter (m)	3.895
	Dynamic pressure (Pa)	2587.81
Exit	Shape	Octagon
	Area (m²)	12.566
	Wetted perimeter (m)	12.906
	Hydraulic diameter (m)	3.895
	Dynamic pressure (Pa)	2587.81
Calculated data	Local loss coefficient	0.005772
	Loss coefficient wrt flight chamber	0.005772
	Pressure loss (Pa)	14.935

2.2.2.3. Flight Diffuser

After the flight chamber, there is a flight diffuser section in the design. This diffuser has a small equivalent cone angle. It can still be used by the trained paratroopers to fly higher and some acrobatic maneuvers in vertical direction. The flight diffuser data and calculated values are given in Table 6. Equation (20) is used for calculating the pressure loss coefficients. The equivalent cone angle is 2.40 degrees.

Table 6 Flight diffuser pressure loss calculation results

Basic Data	Length (m)	5.00
Inlet	Shape	Octagon
	Area (m²)	12.566
	Wetted perimeter (m)	12.906
	Hydraulic diameter (m)	3.895
	Dynamic pressure (Pa)	2587.81
Exit	Shape	Octagon
	Area (m²)	13.920
	Wetted perimeter (m)	13.583
	Hydraulic diameter (m)	4.099
	Dynamic pressure (Pa)	2108.86
Calculated data	Local loss coefficient	0.009042
	Loss coefficient wrt flight chamber	0.009042
	Pressure loss (Pa)	23.398

2.2.2.4. First Diffuser

After the flight diffuser, there is the first diffuser section in the design. This diffuser has relatively large equivalent cone angle. It is main aim is to slow down the velocity before the first corner where the maximum pressure loses occur in wind tunnels. Some professional paratroopers can still fly in the first diffuser if there is enough power in the power section to supply necessary flow rate. The first diffuser data and calculated values are given in Table 7. Equation (20) is used for calculating the pressure loss coefficients. The equivalent cone angle is 7.54 degrees. The cross sectional area is also transformed from octagon to square shape in the first diffuser.

Table 7 First diffuser pressure loss calculation results

Basic Data	Length (m)	12.74
Inlet	Shape	Octagon
	Area (m²)	13.920
	Wetted perimeter (m)	13.583
	Hydraulic diameter (m)	4.099
	Dynamic pressure (Pa)	2108.86
Exit	Shape	Square
	Area (m²)	27.225
	Wetted perimeter (m)	20.871
	Hydraulic diameter (m)	5.218
	Dynamic pressure (Pa)	551.30
Calculated data	Local loss coefficient	0.03509
	Loss coefficient wrt flight chamber	0.028595
	Pressure loss (Pa)	74.000

2.2.2.5. First Corner

After the first diffuser, there is the first corner section in the design. The first corner divides the flow into two half and turns it 90 degrees. The turning vanes are used for rotation. Same turning vanes geometry is used for all corners. For the first corner, eight rows of the turning vanes are used. The first corner is the component generally the maximum pressure loses occur. The first corner data and calculated values are given in Table 8. Equation (39) is used for calculating the pressure loss coefficients. For the friction calculation a characteristic centerline length from the center of inlet to the center of exit areas are used.

Table 8 First corner pressure loss calculation results

Basic Data	Length (m)	3.20
Inlet	Shape	Rectangle
	Area (m²)	13.612
	Wetted perimeter (m)	15.653
	Hydraulic diameter (m)	3.478
	Dynamic pressure (Pa)	551.30
Exit	Shape	Rectangle
	Area (m²)	13.612
	Wetted perimeter (m)	15.653
	Hydraulic diameter (m)	3.478
	Dynamic pressure (Pa)	551.30
Calculated data	Local loss coefficient	0.164526
	Loss coefficient wrt flight chamber	0.03505
	Pressure loss (Pa)	90.70

For turning vanes, the chord length is 0.897 m which is used for calculation of Reynolds number Re_v used in the equations.

The shape of the turning vane given in Figure 20 is constructed as to keep the flow area constant. Also, it is easy to manufacture and inside the shell some materials can be applied to have acoustic treatment. The skin can also be perforated with some small holes to make the material contact with the flowing air. Since empirical methods are used for calculating the pressure loss coefficients. The dimensions of the turning vanes are not given.

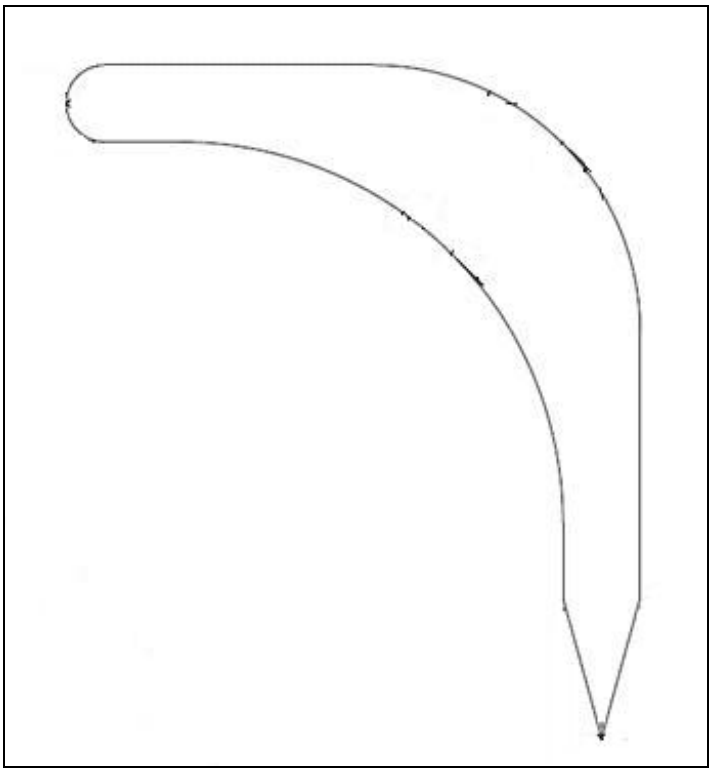

Figure 20 Turning vanes

2.2.2.6. Second Diffuser

After the first corner, there is the second diffuser section in the design. This diffuser has relatively small equivalent cone angle. It is main aim is to slow down the velocity before the second corner. The second diffuser data and calculated values are given in Table 9. Equation (20) is used for calculating the pressure loss coefficients. The equivalent cone angle is 2.83 degrees. There are two second diffuser sections since the wind tunnel is double return type.

Table 9 Second diffuser pressure loss calculation results

Basic Data	Length (m)	12.650
Inlet	Shape	Rectangle
	Area (m²)	13.612
	Wetted perimeter (m)	15.653
	Hydraulic diameter (m)	3.478
	Dynamic pressure (Pa)	551.30
Exit	Shape	Rectangle
	Area (m²)	18.000
	Wetted perimeter (m)	18.000
	Hydraulic diameter (m)	4.00
	Dynamic pressure (Pa)	315.30
Calculated data	Local loss coefficient	0.023846
	Loss coefficient wrt flight chamber	0.00508
	Pressure loss (Pa)	13.15

2.2.2.7. Second Corner

After the second diffuser, there is the second corner section in the design. The second corner turns the flow 90 degrees. The turning vanes are used for rotation. For the second corner, nine rows of the turning vanes are used. The second corner data and calculated values are given in Table 10. Equation (39) is used for calculating the pressure loss coefficients. For the friction calculation a characteristic centerline length from the center of the inlet area to the center of the exit area are used.

For turning vanes, the chord length is 0.897 m which is used for calculation of Reynolds number Re_v used in the equations.

Table 10 Second corner pressure loss calculation results

Basic Data	Length (m)	3.60
Inlet	Shape	Rectangle
	Area (m²)	18.000
	Wetted perimeter (m)	18.000
	Hydraulic diameter (m)	4.00
	Dynamic pressure (Pa)	315.30
Exit	Shape	Rectangle
	Area (m²)	18.000
	Wetted perimeter (m)	18.000
	Hydraulic diameter (m)	4.00
	Dynamic pressure (Pa)	315.30
Calculated data	Local loss coefficient	0.167894
	Loss coefficient wrt flight chamber	0.020456
	Pressure loss (Pa)	52.94

2.2.2.8. Air Exchange Section

There is one air exchange section on every return. There two doors, one is at the inner side and the other is at the outer side. The air is discharged from outer side and fresh air is taken inside from the inner side. For air exchange section, basic data and calculated values are given in Table 11. Since this section is a constant area cross section, equation (17) is used for calculating the pressure loss coefficients.

Table 11 Air exchange section pressure loss calculation results

Basic Data	Length (m)	4.67
Inlet	Shape	Rectangle
	Area (m²)	18.000
	Wetted perimeter (m)	18.000
	Hydraulic diameter (m)	4.00
	Dynamic pressure (Pa)	315.30
Exit	Shape	Rectangle
	Area (m²)	18.000
	Wetted perimeter (m)	18.000
	Hydraulic diameter (m)	4.00
	Dynamic pressure (Pa)	315.30
Calculated data	Local loss coefficient	0.010149
	Loss coefficient wrt flight chamber	0.001237
	Pressure loss (Pa)	3.20

2.2.2.9. Fan Collector

There is one fan collector for each fan used in the design. The flow is split in to two in each return. Also the cross section is changed from circular to square cross section. Also, the area is decreased to the area of one fan for each collector. For fan collector section basic data and calculated values are given in Table 12. Since this section is a constant are cross section, equation (38) is used for calculating the pressure loss coefficients.

Table 12 Fan collector section pressure loss calculation results

Basic Data	Length (m)	9.45
Inlet	Shape	Square
	Area (m²)	9.000
	Wetted perimeter (m)	12.000
	Hydraulic diameter (m)	3.00
	Dynamic pressure (Pa)	315.30
Exit	Shape	Circle
	Area (m²)	7.793
	Wetted perimeter (m)	9.896
	Hydraulic diameter (m)	3.15
	Dynamic pressure (Pa)	420.53
Calculated data	Local loss coefficient	0.008465
	Loss coefficient wrt flight chamber	0.001376
	Pressure loss (Pa)	3.56

2.2.2.10. Fan Inlet Duct

There is one fan inlet duct for each fan. It is a circular cross section, constant area duct and it has the same diameter as fan. It is used for having a smooth and homogeneous flow before the fan. For fan inlet duct section, basic data and calculated values are given in Table 13. Since this section is a constant area cross section, equation (17) is used for calculating the pressure loss coefficients.

Table 13 Fan inlet duct section pressure loss calculation results

Basic Data	Length (m)	3.00
Inlet	Shape	Circle
	Area (m²)	7.793
	Wetted perimeter (m)	9.896
	Hydraulic diameter (m)	3.15
	Dynamic pressure (Pa)	420.53
Exit	Shape	Circle
	Area (m²)	7.793
	Wetted perimeter (m)	9.896
	Hydraulic diameter (m)	3.15
	Dynamic pressure (Pa)	420.53
Calculated data	Local loss coefficient	0.008398
	Loss coefficient wrt flight chamber	0.001365
	Pressure loss (Pa)	3.53

2.2.2.11. Fan Exit Duct

There is one fan exit duct for each fan. It is a circular cross section, constant area duct and it has the same diameter as fan. It is used for having a smooth flow before the fan. For fan exit duct section, basic data and calculated values are given in Table 14. Since this section is a constant area cross section, equation (17) is used for calculating the pressure loss coefficients.

Table 14 Fan exit duct section pressure loss calculation results

Basic Data	Length (m)	1.00
Inlet	Shape	Circle
	Area (m²)	7.793
	Wetted perimeter (m)	9.896
	Hydraulic diameter (m)	3.15
	Dynamic pressure (Pa)	420.53
Exit	Shape	Circle
	Area (m²)	7.793
	Wetted perimeter (m)	9.896
	Hydraulic diameter (m)	3.15
	Dynamic pressure (Pa)	420.53
Calculated data	Local loss coefficient	0.008398
	Loss coefficient wrt flight chamber	0.001365
	Pressure loss (Pa)	1.18

2.2.2.12. Third Diffuser

After the fan exit ducts, there is the third diffuser section in the design. It is main aim is to slow down the velocity before the third corner. The third diffuser data and calculated values are given in Table 15. Equation (20) is used for calculating the pressure loss coefficients. The equivalent cone angle is 5.45 degrees. There are four third diffuser sections since the wind tunnel is a double return type and ducts are divided for each fan. Also, the divided ducts for each fan are combined at the exit of the diffuser.

Table 15 Third diffuser pressure loss calculation results

Basic Data	Length (m)	4.500
Inlet	Shape	Circle
	Area (m²)	7.793
	Wetted perimeter (m)	9.896
	Hydraulic diameter (m)	3.15
	Dynamic pressure (Pa)	420.53
Exit	Shape	Square
	Area (m²)	10.055
	Wetted perimeter (m)	12.684
	Hydraulic diameter (m)	3.171
	Dynamic pressure (Pa)	252.58
Calculated data	Local loss coefficient	0.013378
	Loss coefficient wrt flight chamber	0.002056
	Pressure loss (Pa)	5.32

2.2.2.13. Third Corner

After the third diffuser, there is the third corner section in the design. The third corner turns the flow 90 degrees. The turning vanes are used for rotation. For the third corner, 10 rows of the turning vanes are used. The third corner data and calculated values are given in Table 16. Equation (39) is used for calculating the pressure loss coefficients. For the friction calculation a characteristic centerline length from the center of the inlet area to the center of the exit area are used.

For turning vanes, the chord length is 0.897 m which is used for calculation of Reynolds number Re_v used in the equations.

Table 16 Third corner pressure loss calculation results

Basic Data	Length (m)	3.80
Inlet	Shape	Rectangle
	Area (m²)	20.111
	Wetted perimeter (m)	19.026
	Hydraulic diameter (m)	4.228
	Dynamic pressure (Pa)	252.58
Exit	Shape	Rectangle
	Area (m²)	20.111
	Wetted perimeter (m)	19.026
	Hydraulic diameter (m)	4.228
	Dynamic pressure (Pa)	252.58
Calculated data	Local loss coefficient	0.169366
	Loss coefficient wrt flight chamber	0.0165331
	Pressure loss (Pa)	42.78

2.2.2.14. Fourth Diffuser

After the third corner, there is the fourth diffuser section in the design. It is main aim is to slow down the velocity before the fourth corner and expand the area before the contraction cone. The fourth diffuser data and calculated values are given in Table 17. Equation (20) is used for calculating the pressure loss coefficients. The equivalent cone angle is 6.45 degrees.

Table 17 Fourth diffuser pressure loss calculation results

Basic Data	Length (m)	11.215
Inlet	Shape	Rectangle
	Area (m²)	20.111
	Wetted perimeter (m)	19.026
	Hydraulic diameter (m)	4.228
	Dynamic pressure (Pa)	252.58
Exit	Shape	Rectangle
	Area (m²)	31.415
	Wetted perimeter (m)	23.780
	Hydraulic diameter (m)	5.284
	Dynamic pressure (Pa)	103.51
Calculated data	Local loss coefficient	0.036602
	Loss coefficient wrt flight chamber	0.003572
	Pressure loss (Pa)	9.24

2.2.2.15. Fourth Corner

After the fourth diffuser, there is the fourth corner section in the design. The fourth corner turns the flow 90 degrees. The turning vanes are used for rotation. For the third corner, 13 rows of the turning vanes are used. The fourth corner data and calculated values are given in Table 18. Equation (39) is used for calculating the pressure loss coefficients. For the friction calculation a characteristic centerline length from the center of the inlet area to the center of the exit area are used. The flow is combined after the fourth corner.

For turning vanes, the chord length is 0.897 m which is used for calculation of Reynolds number Re_v used in the equations.

Table 18 Fourth corner pressure loss calculation results

Basic Data	Length (m)	4.60
Inlet	Shape	Rectangle
	Area (m²)	31.415
	Wetted perimeter (m)	23.780
	Hydraulic diameter (m)	5.284
	Dynamic pressure (Pa)	103.51
Exit	Shape	Rectangle
	Area (m²)	31.415
	Wetted perimeter (m)	23.780
	Hydraulic diameter (m)	5.284
	Dynamic pressure (Pa)	103.51
Calculated data	Local loss coefficient	0.175576
	Loss coefficient wrt flight chamber	0.007023
	Pressure loss (Pa)	18.17

2.2.2.16. Settling Chamber

There is settling chamber after the fourth corner in the wind tunnel design. The air is collected just before it enters to the contraction cone. It has a square cross section, constant area duct. For settling chamber, section basic data and calculated values are given in Table 19. Since this section is a constant area cross section, equation (17) is used for calculating the pressure loss coefficients. Since the flow is the slowest in all ducts. The pressure loss is small and for short settling chambers, it can be ignored.

Table 19 Settling chamber section pressure loss calculation results

Basic Data	Length (m)	0.50
Inlet	Shape	Square
	Area (m²)	62.830
	Wetted perimeter (m)	31.706
	Hydraulic diameter (m)	7.927
	Dynamic pressure (Pa)	103.51
Exit	Shape	Square
	Area (m²)	62.830
	Wetted perimeter (m)	31.706
	Hydraulic diameter (m)	7.927
	Dynamic pressure (Pa)	103.51
Calculated data	Local loss coefficient	0.000538
	Loss coefficient wrt flight chamber	0.000022
	Pressure loss (Pa)	0.06

2.2.2.17. Contraction Cone

There is a contraction cone after the fourth corner in the design. The contraction cone is the section where the area is reduced and flow is accelerated to the desired flight chamber velocity. The flow quality and homogeneity in the flight section depends on the design of the contraction cone. The flow quality must be studied by either experimental methods or numerical methods before manufacturing. Also, the cross section is changed from square to octagonal cross section. For contraction cone, basic data and calculated values are given in Table 20. Since this section is a constant are cross section, equation (38) is used for calculating the pressure loss coefficients.

Table 20 Contraction cone section pressure loss calculation results

Basic Data	Length (m)	5.00
Inlet	Shape	Square
	Area (m²)	62.830
	Wetted perimeter (m)	31.706
	Hydraulic diameter (m)	7.927
	Dynamic pressure (Pa)	103.51
Exit	Shape	Octagon
	Area (m²)	12.566
	Wetted perimeter (m)	12.906
	Hydraulic diameter (m)	3.895
	Dynamic pressure (Pa)	2587.81
Calculated data	Local loss coefficient	0.003078
	Loss coefficient wrt flight chamber	0.003078
	Pressure loss (Pa)	7.97

2.2.2.18. Safety Net

There is safety net at the inlet of the flight chamber. The net provides a safety measure and a platform where the trainer can train the paratroopers. Since, the safety net is located at the fastest part of the wind tunnel, the pressure loss across it a considerable amount. The mesh density, the shape of each cell must be designed carefully. The net is composed of steel wires weaved together. The mesh size must be designed to minimize the pressure loss while it must be suitable for paratroopers stand or lay on it. For safety net, basic data and calculated values are given in Table 21. Equation (46) is used for calculating the pressure loss coefficients.

Table 21 Safety net pressure loss calculation results

Basic Data	Cell Shape	Square
	Wire diameter (m)	0.003
	Mesh Size	0.06
	K_{Rn}	1.00
	K_{mesh}	1.3
	Porosity β	0.926
	Solidity σ	0.074
	Dynamic pressure (Pa)	2587.81
Calculated data	Local loss coefficient	0.101983
	Loss coefficient wrt flight chamber	0.101983
	Pressure loss (Pa)	263.91

2.2.2.19. Air Exchange Loss

The air is exchanged with the surroundings at the air exchange sections. Proper doors are can be designed to arrange that some of the air is discharged to surroundings and same amount of fresh air taken in to the tunnel. This process helps to refresh the air circulating inside the tunnel. Another benefit is the temperature rise because of friction can be kept at a certain level above the ambient temperature by adjusting the air exchange amount. Since some energy is discharged with the air discharged and some energy must be spent to accelerate the fresh air joining the tunnel, the amount must be found like a pressure loss. The local pressure loss coefficient for inlet and exit of air is selected as 1.0 [6]. In Table 22 the pressure loss for different amount of air is given.

Table 22 Air exchange pressure loss calculation results

% Air exchange	Local loss coefficient	Loss coefficient (flight chamber)	Pressure loss (Pa)
0.00	1.00	0.000000	0
5.00	1.00	0.006092	15.76493
10.00	1.00	0.012184	31.52985
15.00	1.00	0.018276	47.29478
20.00	1.00	0.024368	63.0597
25.00	1.00	0.030460	78.82463
30.00	1.00	0.036552	94.58955

2.2.2.20. Paratroopers

In scientific wind tunnels, the model cross sectional area is around 5 to 10 percent of the test section area. Mostly, test objects are well designed with relatively low drag. But in the vertical wind tunnel, the test objects are parachutists flying in the flight chamber. The area and drag coefficient of the parachutists are high compared to the test objects in scientific wind tunnels. So the energy required to overcome the energy loss caused by the paratroopers must be calculated.

There are infinitely many combinations of paratroopers having different height and weight can fly in the flight chamber. In this manuscript, four paratroopers having additional equipment weighing 130kg each is used to calculate the pressure loss for the design purposes. Equation (55) is used to calculate the loss coefficient. The data is given in

Table 23 Paratroopers pressure loss

Number of paratroopers	Total Weight	Loss coefficient (flight chamber)	Pressure loss (Pa)
1	130	0.0392166	101.49
2	260	0.0784332	202.97
3	390	0.1176497	304.46
4	520	0.1568663	405.94

2.2.2.21. Total Loss and Power Calculations

The total loss coefficient can be calculated by simply adding the loss coefficients referenced to the flight chamber dynamic pressure. There are many flight configurations depending on the tunnel speed, number of paratroopers in the flight chamber and the amount of air exchange. The

total pressure loss is calculated for four paratroopers with 130kg in weight, flight chamber speed is 65 m/s and 20% air exchange is performed.

Then the total pressure loss of the circuit is 1097.30 Pa. The total pressure loss coefficient is calculated as 0.424025. And by using equation (15), energy ratio is calculated as 2.358. If we consider just the wind tunnel itself, the energy ratio is 7.102 which is a very good number for typical subsonic wind tunnels.

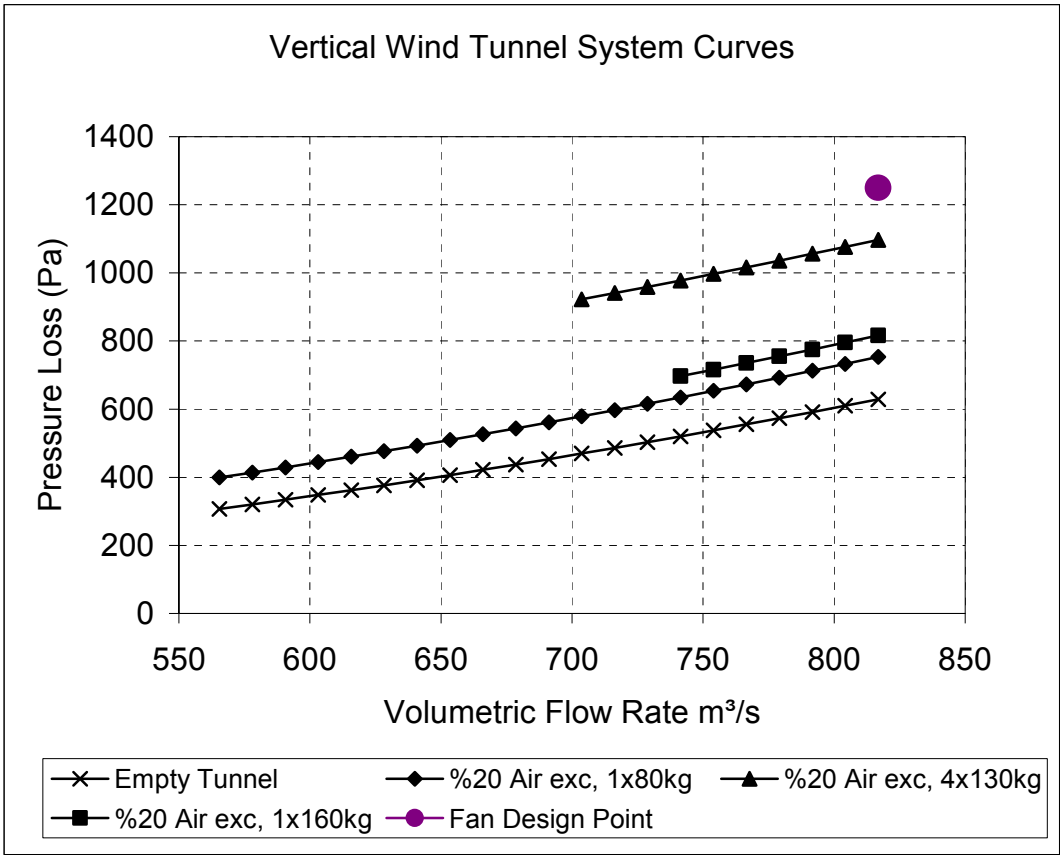

Figure 21 System curves

In Figure 21, some calculated values are used to construct system curves, different number of paratroopers and air exchange configurations are used to calculate the pressure loss coefficients. The values are plotted against the mass flow rate for that given configuration.

It is suggested in references [3]and [6] to add some values to the total pressure loss to compensate some construction errors, leaks and other errors that will be introduced to wind tunnel by time.

For that reason, 1250 Pascal and 816.79 m^3/s values are selected as the design point input for the fan.

The flow power is also calculated as the product of the volumetric flow rate and the total pressure loss. The flow power is 1020987.5 Watts. The motor, which is selected to be used in the fan, must supply that amount of power at the selected RPM.

The required power can also be obtained from the fan design. For preliminary selection it is wise to use 0.8 “total efficiency” and calculate the motor power as around 320 kW per fan.

CHAPTER 3

AXIAL FAN DESIGN

In this chapter of this manuscript, the design approach of the axial fan will be described. Then the data of the fan designed by this approach is given. The design method followed in this manuscript is the method described in reference [6].

3.1. Axial Fan Design Approach

Axial fan design can be considered as designing two dimensional blade sections at various radii. Since the balding is continuous from hub to tip, additional information about the mid blade sections can be interpolated.

The basic equations and assumptions are same for most of the designs but published methods differs in details.. The most important feature of this method is that the design parameters are expressed in terms of two basic velocity ratios.

The swirl coefficient is one of the important velocity ratios. It is given as the ratio of the swirl velocity and the axial velocity at a given radius. The swirl is a measure of rotor torque.

Flow coefficient is another important velocity ratio. It is given as the ratio of the axial velocity and rotational rotor speed at a given radius.

Rotor design is function of swirl coefficient and flow coefficient. Stator design is just the function of the swirl coefficient.

The axial velocity and dynamic pressure based on axial pressure is used to non-dimensionalize static pressures and total pressures.

The task of the fan is generally to produce a pressure rise. If the pressure rise is constant and the axial velocity component is not changing along the radius of the blade, then the flow obeys the free vortex flow. In reality the conditions are not present due to annulus wall boundary layers primarily but the designs using free vortex theory are satisfactory.

A steady, axisymmetric flow without inlet swirl is the necessary condition for the design approach and the flow must be axial and unseparated at the entry of the blade row.

At a given radius, a blade element can be considered as an airfoil. The design approach dictates that the airfoil is a two dimensional airfoil section with an infinitesimal span that is independent of the conditions at other radii. In addition, the flow conditions are steady over the area that is swept by the rotor blades. Both conditions dictate that blade is formed by infinite number of blade sections.

The total pressure rise that can be introduced to the flow by the rotor blades have limit. The total pressure increase is closely related to the lift of the blade sections. The lift of the blade section can be expressed as a function of four parameters. The parameters are, the dynamic pressure based on the relative velocity, the blade chord, the blade camber and the incidence angle. Any increase in any of these parameters increases the total pressure rise across the rotor blade.

The relative velocity can be changed by playing with the boss diameter or tip diameter of the fan or changing the rotational speed of the fan. But there are always limiting factors, such as the necessity to the diffusion of the flow after the fan or the compressibility effects for the flow speeds relative to the blade exceeding 160 m/s. Noise is also another consideration for the increasing rotational speed.

Another parameter called the solidity, which is the ratio of the blade chord to the circumferential gap. Increasing solidity has an affect on the lift curve of the blades. The lift coefficient decreases by the increase of solidity. In addition, the blade loading factor is a limiting parameter and it is function of stagger angle.

Blade camber is another factor affecting the total pressure rise over the fan. But the loading factor must be kept in mind when playing with the blade camber. There are also some disadvantages of excessive camber, such that, increase in noise, dust erosion on the blades and decrease in efficiency.

Increasing blade incidence to have higher pressure rise decreases the margin between the operating point and maximum duty point. Also, the drag coefficient increases as a result of drag polar. The stall may occur on the rotor blades.

Although the rotor is the most important part of the fan, stator blades must be designed appropriately. The swirl imparted by the rotor must be removed by the stators in a rotor-stator unit.

The prerotators are used to deflect the air before entering the blade passage. As the deflection is increased, the static pressure rise across the rotor increases. However, the rotor stalling may limit the amount of air deflection.

Axial flow fans are different compared with the radial fans. The pressure increase in radial fans is through the medium of centrifugal forces. However, in axial flow fans, the pressure increase is attained by the interchange between the dynamic and static pressures. For best efficiency, the diffusion process in the blade cascade and downstream diffuser must be designed carefully. Furthermore, downstream flow must be free of significant swirl.

An optimized rotor, stator, nose fairings, tail fairings and downstream diffuser yield in a high efficiency axial fan. Highest efficiency is obtained by studying the sources of losses separately, in other words loss results from shear, separated and secondary flows must be taken into account.

Secondary flows losses are dependent on blade surface condition, air turning angle, blade solidity, aspect ratio, tip clearance and Reynolds number.

In literature, Howell [32] and Carter [33] have studies with limited success using an analogy of the induced drag of an aircraft wing for compressor blades. The same relations are used for the axial fans since no further data is available.

The loss generated by the nose and tail fairings for the well designed fans does not compromise the design. If the flow does not have swirl and steady, it is very easy to calculate the losses.

The design theory is derived for prerotator, rotor and stator units in reference [6]. In this manuscript only the rotor, stator unit will be considered. The theory is based on the free vortex flow through the rotor and stator.

The total pressure rise and the volumetric flow rate can be converted into nondimensional quantities if the fan and boss diameter is known. It is possible to estimate the fan diameter and boss diameter using a parameter called specific speed.

$$n_s = nQ^{\frac{1}{2}} \left(\Delta H\right)^{\frac{-3}{4}}$$

Where n is the fan rotational speed, Q is the volumetric flow rate and ΔH is the total pressure rise across the fan.

3.1.1. General Momentum Equations

The total pressure rise across the fan unit can be related to the cascade airfoil data that can also be related to general momentum equations. Then the parameters can be defined as functions of velocities defining the flow at each section. In Figure 22, a schematic representation of cascade flow is given. The control volume is enclosed by the inlet and exit of the blade row and the two streamlines with a distance s between them.

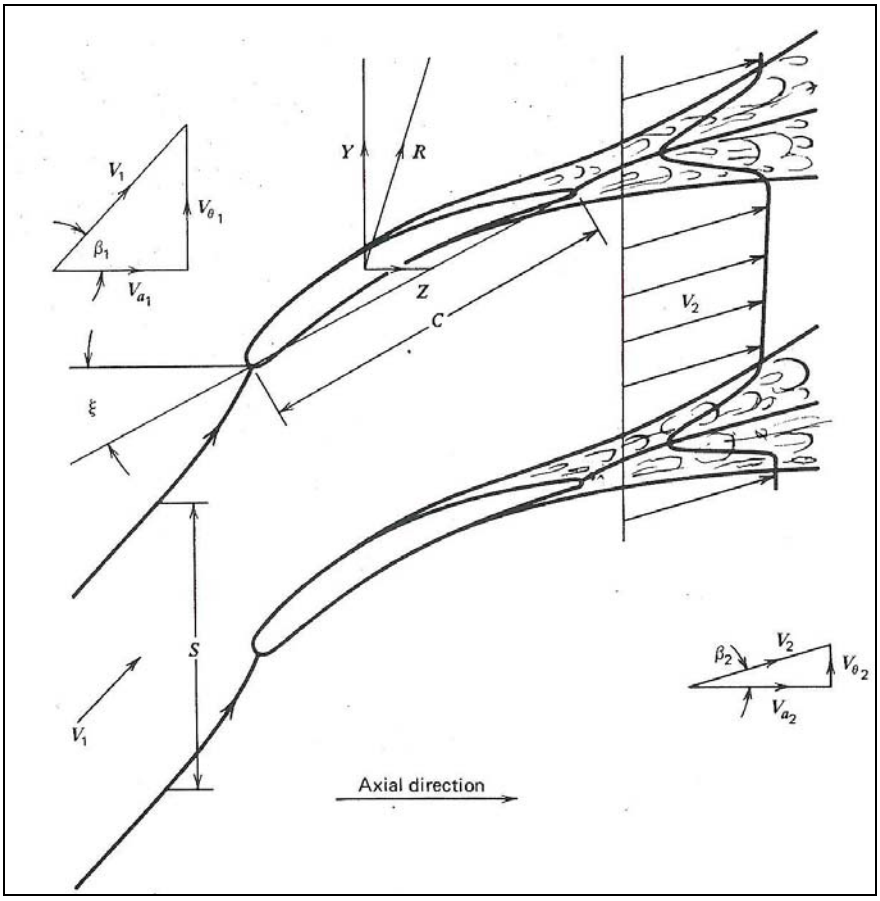

Figure 22 Cascade flow[6]

The general momentum equation can be written in Z and Y direction as follows:

$$Z = \left[\rho s dr V_{a1}^2 - \int_0^s \rho dr V_{a2}^2 dy \right] + \left[p_1 s dr - \int_0^s p_2 dr dy \right] \quad (56)$$

$$Y = \rho s dr V_{a1} V_{\theta 1} - \int_0^s \rho dr V_{a2} V_{\theta 2} dy + E \quad (57)$$

Z and Y are the forces acting on the blade element of length dr for constant inlet velocity. E in equation (57) is the shear stress term due to wake flow shown in Figure 22.

The equations are simplified assuming E is negligible, axial velocity component is constant, pressures at inlet and exit planes does not change in Y direction.

$$Z = \left(p_2 - p_1 \right) s dr \quad (58)$$

$$Y = \rho s V_a \left(V_{\theta 1} - V_{\theta 2} \right) dr \quad (59)$$

The theoretical pressure rise can be expressed as follows:

$$\Delta p_{th} = p_2 - p_1 + \bar{w} \quad (60)$$

In equation (60) $\bar{w}$ is the mean total pressure loss due to the presence of wake.

Conditions in an annulus radius r and width dr shown in Figure 23 are given at various stations. The blading arrangement is given for the most general single stage axial fan. The flow is deflected tangentially by the prerotators in opposite direction of rotor rotation. The air leaves the rotor section with a swirl component and then the swirl component is removed by the help of stators.

Free vortex flow assumption is valid. That is the axial velocity component is constant throughout the fan. There is no radial velocity component and the pressure rise is constant in radial direction.

If any component is missing in the fan design, that is if prerotators are not exist. The equations are simplified simply setting the related terms to zero.

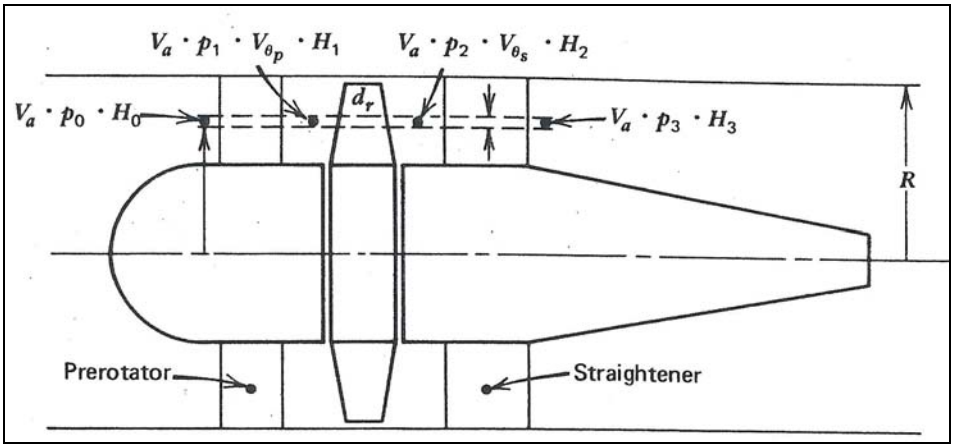

Figure 23 General blading arrangement [6]

The total pressure equations are written as follows for the stations shown in Figure 23:

$$H_0 = p_0 + \frac{1}{2}\rho V_a^2 \tag{61}$$

$$H_1 = p_1 + \frac{1}{2}\rho V_a^2 + \frac{1}{2}\rho V_{\theta p}^2 \tag{62}$$

$$H_2 = p_2 + \frac{1}{2}\rho V_a^2 + \frac{1}{2}\rho V_{\theta s}^2 \tag{63}$$

$$H_3 = p_3 + \frac{1}{2}\rho V_a^2 \tag{64}$$

The total pressure change across the fan can be written as the difference between station three and station zero.

$$H_3 - H_0 = \Delta H_{th} - \Delta h_R - \Delta h_p - \Delta h_s \tag{65}$$

In equation (65) ΔH_{th} is the theoretical pressure rise, other terms are the losses coming from the prerotator, rotor and stators. The equation can be

written in nondimensional form by using the dynamic pressure based on the axial flow.

$$\frac{H_3 - H_0}{\frac{1}{2}\rho V_a^2} = K_{th} - k_R - k_p - k_s \tag{66}$$

Defining the swirl coefficient $\varepsilon = \frac{V_\theta}{V_a}$ and flow coefficient $\lambda = \frac{V_a}{\Omega r}$, theoretical pressure rise coefficient can be expressed as:

$$K_{th} = \frac{2}{\lambda}\left(\varepsilon_p + \varepsilon_s\right) \tag{67}$$

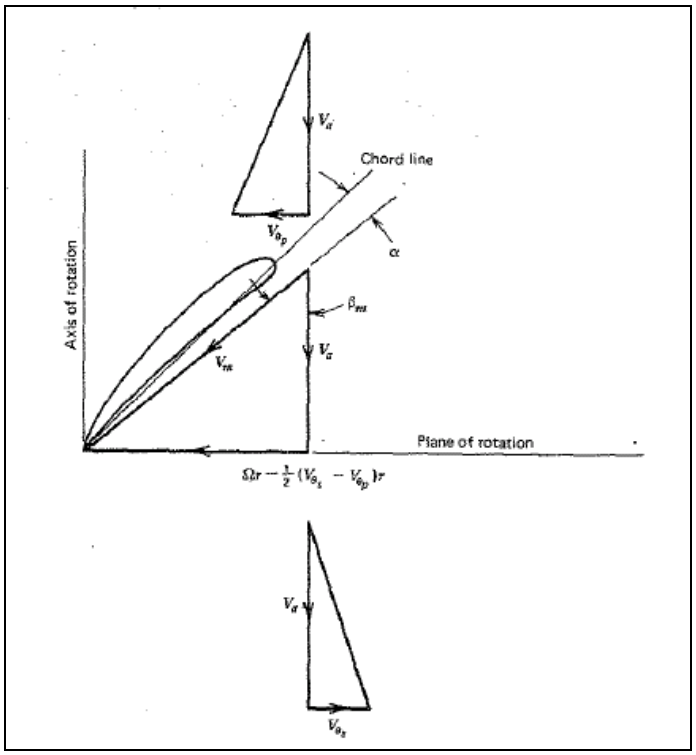

Figure 24 Relative velocity vectors [6]

The flow over the rotor blades can be represented by either absolute velocities or relative velocities. The schematics of velocity vectors for relative and absolute velocities are given in Figure 24 and Figure 25 respectively.

The angle β_m, between the mean velocity vector and plane of rotation is given as:

$$\beta_m = atan\left(\frac{1-\frac{1}{2}\left(\varepsilon_s-\varepsilon_p\right)\lambda}{\lambda}\right) \tag{68}$$

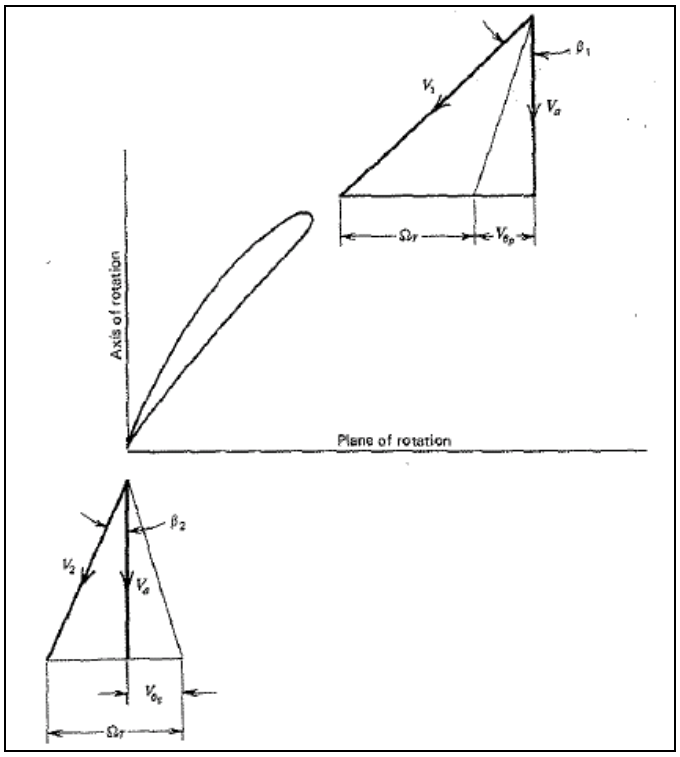

Figure 25 Absolute velocity vectors [6]

The blade lift and drag coefficients are related by equation (69).

$$C_L\sigma = 2\left(\varepsilon_s + \varepsilon_p\right)\cos\beta_m - \sigma C_D \sin\beta_m \tag{69}$$

The blade loss can be calculated from the following formula:

$$C_D = \frac{s}{c} k_r \cos^3\beta_m \tag{70}$$

The solidity $\sigma = \frac{c}{s}$ is defined as the ratio of the chord length and length between blades.

The drag coefficient for F series airfoils can be calculated by using the chart given in Figure 26 and equation

$$C_{Ds} = 0.018 C_L^2 \tag{71}$$

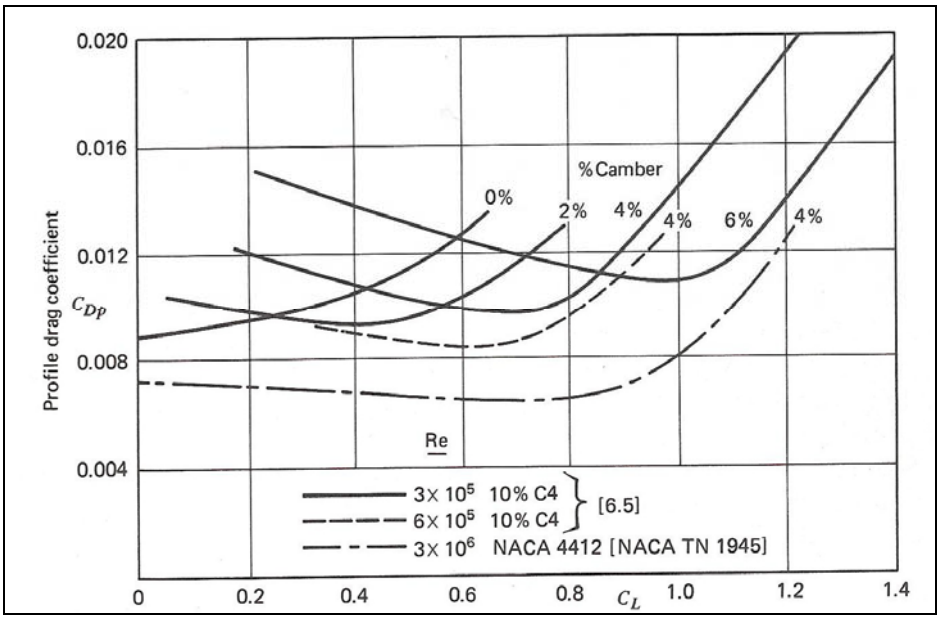

Figure 26 Profile drag vs lift coefficient for F series airfoil [6]

The absolute inlet and outlet angles for the blades as functions of swirl and flow coefficients are given as follows:

$$tan\beta_1 = \frac{1+\varepsilon_p\lambda}{\lambda} \tag{72}$$

$$tan\beta_2 = \frac{1-\varepsilon_s\lambda}{\lambda} \tag{73}$$

$$tan\beta_1 - tan\beta_2 = \varepsilon_s + \varepsilon_s \tag{74}$$

$$tan\beta_m = \frac{1}{2}\left(tan\beta_1 + tan\beta_2\right) \tag{75}$$

The thrust and torque exerted on the flow by the rotor blades can be calculated by using the following equations:

$$Th = Th_c\left(\frac{1}{2}\rho V_a^2 \pi r_{tip}^2\right) \tag{76}$$

$$dTh_c = \frac{\Delta p}{\frac{1}{2}\rho V_a^2} 2xdx \tag{77}$$

$$\frac{dTh_c}{dx} = 2x\left(K_{th} - k_r + \varepsilon_p^2 - \varepsilon_s^2\right) \tag{78}$$

$$T = T_c\left(\frac{1}{2}\rho V_a^2 \pi r_{tip}^3\right) \tag{79}$$

$$\frac{dT_c}{dx} = 4x^2\left(\varepsilon_p + \varepsilon_s\right) \tag{80}$$

The total drag coefficient is defined as:

$$C_D = C_{Dp} + C_{Ds} \tag{81}$$

3.1.2. Rotor Blade Design

For the rotor blade design, there are some important factors. For each blade section, through hub to tip, these factors must be calculated. Also some empirical curves are used to obtain the relevant blade parameters. The geometric details of rotor blade are given in Figure 27.

The formulae and curves are given in this section. Figure 28 shows the deviation angle coefficient relation with the stagger angle.

Then the deviation angle is calculated using the following relation:

$$\delta = m\theta\sqrt{\frac{s}{c}} \tag{82}$$

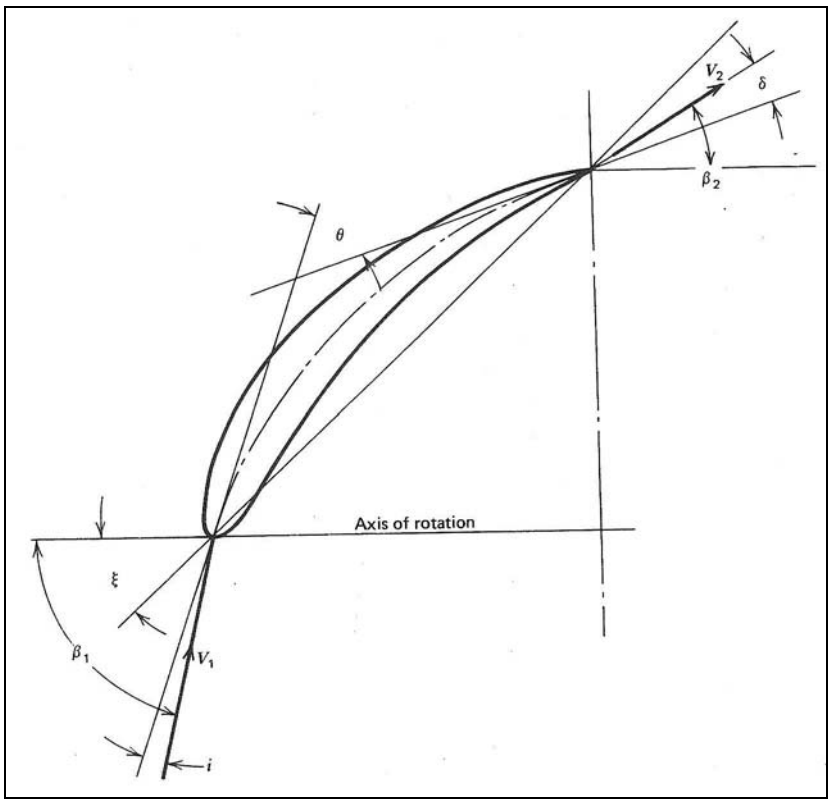

Figure 27 Rotor blade element geometry [6]

In equation (82), m is obtained from Figure 28 and iterative solution developed using the following equations:

$$\theta = \frac{(\beta_1 - \beta_2) - i}{1 - m\sqrt{\frac{s}{c}}} \tag{83}$$

and

$$\xi = (\beta_1 - i) - \frac{\theta}{2} \tag{84}$$

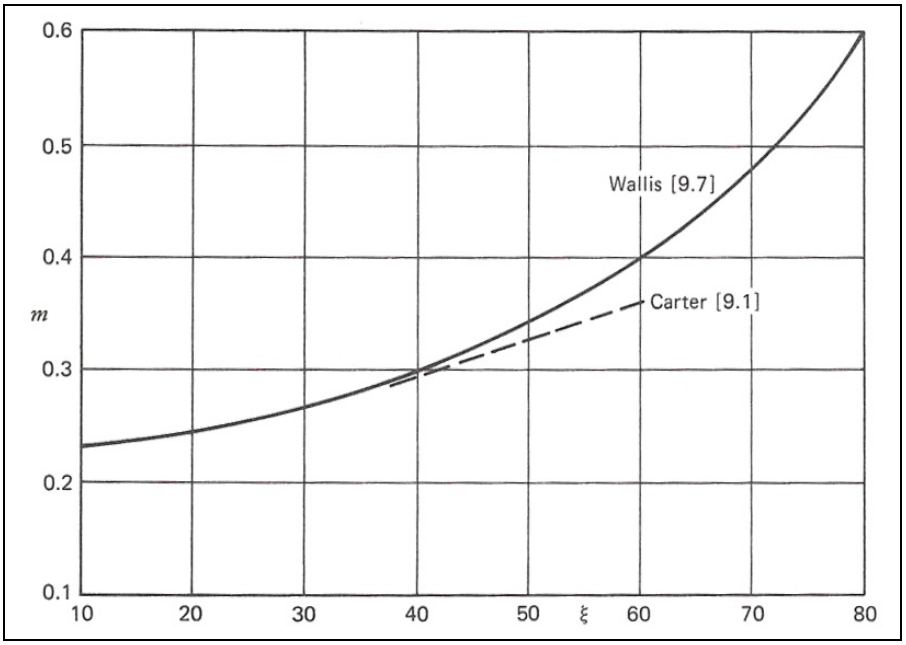

Figure 28 Deviation angle coefficient vs. stagger angle [6]

The rotor loss expression can be calculated for each blade element but it is generally calculation at the mid span section is enough. The loss is obtained from equation (85)

$$\frac{k_R}{K_{th}} = \left(\frac{\lambda}{\frac{C_L}{C_D} \cos^2 \beta_m} \right)_{MS} \tag{85}$$

3.1.3. Stator Design

Stators are designed in a very similar way to the rotors except they are stationary. Generally, local incidence is set to zero for the stator design. The schematic view of stator vane element is given in Figure 29.

$$\beta_m = atan\left(\frac{\varepsilon_s}{2}\right) \tag{86}$$

The following equations are used to obtain stator blade data having F series airfoil section:

$$\theta = \beta_1 + \delta \tag{87}$$

$$\xi = \beta_1 - \frac{\theta}{2} \tag{88}$$

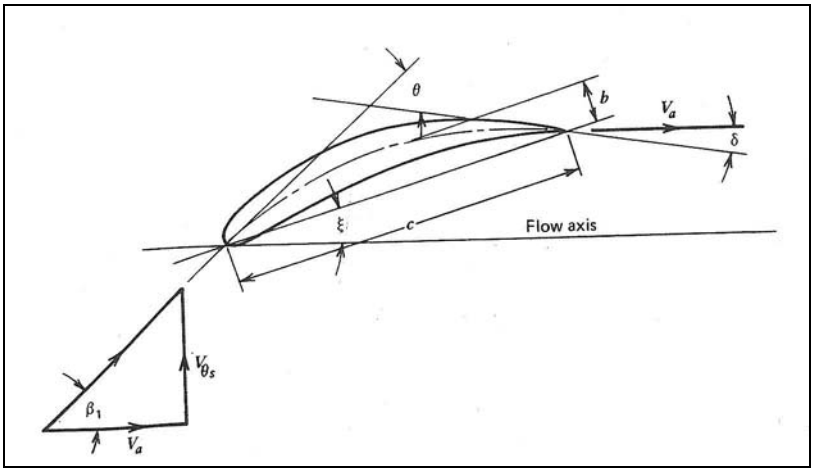

Figure 29 Stator vane element geometry [6]

The loss of the stator section is calculated in a similar manner as in rotor loss calculation. The equation is given as:

$$\frac{k_S}{K_{th}} = \left(\frac{\lambda}{\frac{C_L}{C_D}\cos^2\beta_m}\right)_{MS} \tag{89}$$

Stator vanes design data can be obtained from the Figure 30and Figure 31. Starting with the swirl coefficient, σ and C_L data is obtained. After that, camber angle θ and stagger angle ξ is obtained.

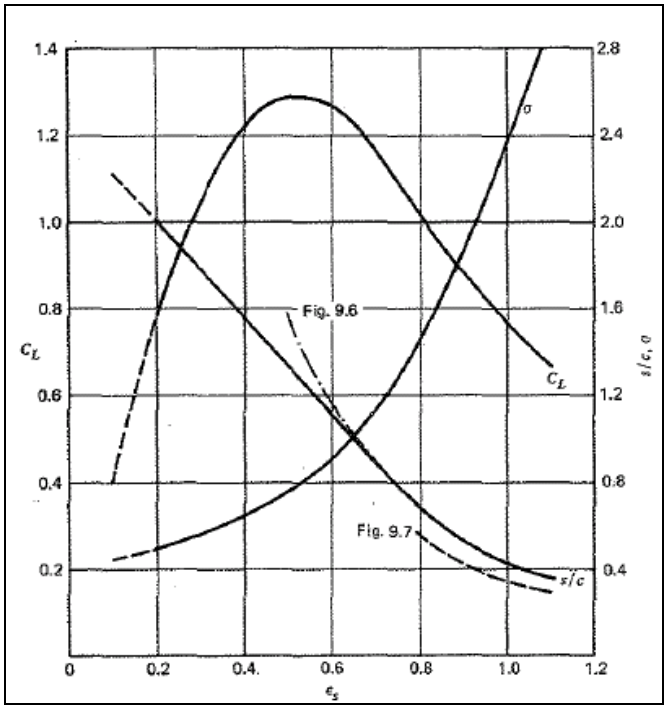

Figure 30 Stator vane design data [6]

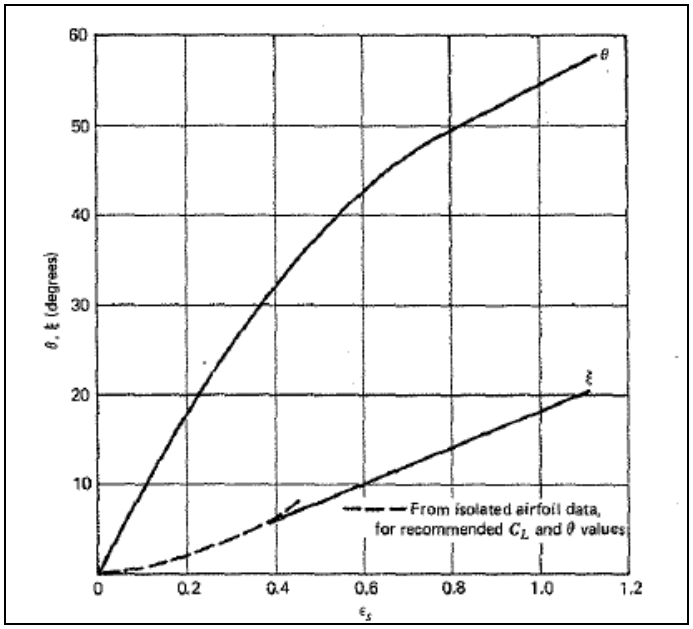

Figure 31 Stator vane camber and stagger angle [6]

3.2. Axial Fan Design and Calculations

In this section basic design of axial fan is given. Also, the assumptions and calculations are carried out.

3.2.1. Basic Assumptions

The fan will be designed according to the fan design point shown in the system curves of vertical wind tunnel designed in the previous chapter.

$$Q = 816.79 \ \frac{\text{m}^3}{\text{s}} \text{ and } \Delta p = 1250 \text{ Pascal}$$

There are four fans in the design. The volumetric flow rate for single fan unit is calculated from the total volumetric flow rate.

$$Q_{fan} = 204.20 \ \frac{\text{m}^3}{\text{s}}$$

Fan diameter is chosen as 3.15 m and wind tunnel is designed accordingly. There are commercially available axial flow fans of different companies with same diameter. The hub to tip ratio, which is another important parameter is chosen as 0.5. That is the boss diameter is half of the fan diameter.

$$D_{fan} = 3.15 \text{ m}, \ D_{hub} = 1.575 \text{ m} \text{ and } x_{hub} = 0.5$$

Also the chord length is considered as constant along the span of the rotor. The aspect ratio is defined as the ratio of span to chord.

$$AR = \frac{b}{c} = 2.00$$

Span is calculated

$$b = \frac{D_{fan} - D_{hub}}{2} = \frac{3.15 - 1.575}{2} = 0.7875 \text{ m}$$

Chord length is calculated as

$$c = \frac{b}{AR} = \frac{0.7875}{2} = 0.3938 \text{ m}$$

The number of rotor blade is chosen as 14 and number of stator blade is chosen as 15.

The design RPM is chosen as 600, because 1000 RPM and 750 RPM electrical motors are available in the market and they can provide sufficient power with very high efficiency.

Standard atmosphere values are used for calculations.

Axial velocity is calculated from the continuity equation.

$$V_a = \frac{A_{fan} V_{fan}}{A_{anulus}} = \frac{Q_{fan}}{\frac{\pi}{4}\left(D_{fan}^2 - D_{hub}^2\right)} = 34.94 \ \frac{m}{s}$$

The fan design is an iterative process. For starting the calculations, blading efficiency, $\eta_{bl} = 0.91$ is assumed as an initial guess. After blading is completed, efficiency is calculated and checked for convergence.

Using equation (66) and setting the prerotator values to zero. We obtain

$$\frac{H_3 - H_0}{\frac{1}{2}\rho V_a^2} = K_{fan} = K_{th} - k_R - k_s = K_{th}\eta_{bl}$$

Pressure rise coefficient is calculated:

$$K_{th} = \frac{K_{fan}}{\eta_{bl}\frac{1}{2}\rho V_a^2} = \frac{1250.00}{0.91 \times 0.5\left(1.225\right)\left(34.94\right)^2} = 1.837$$

Flow coefficient at the mean diameter is calculated

$$\lambda_{MS} = \frac{V_a}{\Omega r_{MS}} = \frac{34.94}{62.83 \times 1.1813} = 0.471$$

Swirl coefficient of mid span is calculated by using equation (67)

$$\varepsilon_{MS} = \frac{K_{th}\lambda}{2} = \frac{1.837 \times 0.471}{2} = 0.433$$

The relative flow angles with respect to the rotor blades are calculated by using equations (72), (73) and (75).

$$\beta_1 = atan\left(\frac{1}{\lambda}\right) = atan\left(\frac{1}{0.471}\right) = 64.8 \text{ degrees}$$

$$\beta_2 = atan\left(\frac{1-\varepsilon_s\lambda}{\lambda}\right) = atan\left(\frac{1-0.433\times 0.471}{0.471}\right) = 59.4 \text{ degrees}$$

$$\beta_m = \frac{1}{2}\left(tan\beta_1 + tan\beta_2\right) = 62.4 \text{ degrees} \qquad (90)$$

By using equation (69) and neglecting the drag term, blade loading is calculated then using the solidity value for the mid span lift coefficient is calculated.

$$C_L\sigma = 2\left(\varepsilon_s\right)\cos\beta_m = 2\times 0.433\cos(62.4°) = 0.4015$$

Solidity is 0.7427 for the mid span

$$C_L = \frac{C_L\sigma}{\sigma} = \frac{0.4015}{0.7427} = 0.541$$

From Figure 26, $C_{Dp} = 0.011$ is found. Then the secondary drag can be calculated $C_{Ds} = 0.018 \times 0.541^2 = 0.0052$

$$C_D = 0.011 + 0.0052 = 0.0162$$

Then using equation (85), rotor loss coefficient is calculated.

$$\frac{k_R}{K_{th}} = \left(\frac{\lambda}{\frac{C_L}{C_D}\cos^2 \beta_m} \right)_{MS} = \frac{0.471}{\frac{0.541}{0.0162}\cos^2(59.4)} = 0.055$$

A similar calculation is performed for mid span section of the stator using equation

$$\frac{k_s}{K_{th}} = \left(\frac{\lambda}{\frac{C_L}{C_D}\cos^2 \beta_m} \right)_{MS} = \frac{0.471}{\frac{1.2791}{0.0444}\cos^2(12.2)} = 0.028$$ where the drag coefficient is calculated from equation (81).

Then the efficiency is calculated again:

$$\eta_{bl} = 1 - \frac{k_R}{K_{th}} - \frac{k_s}{K_{th}} = 1 - 0.055 - 0.028 = 0.917$$

The calculated efficiency is 0.917, which a little bit greater than the assumed value. Since the loss coming from other parts of the fan is not calculated like annulus and nose fairing, the difference is accepted as convenient.

Using the above values and the airfoil section data given in Appendix B, airfoil coordinates are calculated at 21 stations from root to tip for both rotor and stator.

The both stators and rotors, airfoil is F series airfoil with thickness to chord ratio of 10%. To construct rotor and stator blades, area centers of each section is aligned and the sections are rotated by stagger angles calculated.

In Table 24 and Table 25, the calculated data for building rotor and stator blades are summarized respectively.

Table 24 Rotor parameters summary

x	0.50	0.75	1.00
r	0.7875	1.1813	1.575
ε	0.6492	0.4328	0.3246
λ	0.7055	0.4703	0.3528
β_m	47.5396	62.3619	69.4854
$C_L\sigma$	0.8765	0.4015	0.2275
β_1	54.7967	64.8106	70.5695
β_2	37.5326	59.436	68.2793
σ	1.1141	0.7427	0.557
C_L	0.7867	0.5406	0.4084
α	2.00	2.00	2.00
θ	21.6766	6.3629	0.7767
ξ	41.9585	59.6291	68.1812
c	0.3938	0.3938	0.3938
s	0.3534	0.5301	0.7069

Table 25 Stator parameters summary

x	0.5	0.75	1
σ	0.9952	1.4968	1.7388
β_1	32.9911	23.4025	17.9831
β_m	17.9831	12.2103	9.2185
θ	44.3196	33.7971	26.8188
ξ	10.8803	6.4064	4.248
C_L	1.2243	1.2559	1.1016
c	0.3315	0.3306	0.3794

The hub, tip and mid span profiles are given in Figure 32 and Figure 33 with respect to flow direction. The constructed rotor and stator models are given in Figure 34 Figure 35. The models are used to build a full aerodynamic fan model to be used in CFD analyses.

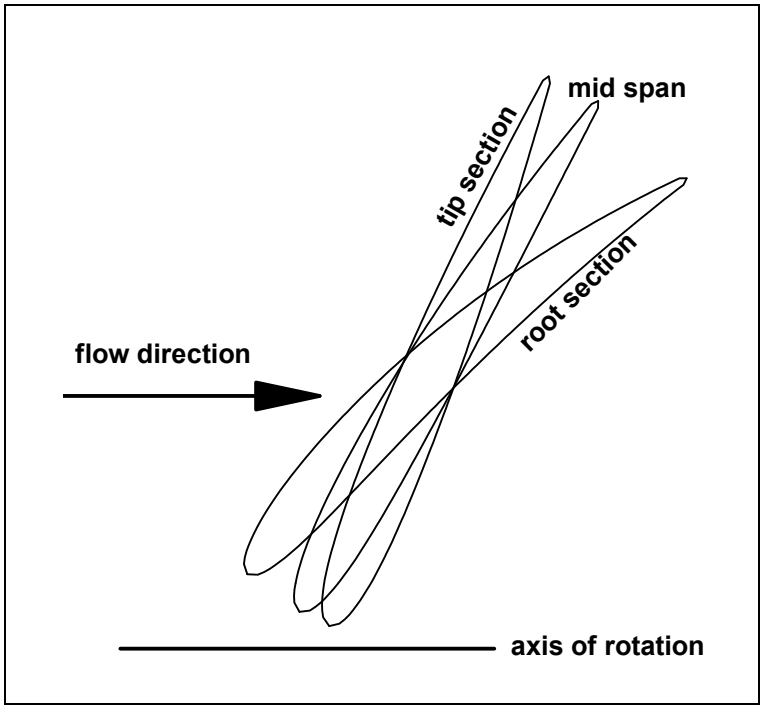

Figure 32 Rotor section profiles

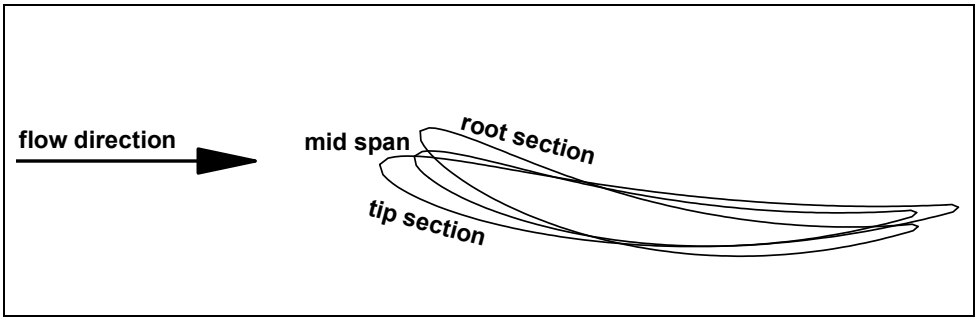

Figure 33 Stator section profiles

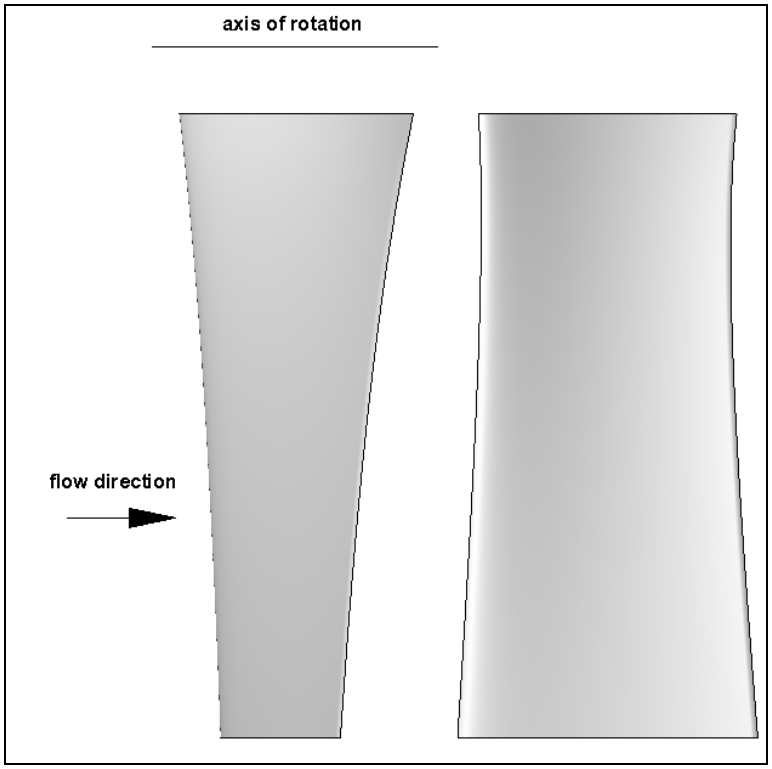

Figure 34 Rotor and stator model (top view)

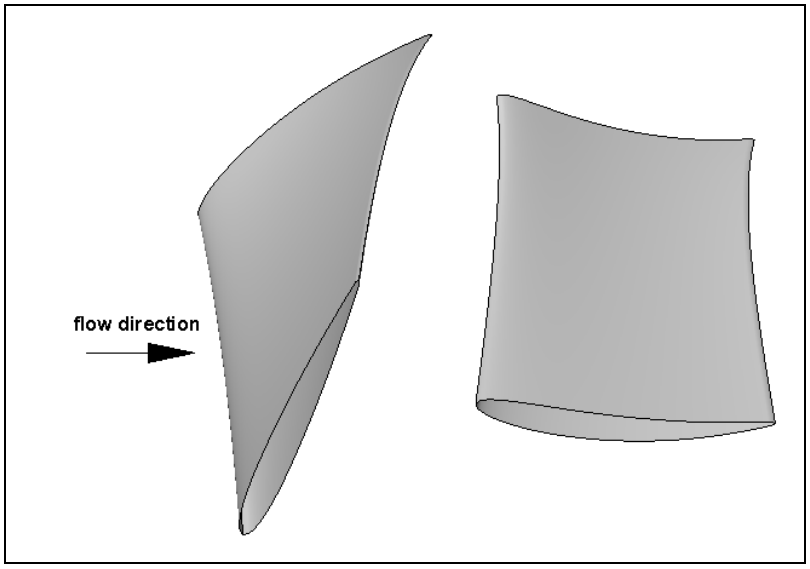

Figure 35 Rotor and stator model (oblique view)

CHAPTER 4

FAN CFD MODEL

4.1. Introduction

The CFD analyses of the designed fan are performed by the FLUENT commercial software version 6.3.26. The input geometry and mesh is prepared by GAMBIT software version 2.3.16. Gambit is a pre-processor software used for preparing input data for CFD programs.

The rotor and stator blades are generated by importing data points to the program. The data of the rotor and stator blades are generated by the approach listed in Appendix BAPPENDIX B and the angles calculated in the previous chapter. After that, geometry generation options such as “building geometries” and “revolution of faces” are used for constructing the full model of the axial flow fan.

1 cm tip clearance is used for the rotor blades. The tip of the rotor blades are truncated by the use of a cylinder having a diameter of 313 cm.

The nose and tail fairing are generated by the ellipse sections that are revolved about the flow axis. The whole geometry, composed of rotor blades, stator blades, and hub, nose and tail fairings is placed in a 12.5 meters long duct.

In this section of the thesis, the CFD analysis results are presented and compared with the analytical result obtained in previous chapter. First, the mesh is described. Then the boundary conditions and solution parameters

are presented. After that the fan performance curve for 600 RPM and 450 RPM are given.

4.2. Computational Mesh

The computational mesh is divided in to two zones. One zone is the part where the flow is axial and the other zone is the part where the flow has swirl components due to the rotation of rotor blades.

The mesh is composed of triangular prisms and tetrahedral elements. There are approximately 2438000 cell elements and 456500 nodes in the solution domain.

The surface mesh elements of the fan rotor, stator, hub, nose and tail fairings are given in Figure 36. In Figure 37, the casing of the axial fan is added to the view and in Figure 38, the tip clearance between the rotor blade and casing is shown. As seen from the figure the tip of the rotor blade is truncated by using a circular cut that follows the contour of the casing.

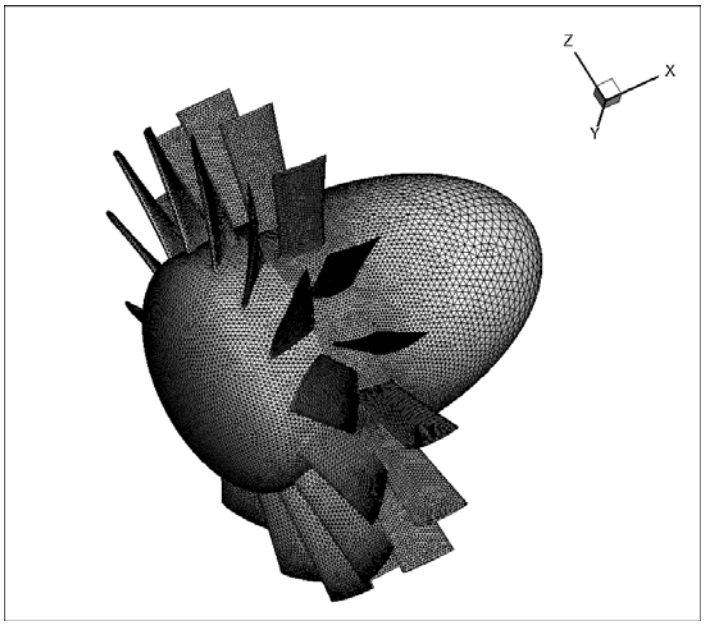

Figure 36 Rotor and stator surface mesh

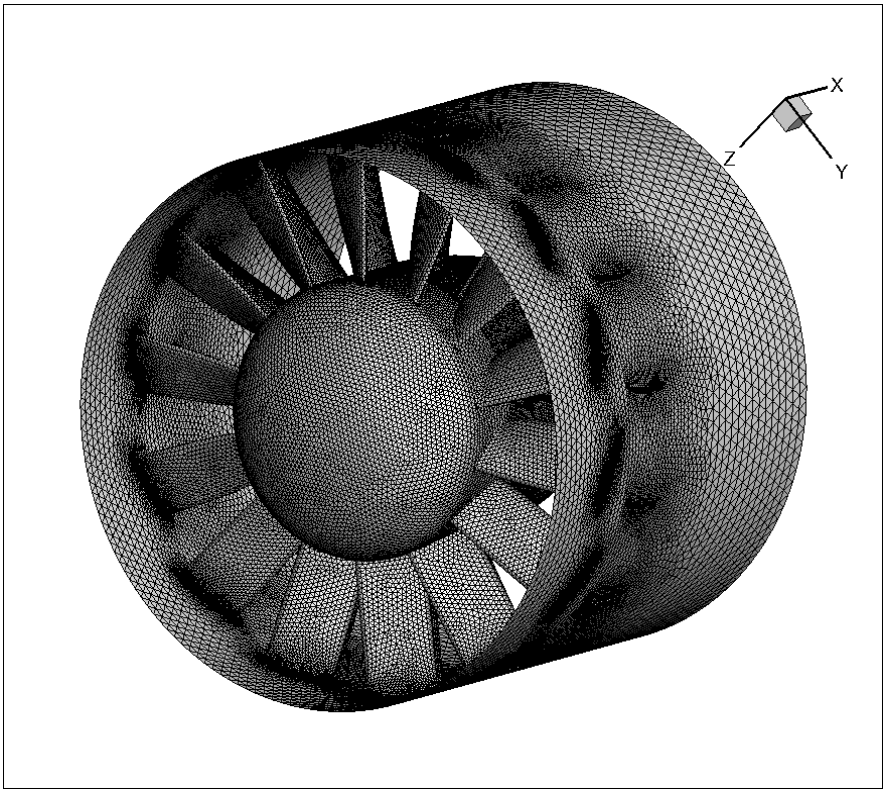

Figure 37 Rotor and stator surface mesh with casing

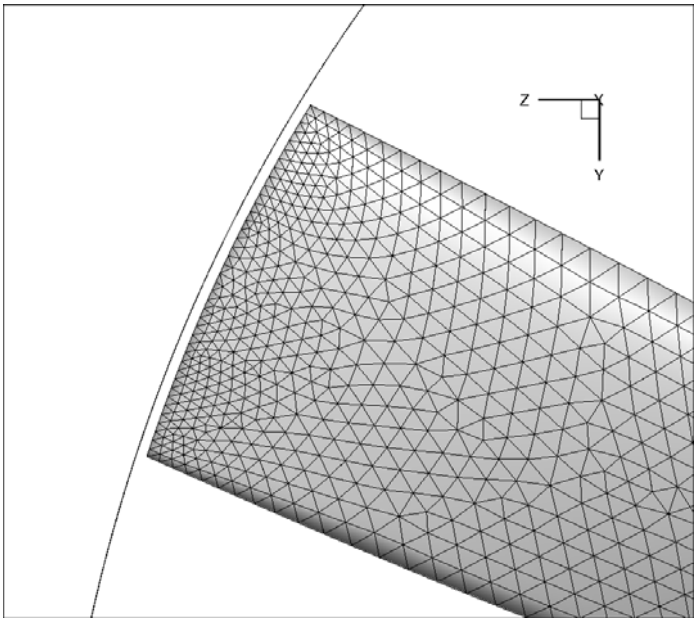

Figure 38 Rotor tip clearance

4.3. Boundary Conditions and Solution Controls

4.3.1. Boundary Conditions

There are two options to find the solution to the problem in FLUENT program. The first option is to define the inlet end exit of the duct as pressure inlet and outlet type boundary conditions, respectively. The total gauge pressure at the inlet is entered by the user and the static gauge pressure at the exit is entered. After the solution is converged a volumetric flow rate and corresponding static or total pressure rise is calculated from the surface integrals. The second option is to define a velocity inlet boundary condition at the inlet section and pressure outlet at the exit. After a steady state solution is obtained, the pressure difference is calculated by using the surface integral options of the fluent program.

The second option has a fast convergence and it is good to control the volumetric flow rate.

There are two flow zones described for the full model. One zone is the fluid where the flow is axial and the other zone is fluid where the flow is rotationary with respect to the rotor. The rotationary fluid zone is defined by a moving reference frame. Zones are shown in Figure 39.

The inlet boundary is defined by using the velocity inlet panel in the FLUENT program. The velocity for the design point is 26.181 m/s. It corresponds to 204 m^3/s volumetric flow rate approximately. Also, the turbulent intensity is assumed as 1% and the hydraulic diameter is entered as 3.15 meters. The velocity inlet panel is given in Figure 40.

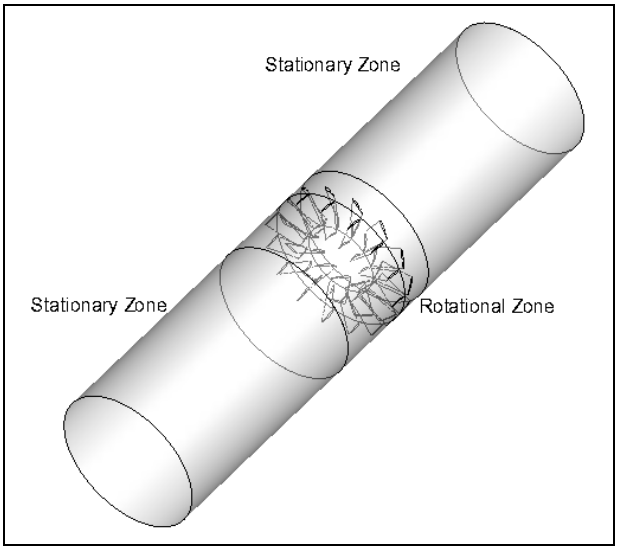

Figure 39 Fluid zones

The exit boundary is defined as a pressure outlet boundary. The gauge static pressure is defined as zero for the exit pressure. In addition, backflow turbulent intensity and backflow hydraulic diameter is defined as 2% and 3.15 meters respectively. The pressure outlet panel is given in Figure 41.

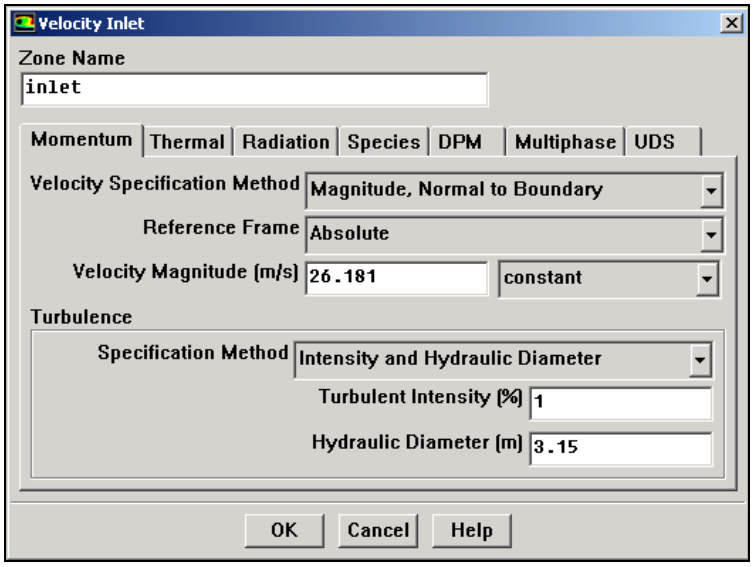

Figure 40 Inlet boundary condition

To simulate the rotation of the rotor, fluid zone around is defined by a moving reference frame with no translational velocity and rotational speed about the flow axis. The fluid panel is given in Figure 42.

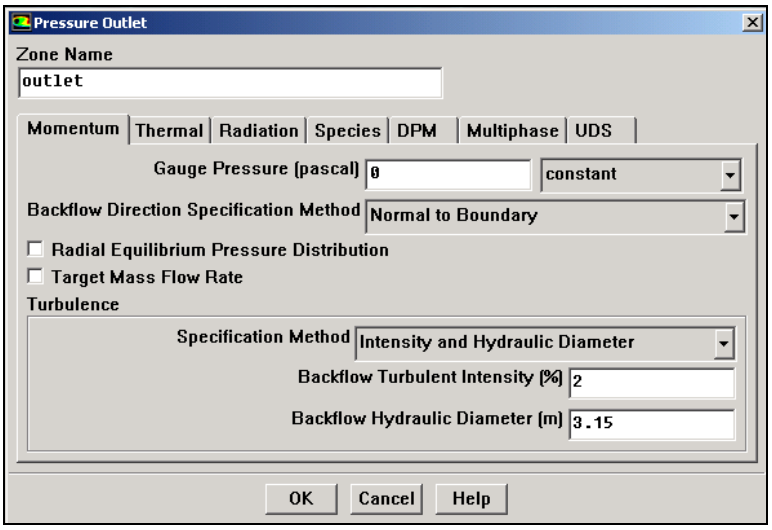

Figure 41 Exit boundary condition

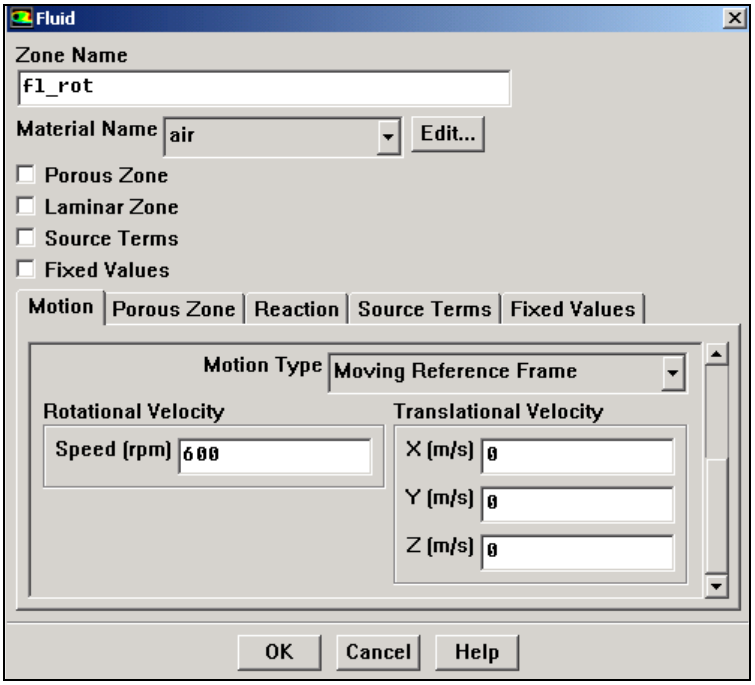

Figure 42 Fluid zone definition around rotor

Since some part of the fluid zone is defined by a moving reference frame and some part of the fluid is stationary, grid interface panel is used to define the interactions. Three grid interfaces are defined between the forward duct-rotor, rotor-stator and stator and aft duct. The grid interfaces panel is shown in Figure 43.

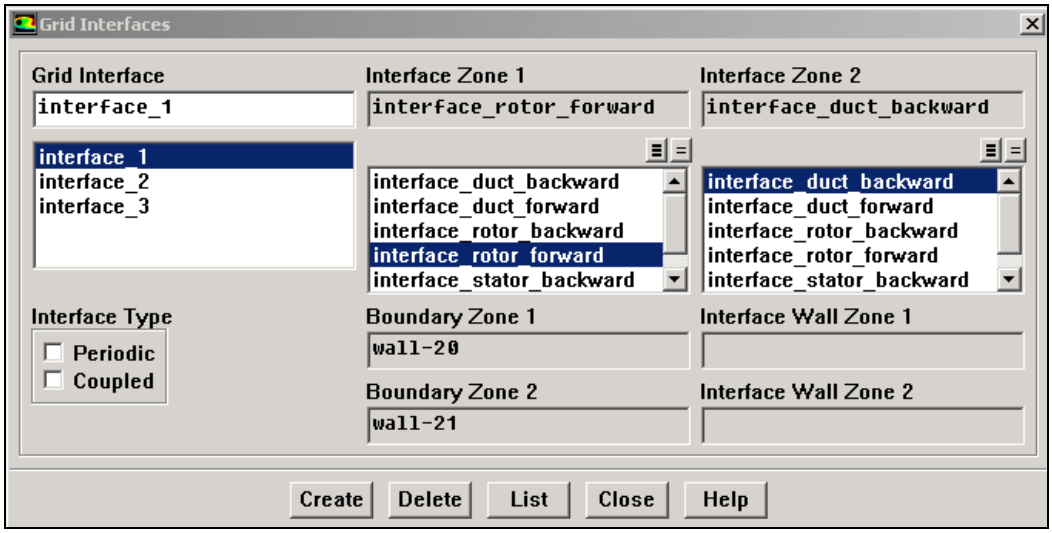

Figure 43 Grid interface definitions

4.3.2. Solution Controls

The solver used in the solution is pressure based solver. This solver is originally, defined as the solver for low speed incompressible flows. However, in FLUENT documentation, it is clearly stated that both pressure and density based solvers are extended to solve various kinds of problems. The solution domain is 3D and steady state solution is sought. The velocity definitions are absolute. The solver form of the FLUENT program is given in Figure 44.

The turbulence model used in the solution is selected as RNG $k-\varepsilon$ model. Koktürk in his thesis[34] has satisfactory results using the RNG $k-\varepsilon$ turbulence model in designing of a reversible axial flow fan. This model is used for complex shear flows having rapid gradients, moderate

swirl, vortices and local translations. Standard wall functions are used and the swirl dominated flow option is activated. The viscous panel is shown in Figure 45.

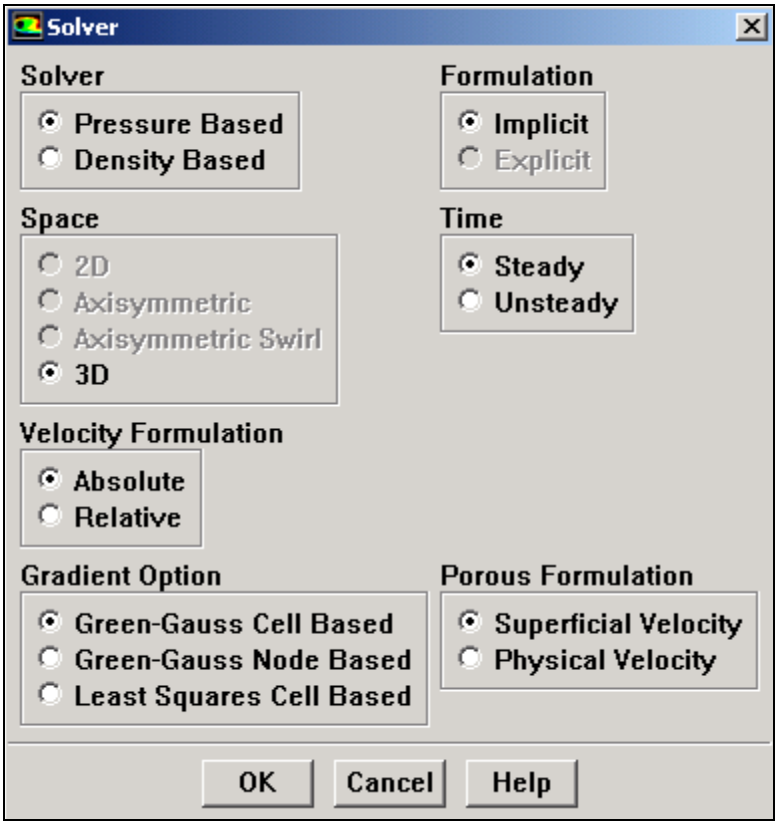

Figure 44 Solver form

For the solution, first order upwind numerical schemes are selected for pressure, momentum, turbulent kinetic energy and turbulent dissipation rate equations. SIMPLE algorithm is used for solving the equations. The solution control panel is shown in Figure 46.

All parameters in FLUENT program in viscous panel and under-relaxation factors are not changed and left as they are.

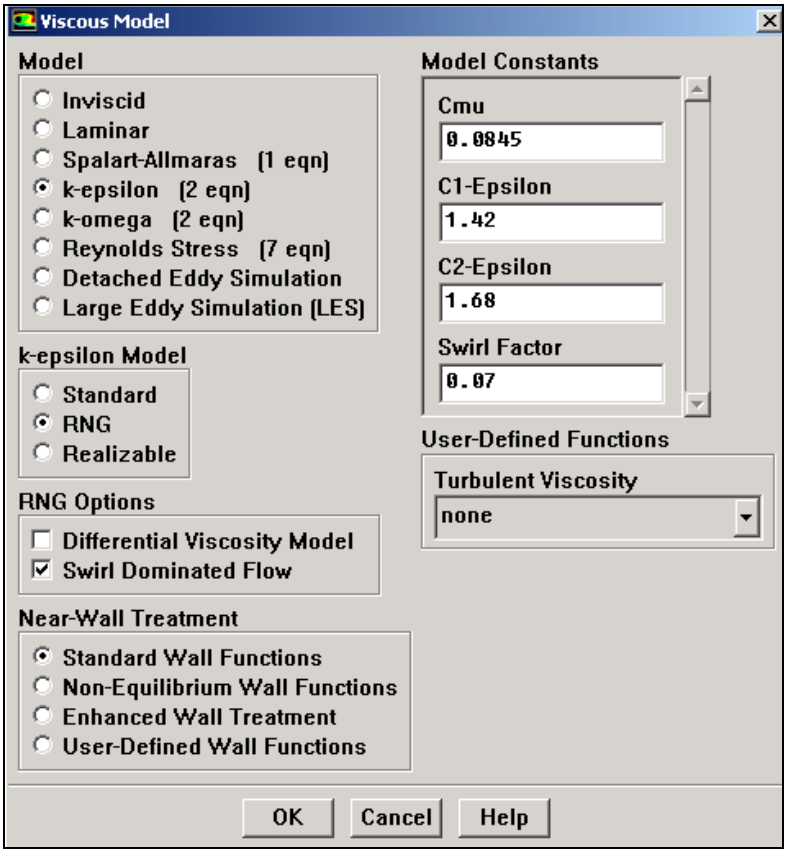

Figure 45 Viscous panel options

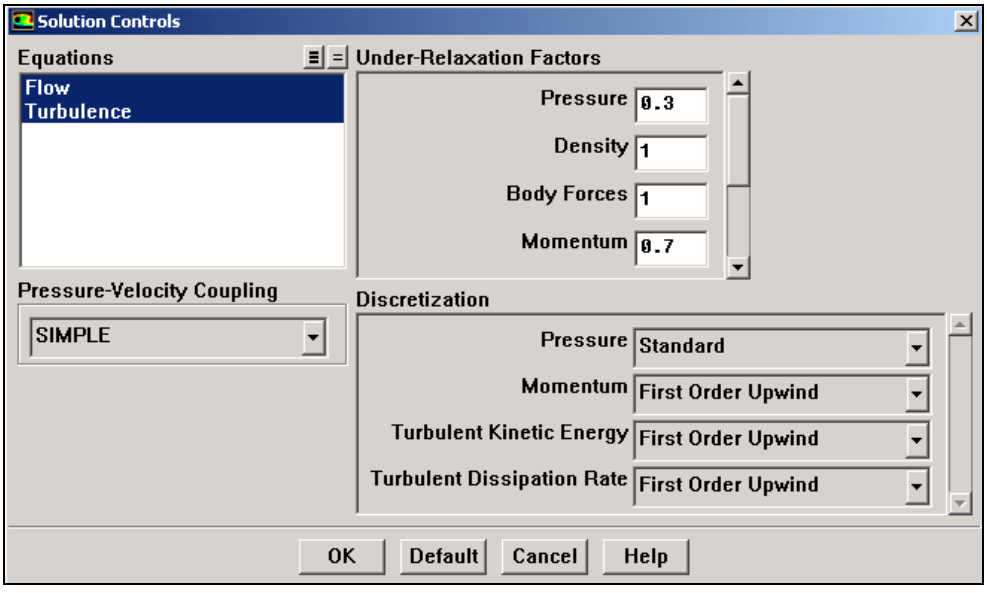

Figure 46 Solution controls

4.4. CFD Results

The CFD runs are performed for six different volumetric flow rates for 600 RPM, fan rotational speed and five different volumetric flow rates for 450 RPM. The circuit loss of the vertical wind tunnel calculated in Chapter 2 is the maximum value that can be possible when operating the wind tunnel. However, a 16% higher volumetric flow rate point is checked with CFD if there is a fan stall.

4.4.1. CFD Results for Design Point

In Chapter 3, the fan design point is defined as 1250 Pascal with a volumetric flow rate of 816.79 m³/s for 4 fans.

The pressure rise is found by taking the difference of the total pressures at the interface planes just in front of rotor and stator. The values are given in Table 26.

The efficiency is calculated by the equation (91)

$$\eta_{hyd} = \frac{\Delta p Q}{T \omega} \tag{91}$$

Where the numerator is the fluid power and denominator is the shaft power.

Table 26 Gauge total pressures about rotor

Section	Q m³/s	p_{total} Pa
Rotor forward plane	203.491	-708.217
Stator forward plane	203.491	527.5875

Total pressure increase is $\Delta p = 527.6 - (-708.2) = 1235.4$ Pa.

The moment about the shaft axis is calculated by FLUENT and it is 4643.34 Nm as magnitude.

Then the hydraulic efficiency is calculated as:

$$\eta_{hyd} = \frac{203.5 \times 1235.4}{4643.34 \times 600} \frac{60}{2\pi} 100 = 86.2 \ \%.$$

The hydraulic efficiency value is lower than the analytical value. It is mainly because of the cascade data for F series airfoils are not sufficient. But 86.2% is still an acceptable and good value for axial flow fan about this size.

4.4.2. CFD Results for Off-Design Points.

The designed axial fan will be operated in a vertical wind tunnel. Compared with other applications, the operating range can be considered very narrow. For 600 RPM, case the tunnel maximum pressure loss which is the design case corresponds to a configuration where there are four paratroopers and some air is exchanged by surroundings. The minimum pressure loss will be achieved when there is no paratrooper in the flying chamber and no air exchanged with the surroundings. In this case, the total pressure loss is 750 Pascal approximately. This case is also considered in CFD runs.

The results of the CFD runs for 600 RPM and 450 RPM are given in Table 27 and Table 28 respectively.

The results are also presented in graphical form in Figure 47. Total pressure rise and efficiency values are plotted with respect to the volumetric flow rate. As described previously, the operating range of the fan is very narrow, so the calculations do not cover fan stall regions, closed valve regions and zero pressure loss regions.

Table 27 CFD results for 600 RPM

V_{axial} m/s	η_{hyd}	Q m³/s	Δp_{total}
20.00	84.21	155.86	1917.89
23.00	85.82	179.24	1619.03
24.50	86.32	190.93	1444.16
26.18	86.20	204.03	1235.81
27.50	85.39	214.31	1065.24
30.00	81.32	233.79	732.54

Table 28 CFD results for 450 RPM

V_{axial} m/s	η_{hyd}	Q m³/s	Δp_{total}
15.00	84.08	116.90	1026.23
18.00	86.18	140.28	844.41
21.00	84.81	163.66	560.69
23.00	79.17	179.24	359.99
25.00	61.33	194.83	157.07

It can be seen from Figure 47 that the maximum efficiency is calculated at the design point that is consistent with the analytical design. Also, the fan analytical design point is very close to the CFD results. An error can be defined as the difference of total pressure rise between analytical result and computational result as a percentage of the analytical result. The error can be calculated by equation (92). The error is calculated as 1.2 %.

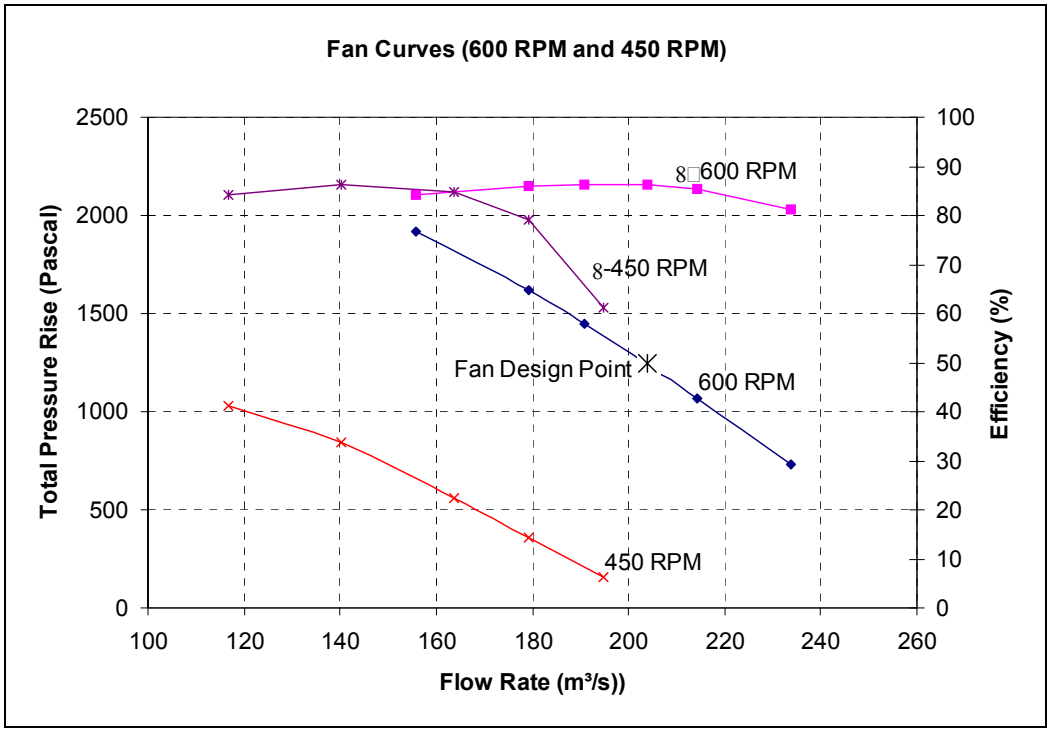

Figure 47 Fan performance curve

$$error = \frac{\Delta p_{CFD} - \Delta p_{analytical}}{\Delta p_{analytical}} \times 100 \qquad (92)$$

For 600 RPM, the axial fan will be operated between 1250 and 750 Pascal pressure loss range. For 450 RPM, case the efficiency is dropped to 60 % approximately. Nevertheless, the system will not operate at that region also.

The efficiency calculated from CFD results is about 6% less than the blading efficiency. The difference is coming from the tip effects and the losses coming from nose faring, tail fairing and fan duct.

4.4.3. Rotor and Stator Pressure and Velocity Contours

This section presents static pressure contours on rotor and stator blades. The absolute velocity contours are also presented in this section.

In Figure 48, the static pressure contours for the rotor suction side is shown. The pressure contour lines can be considered parallel from hub to tip. This situation is convenient since the fan is designed according to the free vortex theory, which dictates that there is no flow in radial direction.

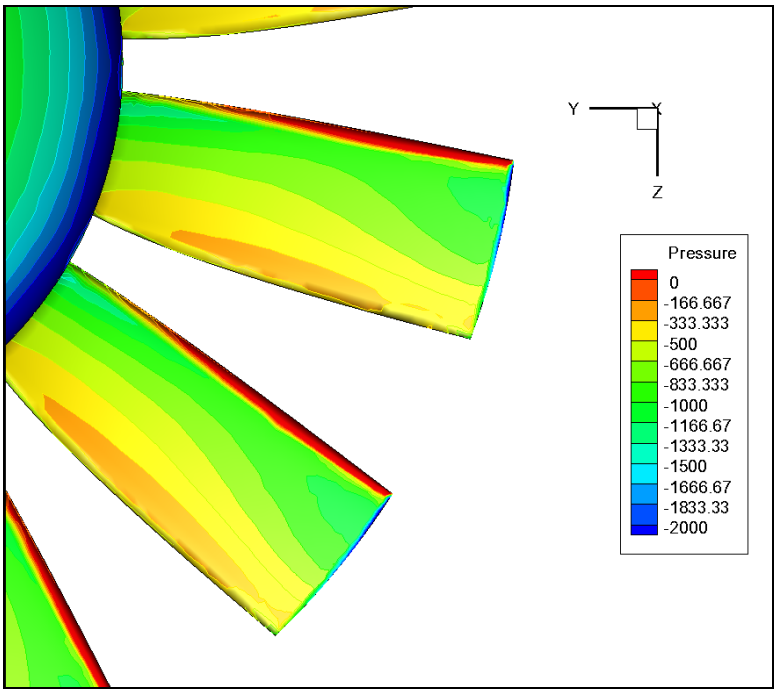

Figure 48 Rotor static pressure contours (pressure side)

The static pressure contours for suction side of the rotor blades are given in Figure 49. The pressure contours for the suction side of the rotor blade is also in good agreement with the free vortex theory.

The pressure contours for stator blades are given in Figure 51. The suction side has parallel pressure contour lines that lie from hub to tip. The pressure side of the stator blades does not have parallel pressure contour lines, but from the figure, it can be concluded that the static pressure is not changing much, that is, the pressure gradient on the pressure side of the stator blades are small compared to the suction side.

The off design pressure contours on the pressure side of the rotor blades for 233 m³/s flow rate and 750 Pascal system resistance, are given in Figure 50. It can be seen that the pressure contours are deteriorating as the fan operating point is away from the design point.

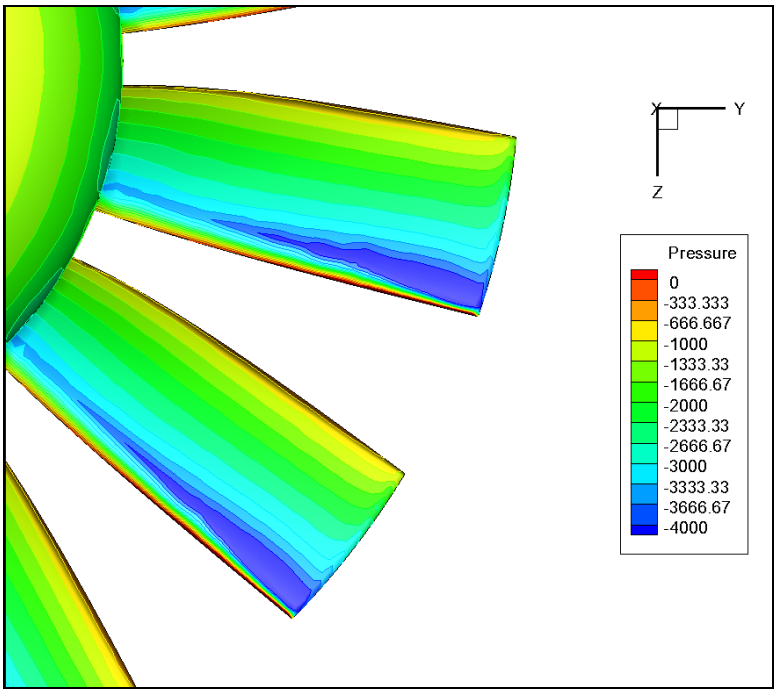

Figure 49 Rotor static pressure contours (suction side)

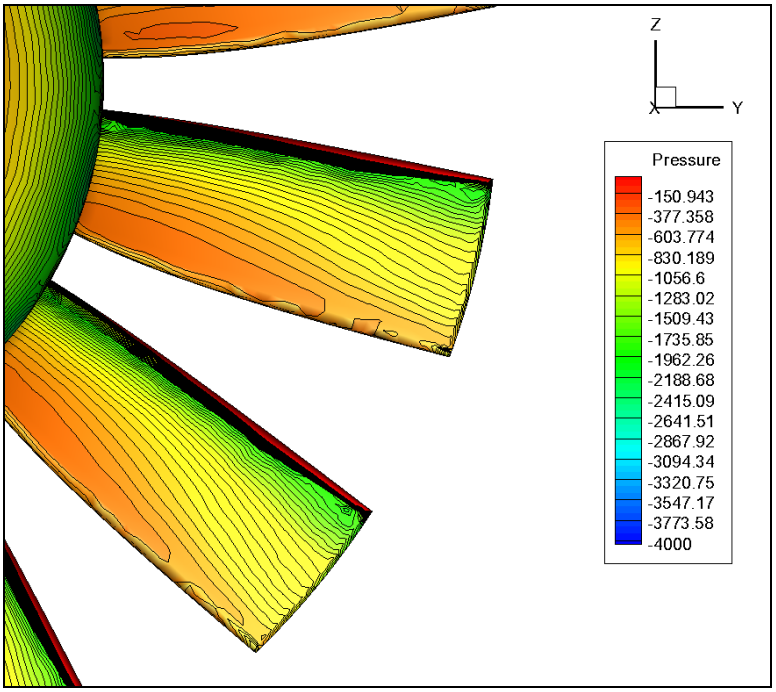

Figure 50 Rotor static pressure contours (Off-design)

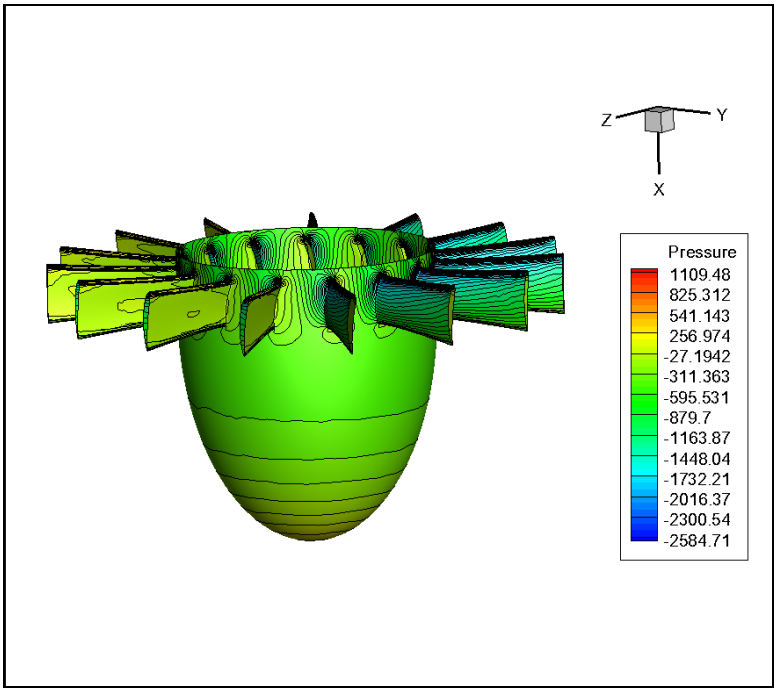

Figure 51 Stator static pressure contours

CHAPTER 5

RESULTS AND DISCUSSION

5.1. General

Special Forces are valuable assets in the military world. They are trained for special missions that require extensive preparation and readiness. Vertical wind tunnel is a mean that simulates the free falling phase. Paratroopers can be trained without any risk in wind tunnel. The training is also much cheaper as compared with real environment. Also, the trainees have chance to correct their mistakes while flying in the tunnel. The trainer and trainee can fly in the flight chamber in a simulated training environment, without thinking of when they are going to open their parachutes.

The manuscript presents a methodology to design a complete vertical wind tunnel with fans. The aerodynamic design of a vertical wind tunnel, aerodynamic design and CFD analysis of an axial flow fan are presented in order.

5.1.1. Wind Tunnel

The wind tunnel is designed as a combination of standard components one after another. The design of each component must satisfy related design requirements coming from either geometrical constraints or related theoretical design limitations coming from researches in the literature. The designed wind tunnel presented in this tunnel obeys the theoretical design limitations.

One important parameter for the wind tunnel is the energy ratio of the circuit. If the energy ratio is greater, then the amount of energy that must be supplied decreases for steady state operation of the wind tunnel.

In reference [9], the energy ratio of some wind tunnel circuit operating in USA is given. Looking at the similar designs, the values 5 – 8 for energy ratio seems a satisfactory design. The energy ratio of open circuit wind tunnels have smaller.

The energy ratio of the designed wind tunnel for the forcible condition is calculated as 2.358. But vertical wind tunnel for human flight has additional loss factors. In this calculation, there is a safety net at the floor of the flight chamber. That section is the fastest section, so the loss contribution of the safety net is considerable amount. Also four flying paratroopers have an additional adverse impact on energy ratio. On scientific tunnels, the model projection area inside the test chamber is usually less than 5%. 20% air exchange is also too much compared to the scientific tunnels.

The energy ratio for clean tunnel is calculated as 7.102 which is a comparable and satisfactory energy ratio value.

5.1.2. Axial Fan Design

There must be a mean to supply momentum to the flow for keeping up steady state flow for different operating conditions. In closed circuit wind tunnels, momentum addition to the flow is generally performed by axial flow fans.

An axial fan is designed by free vortex flow assumption. That is no radial flow inside the fan. There is only a swirl component of flow in absolute frame just after the rotor blades. This swirl is removed by stators or straighteners.

For axial fan design, many parameters must be taken into account. Starting from the outer dimension of the fan, number of rotor blades, number of stator blades, hub diameter, chord length, solidity, and airfoil selection are important factors.

There are empirical methods to select most of the parameters; however axial fans with known performance in the commercial market can also be a good starting point for some basic dimensions like fan diameter, hub to tip ratio.

The design actually depends on airfoil characteristic and data mainly. The required total pressure increase through out the fan corresponding to a required flow rate is the main objective of the fan design. This objective is preformed by carefully designing the local airfoil sections in radial direction.

In this thesis, F-series airfoils are used for local rotor and stator sections. The data of the airfoil is taken from reference [6]. Lift to drag ratio of the airfoil is as other parameter that defines the performance and efficiency of the fan. For F-series airfoil, lift to drag ratio is around 30. Higher lift to drag ratio airfoils is available in literature and they can be used for more efficient fan design. However, the cascade data for airfoil sections are lacking in literature. Most scientific studies about cascade flow are performed with less efficient airfoil sections.

The fan design point is selected from the system operating points. Although there is a range that a system can operate, fan design must be performed for a point in the operating envelope.

By using the F-series airfoils, the orientation data for 20 different sections are generated according to the given flow velocity and pressure rise. The efficiency value is calculated around 91%. The efficiency value is actually an input for structural design and the power supply that will be attached to the rotor.

5.1.3. CFD Analyses

CFD analyses are performed for a full axial fan model. Also inlet and exit duct are added for solution to be more realistic. For nose and tail fairing half ellipsoids are used. The CFD studies are performed by FLUENT commercial software. The volumetric flow rate is used as input and total pressure difference across the fan rotor and torque acting on the fan symmetry axis by the rotor is extracted by the pressure distribution on the rotor surface.

Totally eleven runs are performed. Other than the fan design point, 5 points for 600 RPM and 5 points for 450 RPM are investigated.

The total pressure rise through the rotor is in agreement with the analytical design. However, efficiency values are calculated as 86%, which is lower compared to the 91% analytical blading efficiency.

Also carefully designed nose and tail fairings can increase the efficiency. Using semi spherical nose fairing and conical nose fairing can make a better contour for the flows.

The pressure contours of the CFD results are also in agreement with free vortex flow. The pressure contours are aligned from hub to tip in a parallel way. In addition, when the operating condition is different from the design point the pressure contours deteriorate as expected.

5.2. Recommendations for Future Work

Cooling is an important factor and it must be taken into consideration for scientific wind tunnels and for tunnels built in hot climatic environment. Cooling with air exchange may not be an option, if the environment temperature is high. Cooling option through corner vanes or wind tunnel walls can be studied for future work

The fan noise must be taken into account because it can reach very high decibels and can be very annoying and be a health risk. Sound absorbing through corner vanes and tunnel walls can be studied as future work.

The cascade data of high lift to drag ratio airfoil sections with various solidity ratios can be studied and a fan blade section database can be prepared for efficient axial fan designs.

To reduce the initial construction cost of the wind tunnel, the tunnel dimensions can be reduced. The option of variable area corners can be analyzed and studied as a future work to reduce the dimensions of the wind tunnel.

5.3. Conclusion

By using the model presented in this manuscript, not only vertical wind tunnel but also scientific wind tunnels in subsonic regimes can be designed and built. The design in this manuscript is for standard conditions, if the location is different than standard, the tunnel design must be optimized for these conditions. The terminal velocity, which derives the tunnel design, changes nonlinearly with altitude. This situation must be taken into account during design.

The vertical wind tunnel of Turkish Special Forces is designed using the methodology presented in this manuscript. The wind tunnel is in service more than two years. A commercial set of axial fans is used as the power supply of the wind tunnel. The wind tunnel is designed to achieve wind speed over 70 m/s because it is located over 1100 meter height above sea level.

CFD is used to analyze the total pressure increase across the rotor of the fan. Since the operating region is far from the fan stall point, flow separation or instabilities are not investigated. Although CFD is a powerful tool for flow analysis, it must be backed up by experimental data.

It is concluded that axial fan design method presented in this manuscript can be used for designing high capacity fans and the wind tunnel design method can be used to design scientific and vertical wind tunnels in subsonic regimes to meet different requirements.

REFERENCES

[1] Hansen, J.R.(Editor), Taylor, D.B., Kinney, J., Lee, J.L., “The Wind and Beyond”, The NASA History Series, 2003

[2] Talay, T.A., “Introduction to the Aerodynamics of Flight”, NASA Scientific and Technical Information Office, 1975

[3] Barlow, J.B., Rae W.H., Pope, A., “Low Speed Wind Tunnel Testing”, John Wiley & Sons, 1996

[4] Wattendorf, F.L., “Factors Influencing the Energy Ratio of Return Flow Wind Tunnels”, 5th International Congress for Applied Mechanics, Cambridge, Sept.12-16, 1938, p. 52.

[5] Fluent 6.3.26 Documentation, FLUENT INC.

[6] Wallis, R.A., “Axial Flow Fans and Ducts”, John Wiley and Sons, 1983

[7] Abbot, I.H., Von Doenhoff, A.E., “Theory of Wing Sections”, Dover Publications, 1959

[8] Horlock, J.H., “Axial Flow Compressors, Fluid Mechanics &Thermodynamics”, Robert E. Krieger Publishing Co., 1973

[9] Eckert, W.T., Mort, K.W., Jope, J., “Aerodynamic Design Guidelines and Computer Program for Estimation of Subsonic Wind Tunnel Performance”, NASA TN D-8243, 1976

[10] Stepanoff, A.J., “Turboblowers; Theory, Design and Application of Centrifugal and Axial Flow Compressors and Fans”, John Wiley and Sons, 1955.

[11] Aksel, M.H., “Fluid Mechanics, Volumes I-II”, METU Press, 1999

[12] Bleier, F.P., “Fan Handbook: Selection, Application and Design”, McGraw-Hill, 1998.

[13] Osborne, W.C., “Fans”, Pergamon Press, 1977.

[14] Gostelow, J.P., “Cascade Aerodynamics”, Pergamon Press, 1984.

[15] Agrawal, D.C., “Terminal Velocity of Skydivers”, Physics Education 35 (4), July 2000, p. 281-283

[16] Eck, B., “Fans”, Pergamon Press, 1973

[17] Turner, R.C., “Notes on Ducted Fan Design”, Ministry of Aviation Aeronautical Research Council, C.P. No.895, 1966

[18] Shames, I.H., “Mechanics of Fluids, 3rd ed.”, McGraw-Hill, 1992

[19] White, F.M., “Fluid Mechanics, 4th ed.”, McGraw-Hill, 2001

[20] “Aerodynamics of Wind Tunnel Circuits and Their Component” AGARD CP585, June 1997

[21] Knight, I., “The Design and Construction of a Vertical Wind Tunnel for the Study of Untethered Firebrands in Flight,” Kluwer Academic Publishers. Fire Technology, Vol. 37, pp. 87–100, 2001.)

[22] Morel, T., “Comprehensive Design of Axisymmetric Wind Tunnel Contractions”, Journal of Fluids Eng., ASME, 97, p. 225-233, June 1975

[23] Borger, G.,G, “The Optimization of Wind Tunnel Contractions for Subsonic Range”, NASA TTF 16899, March 1976

[24] Patterson, G.,N., “Note on the Design of Corners in Duct Systems”, ARC R&M 1773, 1937

[25] McPhail, D., C., “ Experiments on Turning Vanes at an Expansion”, ARC 1876, 1939

[26] Krober, G., “Guide Vanes for Deflecting Fluid Contents with Small Loss of Energy”, NACA TM 722, 1932.

[27] Collar, A.,R., “ Some Experiments with Cascades of Airfoils”, ARC R&M 1768, 1937

[28] Prandtl, L., “Attaining A Steady Stream in Wind Tunnels”, NACA TM 726, October 1933

[29] Anderson, J., D., Jr., “Fundamentals of Aerodynamics, 3rd edition”, McGraw-Hill, 2001

[30] “http://www.skyventure.com/”, webpage of “Skyventure LLC”, 21/02/2010

[31] Hoerner, S., F., “Fluid-Dynamic Drag”, Hoerner, 1965

[32] Howell, A., R., “Fluid Dynamics of Axial Compressors”, Proc. Instn. Mech. Eng., London, 153, 441-453, 1945

[33] Carter, A., D., S., “Three Dimensional Flow Theories for Axial Compressors and Turbines” Fluid Dynamics of Axial Compressors”, Proc. Instn. Mech. Eng., London, 159, 255-268, 1948

[34] Köktürk T., “Design and Performance Analysis of a Reversible Axial Flow Fan”, M.Sc. Thesis, Middle East Technical University, June 2005

[35] Vlajinac, M., “Design Construction and Evaluation of a Subsonic Wind Tunnel”, M.Sc. Thesis, Massachusetts Institute of Technology, June 1970

[36] “http://en.wikipedia.org/wiki/File:Windtunnel1-en.svg”, 02/12/2010

[37] “http://www.mi.uni-hamburg.de/index.php?id=423&L=3”, 02/12/2010

[38] “http://www.industrialpressureblower.com/fan.html”, 02/12/2010

[39] “http://www.tech-dist.com/Greenheck/”, 2/12/2010

[40] “http://www.indiamart.com/”, 03/12/2010

[41] “http://www.globalindustrial.com/g/hvac/exhaust-fans/tube-axial/explosion-proof-tube-axial-duct-fan-wet”, 03/12/2010

APPENDIX A

TERMINAL VELOCITY OF PARATROOPERS

A.1. Definitions

To simulate free fall in a vertical wind tunnel we have to supply enough amount of airflow through the flight chamber that will suspend the paratrooper. The question arises “what amount of air is sufficient?” The answer is the terminal velocity. The definition of the terminal velocity is given by different sources.

Most common definition is “the velocity that can be reached by an object in a free fall in the air”.

Also another definition must be introduced “spread eagle position”. The spread eagle position is the horizontal position of the paratrooper facing down and arms are spread like the wings of an eagle. The position is shown in Figure 52.

Figure 52 Spread eagle position

In the wind tunnel, a variety of paratroopers must be trained. That is the velocity in the flying chamber can be adjusted such that it is equal to the terminal velocity of the trainee. The mass and the height of each paratrooper is different so must be the terminal velocity.

International health organization has a definition that relates the height of a person to its mass. It is the famous “Body Mass Index” (BMI). This relation is one of the relations required to calculate the terminal velocity for a variety of paratroopers.

$$BMI = \frac{M}{H^2} \tag{93}$$

BMI for a normal people is between 18.5 and 25. For BMI between 25 and 30, the person is considered overweight. In addition, if BMI is over 30, the person is obese.

In this section a relation between the terminal velocity, mass and height of the paratrooper will be derived

A.2. Drag Force

The drag force exerted on an object by the air is given by the equation [29]

$$D = \frac{1}{2}\rho V^2 C_D S_{ref} \tag{94}$$

Where ρ is the density, V is the air velocity, C_D is the drag coefficient and S_{ref} is the projected area.

When the paratrooper reaches terminal velocity the drag force D is equal to his/her weight and the weight is mass times the gravitational acceleration.

$W = Mg$

$$Mg = \frac{1}{2}\rho V^2 C_D S_{ref} \quad (95)$$

To evaluate the terminal velocity, the density of the air, the drag coefficient, mass and the projected area must be known.

The drag coefficient is given around 1.0-1.3 in reference [31].

A.3. Human Model

D C Agrawal[15] modeled the paratrooper as the combination of sphere and cylinders. The paratrooper's body is divided into 6 sections. These sections are legs, arms, trunk and the head. Each section is modeled as a cylinder except the head. The head modeled as a sphere. The density of the paratrooper is assumed 1000 kg /m³ and distributed homogenously.

In his study, the required projected area for calculating the terminal velocity is given as a function of mass and height.

In Figure 53, six sections of human model are shown. The numbers inside each section defines the mass of the section as a percentage of total mass of the model.

The mass, length, and diameter of the sections of the body are given in Table 29 and Table 30.

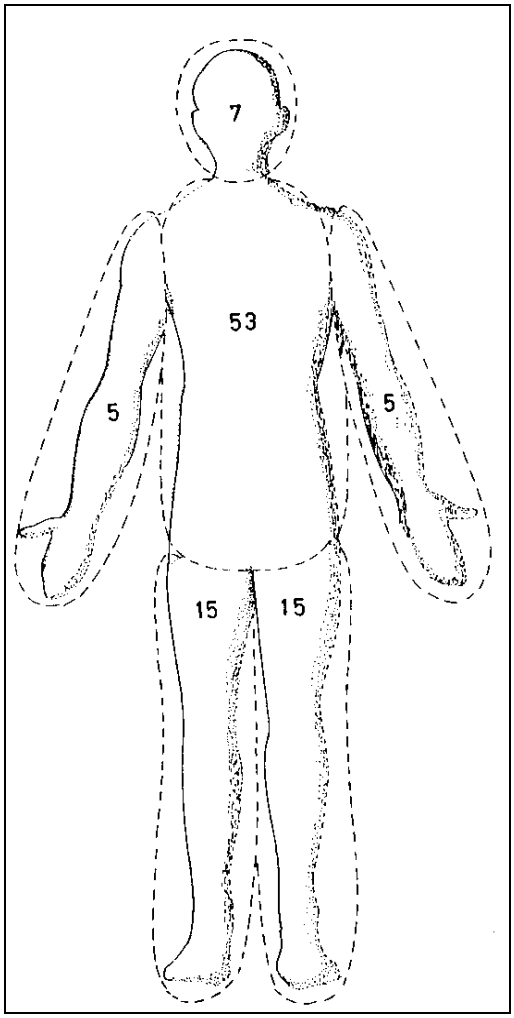

Figure 53 Human Model

Table 29 Human model section weights

Section	**Mass**
m mass of head	0.07M kg
m_1 mass of arm	0.05M kg
m_2 mass of leg	0.15M kg
m_3 mass of trunk	0.53M kg

Table 30 Human model section dimensions

Section	Length / Diameter
L_1 length of arm	$H/2$ m
L_2 length of leg	$H/2$ m
L_3 length of arm	$2H/5$ m
r radius of head	$0.0256M^{1/3}$ m
r_1 radius of arm	$0.0056(M/H)^{1/2}$ m
r_2 radius of leg	$0.0098(M/H)^{1/2}$ m
r_3 radius of trunk	$0.0205(M/H)^{1/2}$ m

By using the equation (96) , it is possible to calculate the projected area of the human model. Since the head is sphere and other body sections are cylinders. The total projected area is given as the sum of the projected areas of the sections.

Head $\pi r^2 =$ $0.0021M^{2/3}$

Arms $4r_1L_1 =$ $0.0112(MH)^{1/2}$

Legs $4r_2L_2 =$ $0.0196(MH)^{1/2}$

Trunk $2r_3L_3 =$ $0.0164(MH)^{1/2}$

Where H is the height in meters and M is the mass in kilograms.

$$S_{ref} = 0.0472(MH)^{1/2} + 0.0021M^{2/3} \quad (96)$$

The projected area is used for calculating blockage effects where necessary. It is also used to calculate the terminal velocity of different paratroopers having different body weight and height.

A.4. Terminal Velocity Calculation

It is now possible to calculate the terminal velocity of anybody knowing the height, and mass and taking the drag coefficient $C_D = 1.0$.

Paratroopers of Special Forces put on additional weight when they are jumping for operations. The additional weight is assumed 60 kg including all the equipments necessary for the operation and the parachute itself.

The terminal velocity is calculated for BMI changing between. 18.5 and 30. The limiting cases for the height and weight are assumed as 1.45 m to 2.0 m and 40 kg to 110 kg respectively. That is, one parameter is chosen as the independent variable one and the other parameter is calculated by using the BMI values. If the parameter is out of range then the data is omitted.

In Figure 54, Figure 55 and Figure 56 the terminal velocity calculations are presented. The additional weight data is obtained from the Special Forces Officers. In the tunnel design, the maximum velocity will be used for pressure loss and power requirement calculations:

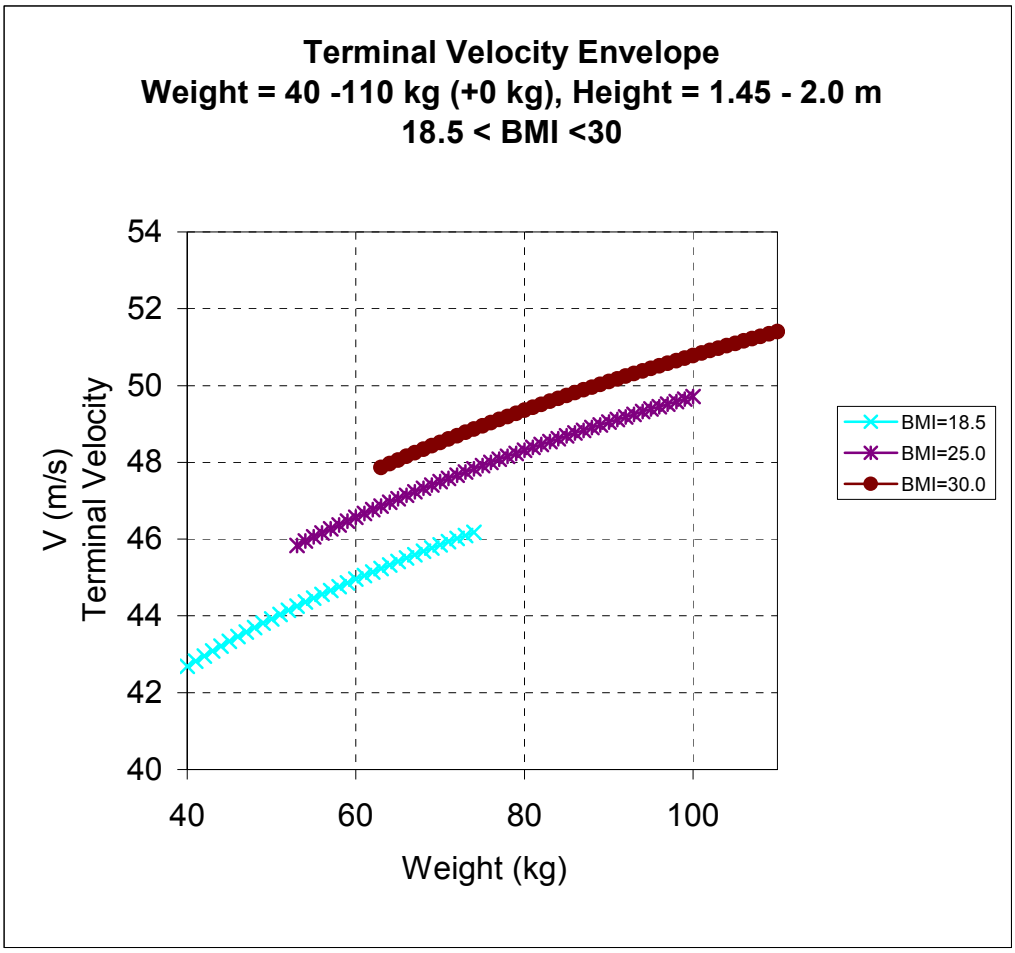

Figure 54 Terminal velocity, no additional weight

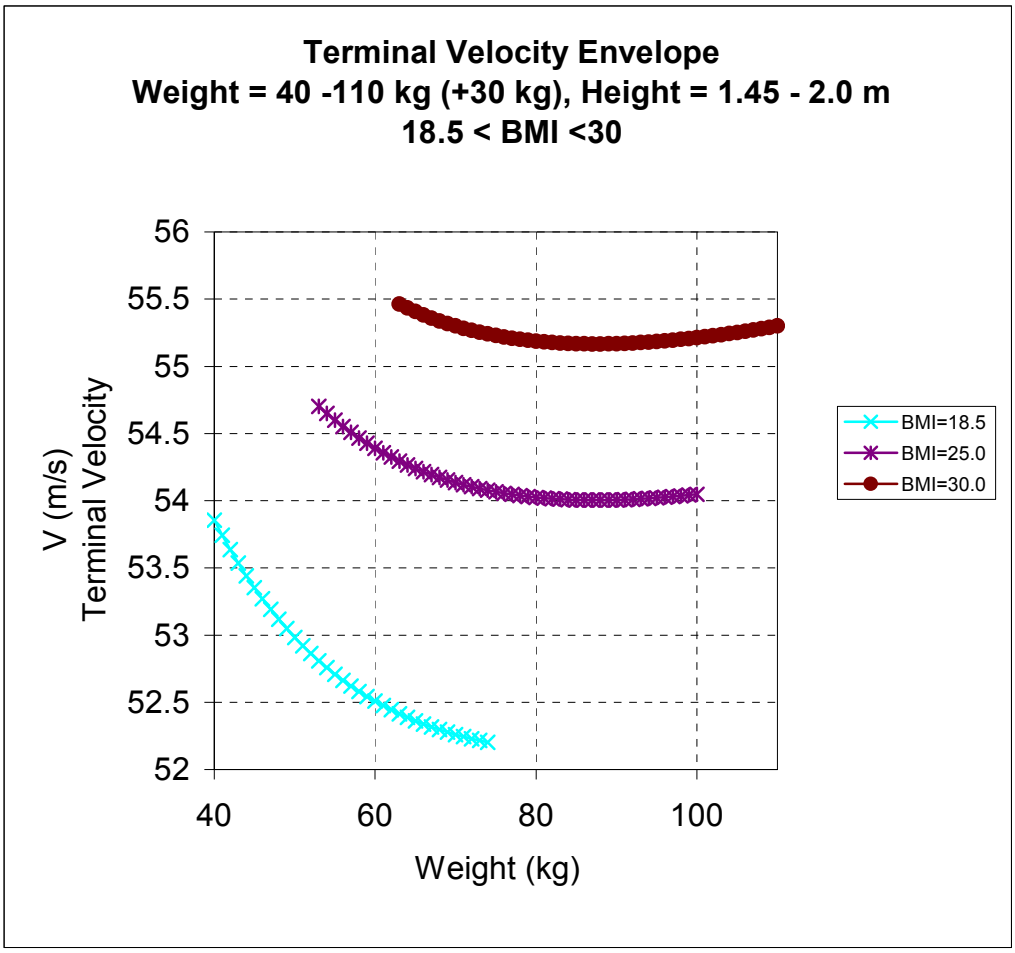

Figure 55 Terminal velocity, 30kg additional weight

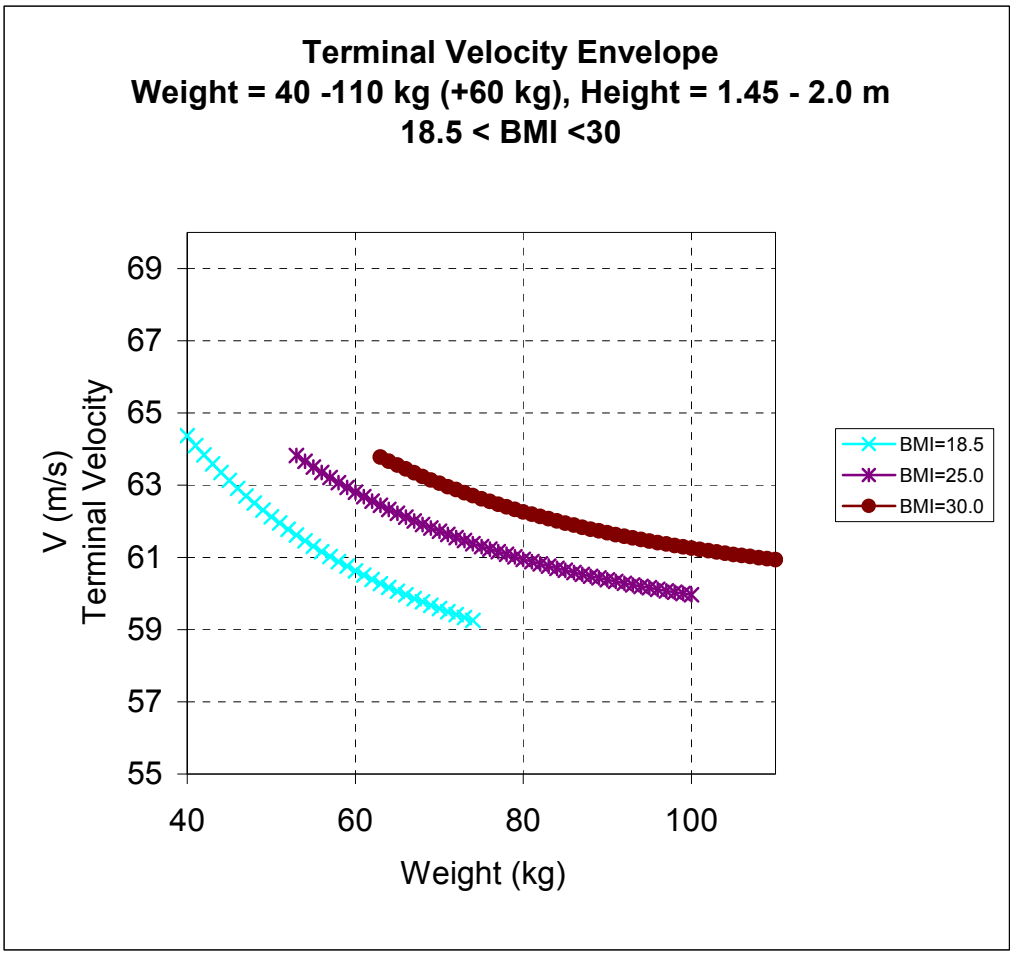

Figure 56 Terminal velocity, 60kg additional weight

APPENDIX B

AIRFOIL SECTIONS AND DATA

B.1. F Series Airfoil

This is an airfoil combination of different airfoil properties. C4 thickness form is used on a circular arc camber line and additional nose camber is based on the NACA 230 camber line. The equations given below are used to calculate the coordinated of the impeller and straightener sections used in the fan design.

The symmetrical C4 profile is given as:

$$\pm y_t = \frac{t}{0.20}\left(\begin{array}{l} 0.3048x^{\frac{1}{2}} - 0.0914x - 0.8614x^2 + 2.1236x^3 \ldots \\ -2.9163x^4 + 1.9744x^5 - 0.5231x^6 \end{array}\right) \qquad (97)$$

The coordinates x, y and the thickness t is in percent of the chord.

The camber as a combination of the circular arc and NACA 230 camber line is defined as follows:

$x < 0.2025$

$$y_c = \left[\left(\frac{0.5}{\sin\left(\frac{\theta}{2}\right)}\right)^2 - \left(x-0.5\right)^2\right]^{\frac{1}{2}} - \ldots \qquad (98)$$

$$\frac{0.5}{\tan\left(\frac{\theta}{2}\right)} + \left[120.5d\left(x^3 - 0.6075x^2 + 0.1147x\right)\right]$$

$x \geq 0.2025$

$$y_c = \left[\left(\frac{0.5}{\sin\left(\frac{\theta}{2}\right)}\right)^2 - \left(x-0.5\right)^2\right]^{\frac{1}{2}} - \frac{0.5}{\tan\left(\frac{\theta}{2}\right)} + d\left(1-x\right) \qquad (99)$$

In the above equations θ is the camber angle in degrees that is directly related with the lift coefficient, d is the nose droop in percentage of the chord. A representative drawing is given in Figure 57.

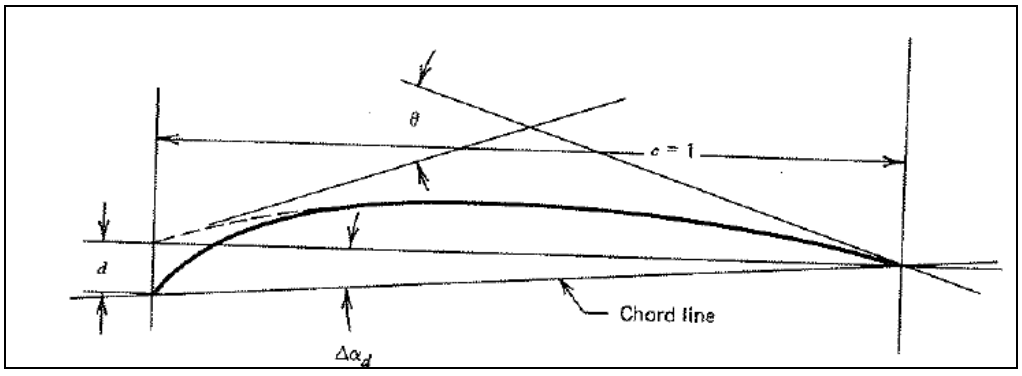

Figure 57 Camber line of F Series airfoil [6]

The coordinates of the upper and lower surface can be determined by applying the thickness formula over the camber line.

The coordinates of the upper and lower surface is calculated using the equations (100) and (101).

$$x_U = x - y_t \sin\varphi$$
$$y_U = y_c + y_t \cos\varphi \qquad (100)$$

$$x_L = x + y_t \sin\varphi$$
$$y_L = y_c - y_t \cos\varphi \qquad (101)$$

Where $\varphi = a\tan\left(\frac{dy_c}{dx}\right)$ is the slope of the camber line. The Figure 58 represents the coordinate determination of airfoils.

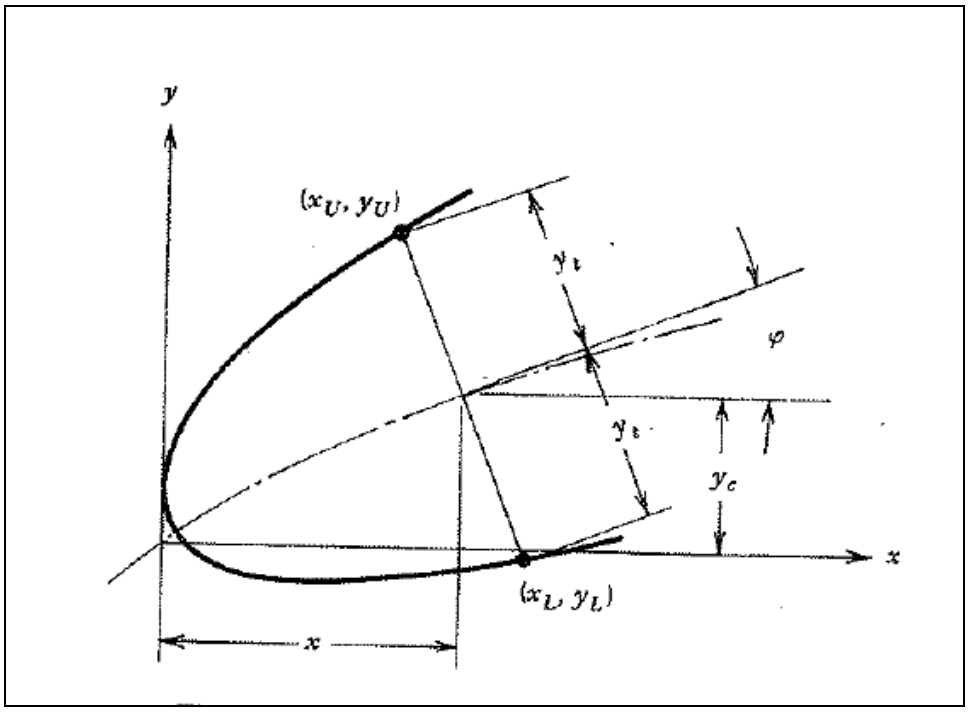

Figure 58 Airfoil coordinate determination [6]

It is important to define some mechanical properties of the airfoils for general use. The mechanical properties are moment of inertia, area

centroid location, etc. for F series airfoil the area centroid location is given by the equation (102). All values in percentage of chord.

$$\bar{X} = 43.5 - 0.0036\theta - 0.048d$$
$$\bar{Y} = 0.164\theta + 53d \qquad (102)$$

A sample airfoil with $\theta = 20$ degrees, d=0.00 is generated with a computer program and it is shown in Figure 59.

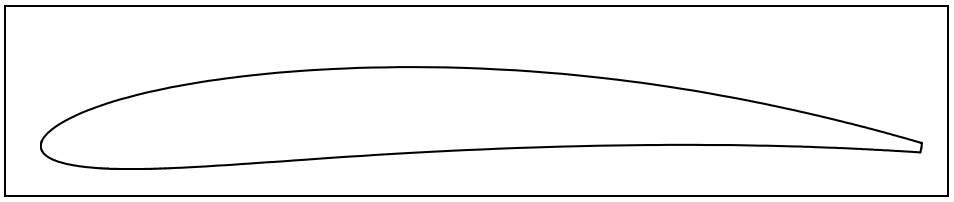

Figure 59 Sample airfoil

B.2. Other Airfoil Sections

There are other airfoil sections which are used in compressor design, fan design and turbine designs. The details of these airfoils will not be given in this manuscript but the names will be mentioned as a reference.

NACA 65 series are famous airfoil sections. There are studies in the literature about the performance of these airfoils. In [8], Horlock gives an extensive data for 65 series airfoils known as “Mellor Charts”. These charts relate the relative velocities, section lift coefficient and solidity. By using these charts, it is possible to obtain the airfoil section and it is orientation with respect to the flow direction.

In addition, some flat undersurface airfoils are used in axial fan designs. These airfoils are called “Clark Y”, “Gö 436”, “Gö 623” and “RAF 6E” airfoil sections. The data about these airfoil sections can be found in literature.